Optimization Framework for Improving Energy Flexibility in Residential Buildings

Optimierungsrahmen für die Verbesserung der Energieflexibilität in Wohngebäuden

Dissertation
zur Erlangung des Grades
des Doktors der Ingenieurwissenschaften
der Naturwissenschaftlich-Technischen Fakultät
der Universität des Saarlandes

von
Muhammad Usman

Saarbrücken
2023

Tag des Kolloquiums:	7. March 2023
Dekan:	Prof. Dr. Ludger Santen
Berichterstatter:	Prof. Dr.-Ing. Georg Frey Prof. Dr. Nadeem Ahmed Sheikh
Akad. Mitglied:	Dr.-Ing. Amine Othmane
Vorsitz:	Prof. Dr.-Ing. Paul Motzki

Abstract

Energy flexibility is balancing the supply and demand of a building according to climate conditions, user preferences, and grid constraints. Energy flexibility in households is a practical approach to achieving sustainability in the building sector. However, the diversity in flexibility potential of energy systems and climatic variability complicate the selection of envelope parameters and building energy systems (BESs). This study aimed to design a framework to improve the energy flexibility of the building. For this purpose, a single-family house and diversified BESs were simulated in a TRNSYS-Python co-simulation platform.

Initially, the bi-objective optimization identified flexible building envelopes in twenty-four locations. Then, the multi-criteria assessment of BESs was conducted using life-cycle energy flexibility indicators. Lastly, the energy flexibility potential of the BES was evaluated by employing steady-state optimization and model predictive control (MPC). The findings of this work set a benchmark for flexible household envelopes. The systematic approach for selecting BES could guide the energy system design, providing insight into energy flexibility. Further, this investigation has established that the dataset of building thermal load, boundary conditions, and control disturbances can be used to develop an MPC-based dynamic control. That controller could be employed on different BESs to achieve energy flexibility.

Kurzfassung

Energieflexibilität ist der Ausgleich von Versorgung und Bedarf eines Gebäudes je nach Klima, Nutzerpräferenzen und Netzbeschränkungen. Energieflexibilität ist damit ein praktischer Ansatz für Nachhaltigkeit in Gebäuden. Die Vielfalt des Flexibilitätspotenzials von Energiesystemen und die klimatischen Unterschiede erschweren jedoch die Auswahl von Hüllparametern und Gebäudeenergiesystemen (BESs). Diese Studie zielte darauf ab, einen Rahmen zur Verbesserung der energetischen Flexibilität von Gebäuden zu entwickeln. Hierzu wurden ein Einfamilienhaus und verschiedene BES in einer TRNSYS-Python Co-Simulationsplattform simuliert.

Zunächst wurden über eine bi-objektive Optimierung flexible Gebäudehüllen an vierundzwanzig Standorten ermittelt. Danach erfolgte eine multikriterielle Bewertung der BES anhand von Energieflexibilitätsindikatoren über den gesamten Lebenszyklus. Schließlich wurde das Energieflexibilitätspotenzial der BES durch den Einsatz statischer Optimierung und modellprädiktiver Regelung (MPC) bewertet. Die Ergebnisse dieser Arbeit setzen einen Maßstab für flexible Gebäudehüllen. Der systematische Ansatz zur Auswahl von BES könnte als Leitfaden für die Auslegung zukünftiger Systeme dienen. Darüber hinaus hat die Untersuchung ergeben, dass Daten zu thermischer Belastung des Gebäudes, Randbedingungen und Regelungsstörungen zur Entwicklung eines MPC verwendet werden können. Dieser Regler könnte bei verschiedenen BES eingesetzt werden, um Energieflexibilität zu erreichen.

Acknowledgment

I express my sincere gratitude to my supervisor, Prof. Dr. Ing. Georg Frey, for his kind support throughout this research work. His guidance, motivation, and provision of a productive working environment made it possible for me to complete this work successfully. I am also very thankful to my colleagues for all the help and support during my stay at the Chair of Automation and Energy Systems.

Table of Contents

List of Figures

List of Tables

1 Introduction

1.1 Background

The building sector accounts for 30% of energy use and 27% of CO_2 emissions worldwide. Residential buildings are responsible for 22% of final energy consumption and 17% of CO_2 emissions globally [1]. The Asian household sector has the largest share of 35% in building energy consumption. The second largest energy consumer for the residential sector is Europe, which accounts for about 28% of total energy use. Annual growth of 1.4% is anticipated in household energy use from 2018 to 2050 [2]. Energy consumption in the residential sector in 2014 was 30% higher than in 1990. In developing economies, this growth was above 50% during that timeline [3]. The energy usage share of heating, ventilation, and air-conditioning (HVAC) applications in buildings was the largest, around 37% in the world, in 2020. HVAC systems in buildings had a final energy consumption share of approximately 61% in Europe in 2019. Consequently, HVAC applications are responsible for a significant portion of buildings' CO_2 emissions [4]. Space heating, air-conditioning, and domestic hot water (DHW) are building end-use services with a substantial energy consumption share. A study produced the energy consumption trend for these three services from 2010 to 2050 based on the population size, household size, floor area, and Gross Domestic Product (GDP). The trend shows that energy consumption of these end uses increased by 65% worldwide in residential buildings from 2010 to 2050. The increase in energy consumption is relatively higher in regions of hot and humid or partially humid climates like Central and South Asia, Latin America, Africa, and the Middle East. However, energy consumption increases at a low rate in North America, Central Europe, and Eastern Europe. Even the energy consumption for space heating and cooling will be lower in 2050 than in 2010 in cold regions of Western Europe and Pacific OECD countries [5]. Based on these facts, modern society requires an economical and reliable energy supply to achieve thermal comfort and living standards. It is challenging to balance supply and demand while meeting climatic and energy efficiency standards like the energy performance of buildings directive [6] and the energy efficiency directive [7] by the European Commission. Current energy standards require management on both the demand and supply sides to accomplish the set energy efficiency and emissions reduction targets. Buildings have an enormous potential for energy savings, and energy efficiency in the building sector would lead to reduced CO_2 emissions [8–10]. It is projected that the building sector will contribute 25% to the reductions in CO_2 emissions by 2030 [11]. Among different building typologies, households are most

imperative for energy management due to the highest share in the final energy consumption. The energy management of a building through demand-side management (DSM) and supply-side management (SSM) can be referred to as energy flexibility. There are different definitions of energy flexibility in the literature. However, the most widely adopted one is defined in IEA EBC Annex 67 as "…*the ability to manage its demand and generation according to local climate conditions, user needs and grid requirements.*" [12]. The DSM may include load shifting, load shaving, and energy consumption reduction. In comparison, the SSM is the generation, storage, and distribution of electric and thermal energy in an efficient way. Energy flexibility can be further categorized into generation flexibility, system flexibility on the supply side, and load/demand flexibility on the demand side [13]. Moreover, two indicators generally assess energy flexibility: potential and performance indicators. The former indicators quantify energy flexibility using a bottom-up approach for demand response. The latter quantifies the energy system's flexibility regarding the economic and/or environmental impacts [14].

Extensive research has been conducted on the modulation of energy demand based on energy tariffs and peak loads, yet assessing flexibility for different energy supply mixes and service systems is unrecognized. The efficient architecture and energy systems with optimal control strategies reduce the energy use of the building. Moreover, renewable energy sources, specifically solar and geothermal, can reduce greenhouse gas (GHG) emissions by substituting conventional fuels [15–19]. The thermal gains/losses of the building envelope control the energy use for thermal comfort, which explicitly impacts total energy consumption in buildings [20]. Consequently, designing the building envelope using an integrative approach at the initial planning stage is imperative to improve buildings' energy flexibility. The energy supply system should be technically and economically feasible and environmentally friendly. Integration of renewable energy into the energy supply system is fundamental to achieving a sustainable future. Although integrating renewable energy technologies in the building sector is growing fast, it only covered 14% of the total energy demand in 2017 [21]. The use of solar energy in building energy systems (BESs) has increased significantly in the last decade, and this growth is expected to be increased in the future [22].

Similarly, the direct use of geothermal energy grew remarkably from 2010 to 2019, when it doubled to 107727 $MW_{thermal}$. From 2010 to 2015, thermal energy utilization increased by 39.8% and 2.3% from 2015 to 2019 [23]. In 2018, the combined share of solar and geothermal heat was 5.1% of total energy consumption for thermal comfort in buildings [21]. Recently, small to large-scale buildings have been equipped with combined solar and geothermal systems

to supply electricity, DHW, and HVAC services [8,24–27]. The optimal control of the HVAC system is also an essential aspect of DSM due to its large share of energy consumption and GHG emissions. Previous studies have proven a substantial energy-saving potential in the building sector by employing automation and control of HVAC systems [8,10,28]. Though the control strategies improve the performance of HVAC systems, integrating HVAC systems with buildings is challenging to time-dependent dynamics and the high number of interactions [29]. The locality of a building is also a decisive factor for building design, selection of energy supply and service systems, and control strategies of an HVAC system. The variation in weather conditions, energy tariffs, renewable energy potential, and GHG emissions from power production strongly influence the choice of BES [30,31]. Summarizing the energy flexibility strategies: generation flexibility includes on-site generation options, system flexibility includes energy storage, improved thermal envelope, and combinations of service systems, and demand flexibility includes control of HVAC thermostats, load shifting, and electric/thermal charging cycles.

1.2 Research questions and objectives

It is anticipated from the literature that residential buildings may have the potential for flexibility on the demand and supply sides. This potential depends on the choice of the energy system and on climate conditions. Energy flexibility gives information on the energy balance of the demand and supply sides. Conventionally, energy flexibility is quantified in terms of energy efficiency, cost reduction, and improvement in the environmental impacts of the energy system during the demand response event (DRE). However, different energy systems have specific life-cycle costs (LCC), life-cycle emissions (LCEs), and RES capacities.

Furthermore, the DSM and SSM strategies result in different levels of energy flexibility for different service systems and energy mixes for a building. Most of the recent research on energy flexibility in residential buildings is focused on demand flexibility [32,33], with some studies [34,35] considering limited options of both demand and supply sides for a specific energy system in residential buildings. The flexibility indicators in the literature mostly quantify only one source of flexibility in a building. Moreover, the flexibility indicators provide information on energy consumption, efficiency, costs, and emissions but are limited to the operational characteristics of the energy system. Potential indicators alone cannot be used to compare energy systems because they only give information on energy flexibility regarding the baseline energy use profile. A BES could most likely accomplish high energy flexibility, yet the life-

cycle energy use or CO_2 emissions are higher than in another energy system with lower energy flexibility potential. Thus, the energy flexibility of different energy systems needs to be assessed at the design stage, considering technical feasibility, economic viability, and environmental impacts during the life cycle. Factually, no systematic methodology has been established to evaluate the potential of different energy systems for the generation, system, and demand flexibilities on an integrated basis. Although explicit flexibility indicators have been used to quantify flexibility during a DRE for different building systems, the methodical flexibility indicators need to be defined to compare and select multiple BESs.

Based on these facts, the following research questions have been defined:

1. What is the energy flexibility potential in residential buildings with multiple energy systems?
2. What are optimal envelope parameters in different climates to improve households' energy flexibility?
3. How can a flexible BES be selected based on the life-cycle flexibility indicators in different climates?
4. How can an optimal dynamic control be developed which can be employed on different energy systems to improve demand flexibility?

Answers to these questions outlined the aim and objectives of this research. The aim was to develop an optimization framework to identify a BES according to the climate conditions, which provides energy flexibility in households without compromising thermal comfort. The optimization framework includes the following tasks:

- Flexibility assessment of the building's optimal passive design (potential indicators).
- Flexibility assessment of multiple BESs with different energy supply mixes and service systems (potential indicators + performance indicators).
- Flexibility assessment of model predictive control (MPC) for thermostat and window shading fraction (potential indicators + performance indicators).

To achieve the aim, a single-family house and diversified BESs were modeled and simulated in a TRNSYS-Python co-simulation platform. The research aim mapped the following research objectives:

1. Establish guidelines for achieving energy flexibility in a residential building by determining optimum envelope design in various climate zones.

For this purpose, household passive design optimization was conducted for twenty-four locations in twenty climates by coupling Transient System Simulation Program (TRNSYS) [36] and a non-dominated sorting genetic algorithm (NSGA-III) using a Python program.

2. Apply a multi-criteria assessment technique for selecting the BES using novel combination of energy flexibility indicators, which provide a comprehensive insight into energy flexibility.

The goal was achieved by a multi-criteria assessment of fourteen diversified BES based on life-cycle energy flexibility indicators. This task was performed in four locations having different climate conditions (severe cold, cold, mild, and hot)

3. Evaluate how much energy flexibility potential exists by steady-state optimization (SSO) of energy storage capacities, heat pump's operational parameters, and heating/cooling setpoints.

This task was accomplished by performing a multi-objective optimization (MOO) using the NSGA-III algorithm for BES from the former task. The optimization variables were battery storage capacity, thermal energy storage volume, source side flow rate of geothermal heat pump, On/off delay of HP, borehole diameter of ground heat exchanger, and heating/cooling set points of the zone. In addition, primary energy ratio (PER) (to be maximized) and electricity consumption of BES (to be minimized) were defined as objective functions with fractional state of charge of battery and thermal comfort as constraints of the optimization problem.

4. Develop an MPC strategy for building service systems and evaluate the demand flexibility from dynamic control.

An MPC strategy was implemented on the BES from the previous step for this task. Firstly, a predictive model was developed for building thermal load considering boundary conditions and time-varying climate uncertainties. An MPC-based supervisory control in Python script interacted with local controllers (PID controllers for temperature set points and shading fraction of windows) in TRNSYS at the beginning of each time step. The supervisory controller optimized the control variable using a genetic algorithm (GA) and predictive model to minimize the energy system's electricity consumption while maintaining the zone's thermal comfort.

1.3 Research contributions

Previous flexibility assessment studies were focused on energy flexibility of generation, system, and demand domains of a specific system, independently. The flexibility assessment indicators

were also limited to demand response flexibility. Further, the performance indicators for cost and emissions are evaluated during the energy system operation without considering the embodied emissions and life-cycle costs of energy supply and BES. The novelty of the research is the development of a systematic framework for estimating the energy flexibility of multiple building energy systems from an integrated energy system perspective. A novel set of flexibility indicators is proposed to calculate an energy system's flexibility potential for the complete life cycle at the design stage. These performance indicators can evaluate the flexibility for generation, system, and demand flexibilities, altogether. Moreover, the MPC strategy can be employed on multiple energy systems using the thermal demand-based predictive model of the building. The novelty of the work is further evinced in chapter 2 by reviewing the current methods for energy flexibility and its quantification in buildings.

The outcomes of this work support different stakeholders of building energy systems to make appropriate decisions for the transition to sustainability in the building sector. The implementation of the optimization framework results in the following research contributions:

- Benchmarking envelope design with climate adaptability overcomes the limitations of the complex modeling of building architecture. Furthermore, since the climate has been changing over the past decades globally, the developed guidelines provide criteria to modify the building design in the future.
- Provide a methodology for comprehensive multi-criteria evaluation of energy systems to identify a flexible BES that provides thermal comfort in the building and is technically feasible, economical, and environmentally friendly.
- An MPC-based supervisory controller improves the demand flexibility of various BESs by coupling an optimization algorithm and a predictive model designed from the dataset of building thermal load, boundary conditions, and control disturbances.

1.4 Thesis structure

The thesis is structured as follows:

Chapter 2 provides an overview of opportunities and sources of energy flexibility in buildings and introduces the optimization strategies in the context of previous findings in the literature.

Chapter 3 describes the designing of BES and quantification of energy flexibility and explains the development of the TRNSYS-Python co-simulation optimization framework. The assumptions and limitations of this work are also described for reference.

Chapter 4 describes the reference building's thermal load model and boundary conditions. Then, it presents the modeling of energy systems and performance characteristics of HVAC equipment. In the end, it explains the modeling of an MPC-based dynamic control.

Chapter 5 provides case studies of achieving energy flexibility by employing the proposed optimization framework. In addition, this chapter presents and discusses the simulation results of the investigated scenarios.

Chapter 6 describes the implications and scope of this study, followed by the research outcomes and perspectives for future work.

1.5 Research publications

Some results of this research work have already been published in journals and conferences. The following research articles are based on this study:

1. M. Usman and G. Frey, "Multi-Objective Techno-Economic Optimization of Design Parameters for Residential Buildings in Different Climate Zones," Sustainability, vol. 14, no. 1, p. 65, Dec. 2021, doi: 10.3390/su14010065. [37]
2. M. Usman, D. Jonas, G. Frey, A methodology for multi-criteria assessment of renewable integrated energy supply options and alternative HVAC systems in a household, Energy Build. 273 (2022) 112397. [38]
3. M. Usman, D.M. Minhas, G. Frey, Energy optimization of a residential building using model predictive control-A case study in temperate oceanic climate, in: 2022 International Conference on Electrical, Computer and Energy Technologies (ICECET), IEEE, 2022: pp. 1–6. [39]

Additional Publications

4. M. Usman, M. Ali, T. ur Rashid, H. M. Ali, and G. Frey, ''Towards zero energy solar households – A model-based simulation and optimization analysis for a humid subtropical climate," Sustainable Energy Technologies and Assessments, vol. 48, p. 101574, 2021, doi: 10.1016/j.seta.2021.101574. [17]

2 Review of materials and methods

The growing energy consumption and GHG emissions in the building sector have inclined the focus of researchers to integrate RES and energy-saving strategies. The flexible building is becoming an increasingly important aspect of sustainability in buildings. However, the energy flexibility of BES involves several elements, from design to the utilization phase. Different energy systems hold diverse flexibility capabilities, operational features, energy consumption, and demand response characteristics [14]. It becomes critical to evaluate these characteristics at the design stage according to the climate uncertainties and boundary conditions to identify the BES with maximum flexibility.

There are various definitions and terminologies for energy flexibility in the literature, as described in Table 2-1. Regardless of the variation in the definitions, the basic principle of building energy flexibility (BEF) can be stated as the ability of a building to operate flexibly by adjusting its energy demand and generation without compromising thermal comfort [40].

Table 2-1: Definitions of energy flexibility in literature (DSM = demand-side management, SSM = supply-side management)

Terminology	Definition	Flexibility domain	Reference
Energy flexibility	*"…the ability to manage its demand and generation according to local climate conditions, user needs and grid requirements."*	DSM	[12]
Energy flexibility	"…the ability to adapt the energy profile without jeopardizing technical and comfort constraints."	DSM	[14]
Demand flexibility	*"…the customers' ability to modify their energy consumption in response to an external signal."*	DSM	[41]
Flexibility	"…the ability to deviate from the reference electric load profile during the flexibility interval."	DSM	[42]
Flexibility	"…the ability of a power system to cope with variability and uncertainty in both generation and demand, while maintaining a satisfactory level of reliability at a reasonable cost, over different time horizons."	SSM	[43]
Power flexibility	"…the ability to continually balance electricity supply and demand with negligible disruption to service for connected loads often in response to variability in RES-based generation."	DSM + SSM	[44]

The studies listed in Table 2-1 mainly differ in the ways of flexibility sources and flexibility strategies. The common attribute of these definitions is the motivation for energy flexibility, which is increasing the share of RES, energy saving, peak load reduction, and grid independence. Another essential characteristic of flexibility is the targeted domains of energy flexibility. Energy flexibility can be applied from the building structure to technologies and individual components of BES. However, most of the studies analyze the flexibility capacity of a DRE. The DRE span is usually seconds, hours, or a day but it could be a month or a year,

depending on the strategies. Summarizing, energy flexibility reduces the building's electric and/or thermal demand from the grid for a certain timespan by using thermal storage, flexible technologies, and applying control strategies. This study uses the terminology of energy flexibility due to its broad spectrum, which covers flexibility for all three domains, generation, system, and demand flexibilities.

2.1 Energy flexibility opportunities

Energy flexibility in a building is determined by thermal load, energy service technologies, energy storage techniques, and control strategies for service systems. Energy flexibility sources include on-site power generation, energy system technologies, active and passive energy storage, thermostatically controlled loads, and load shifting. The energy flexibility can be categorized based on the flexibility sources as follows [13].

- **Generation flexibility:** Renewable generation (solar, wind, etc.), fuel cell, combined cooling, heating, and power (CCHP)
- **System flexibility:** Combination of technologies (heat pump, district heating, absorption chiller, geothermal heat pump, etc.), active energy storage (battery, thermal storage tank, etc.), passive thermal storage (phase change material, structural thermal mass)
- **Demand flexibility:** thermostatically controlled load (HVAC, water heater, refrigerator, etc.), wet appliances, battery-based loads (electric vehicle, laptop, etc.)

Different energy flexibility sources (EFS) provide a certain level of flexibility in the building. A sensitive analysis of building parameters on energy flexibility showed that envelope insulation is the buildings' most influential flexibility source. Thermal inertia of building structure and energy system also proved to be EFS with higher impacts [45]. In a study [46], a sensitivity analysis was performed for building parameters concerning their effect on different aspects of energy flexibility. Table 2-2:Table 2-2 provides the ranking of building parameters for energy flexibility prospects. Envelope insulation is the most critical feature of EFS. Thermal inertia of building structure, the ability to absorb, store, and release heat, can also deliver significant energy flexibility in load shifting but with small durations of DREs. The heating/cooling technology type is another factor that significantly impacts energy cost efficiency. Control strategy comes next in the hierarchy of energy flexibility potential. Therefore, a residential building with a high level of insulation, larger thermal inertia, and an

efficient heating/cooling system with optimal thermostatic modulation can provide energy flexibility with thermal comfort.

Table 2-2: The ranks of envelope parameters according to the energy flexibility potential [46]

General ranking	Parameters	A[1]	B[2]	Δ[3]	ß[4]	Load shifting ability	Energy cost efficiency
1	Insulation level	1	1	1	1	1	1
2	Thermal inertia	2	2	2	6	2	4
3	Heating/Cooling system	5	5	3	5	3	2
4	Control strategy	4	4	5	4	4	5
5	Building topology	3	3	4	7	5	3
6	Outdoor temperature	6	6	6	3	6	6
7	Solar radiation	7	7	7	2	7	7

[1] The total amount of energy shift (downward) in time.

[2] The total amount of energy shift (upward) in time.

[3] The maximum change in the power demand.

[4] The time of reduced energy demand after the control strategy.

This study considers envelope insulation, active thermal storage, RES, and heating/cooling system as flexibility sources. The energy-saving potential and strategies for flexibility sources are discussed in later sections, 2.1.1 to 2.2.3. To get an insight into energy flexibility and its quantification in residential buildings, Table 2-3 gives an overview of the applied flexibility strategies on various sources of flexibility and indicators used to characterize energy flexibility in the literature.

Table 2-3: Overview of flexibility sources with employed control strategies and flexibility indicators in residential buildings

Ref.	Flexibility source			Control strategy	Control inputs	Energy flexibility quantification	
	Generation	*System*	*Demand*			*Performance indicators*	*Potential indicators*
[32]			- heat pump	- MPC	- thermal energy of heat pump - thermal energy of storage tank	- electricity cost - CO_2 emissions	- flexible thermal load
[47]			- district heating	- Rule-based scheduling	- Temp. set points	- cost of heating	- Flexibility indicator
[34]	- PV	- battery - envelope parameters	- HVAC - water heater	- MPC	- Temp. set points - PV power - Battery power - water heater duty cycle	- electricity cost	- peak power reduction - energy demand in peak hours
[48]		- Four buildings with different envelope parameters	- space heating	- schedule-based	- Temp. set points	- thermal comfort	- delayed operation - rebound energy
[49]			- space heating	- MPC + Rule-based control	- Temp. set points with comfort constraint		- flexible energy (savings) - rebound energy - flexible energy efficiency - maximum flexible power
[50]		- building thermal storage - old building and passive house - heating technologies	- radiator heating - floor heating	- schedule-based	- Temp. set points		- flexible heating energy - storage capacity - shifting efficiency - flexibility factor
[51]	- micro-wind - PV - thermal collectors	- battery - DHW tank - Cooling storage tank	- HVAC	- schedule-based - rule-based	- Temp. set points of storage tank recharging - volume of cooling storage tank - battery capacity - control signal for PV and battery supply to the load		- Flexible time duration - Flexible power - Flexible energy - Flexibility factor
[52]	- thermal collectors	- heating technologies - thermal storage tank	- air source heat pump - direct electric heating	- Rule-based control - schedule-based	- Temp. set points for the heating system and DHW	- cost of heating - CO_2 emissions	- flexible energy

Ref.	Flexibility source			Control strategy	Control inputs	Energy flexibility quantification	
	Generation	***System***	***Demand***			***Performance indicators***	***Potential indicators***
[53]	- PV - thermal collectors	- building stock upgradation of envelope and HVAC system	- HVAC			- primary energy consumption - CO_2 Emissions	- renewable energy use - flexible loads
[33]		- 03 buildings with different envelope parameters	- HVAC	- schedule-based	- Temp. set points	- thermal comfort	- storage capacity - storage efficiency
[35]		- 02 buildings with different envelope parameters	- heating system	- schedule-based	- Temp. set points		- added energy - discharged energy - curtailed energy - rebound energy
[54]	- PV	- structural thermal energy storage - thermal storage tank - battery	- GSHP	- schedule-based	- thermal storage tank volume - Temp. set points of thermal storage tank		- storage capacity - storage efficiency - self-consumption
[43]	- wind power - generators			- dynamic optimization	- on/off status of generators	- operational cost - investment cost	- flexibility index
[55]		- structural thermal energy storage - building stock with different envelope properties and heating system	-	- Rule-based control	- Temp set points		- storage capacity - storage efficiency - power shifting capability
[45]		- structural thermal energy storage - building with different envelope parameters - heating technologies	- heating system	- Rule-based control	- Temp set points		- flexibility index

2.1.1 Building architecture

This growing energy demand with associated CO_2 emissions and the large energy flexibility potential of the envelope have led to modern design concepts for energy savings in buildings. Consequently, energy-efficient buildings are a sustainable approach to decreasing energy demand and GHG emissions. As established from the sensitivity analysis of building parameters [45,46], envelope insulation is the most effective technique to improve energy flexibility in buildings. A study on energy efficiency and demand flexibility in 498 dwellings showed 38 – 58% energy saving for various envelope insulation levels in a cold climate. The energy management system with battery storage resulted in an energy cost reduction of $140/year [34]. The envelope parameters are strongly related to the ability of load shifting. It was observed in [48,50] that poorly insulated households had significant potential for load shifting but with shorter periods. In contrast, the well-insulated households had a smaller potential for load shifting due to decreased heating/cooling demand than poorly insulated households for longer periods.

Similarly, Vivian et al. [33] found that storage capacity was higher in new buildings than in old ones. Interestingly, the storage efficiency is higher in new buildings, which means that the energy stored during the demand response was used to its maximum later in new buildings, and a substantial portion of stored energy was lost in old buildings. Reynders et al. [55] also investigated energy flexibility as a function of building topology and control parameters and concluded that the structural thermal energy storage should be activated for a shorter duration to achieve higher energy flexibility. Another study investigated the energy flexibility in 419 dwellings having different envelope retrofits [53]. It was found that each element of the envelope, i.e., external walls, roof, floor, and windows, had substantial energy-saving potential individually. However, the whole building retrofit was most effective with primary energy savings of 35%, CO_2 emissions reduction of 47.6%, renewable energy use reduction of 2%, and flexible load reduction of 5%. The energy demand for thermal comfort is determined by the building envelope's thermal performance, which has direct implications on the total energy need of the building [20]. Thus, an integrative methodology is required to build a passive design to improve energy flexibility at the initial design stage. Designers need extensive details on building performance and must choose from a wide range of design options to achieve the desired energy flexibility.

2.1.1.1 Optimization of envelope parameters

Previous studies depict that a building's operating costs, carbon emissions, and energy efficiency depend on the preliminary design approaches [56]. In the planning phase, the designer must consider building orientation, ventilation rates, solar gain/loss, window area and shading, and thermal transmittance, which influence the building performance altogether or individually[57,58]. Climate is another critical aspect in designing building architecture. Since the envelope design and energy-saving capacity vary with the outdoor environment, the design phase becomes more complex due to the diversity of weather conditions in different regions [30]. Another critical factor to consider when assessing thermal load, particularly the cooling load, is heat gain from household appliances. A realistic appliance's heat gain profile could assist in quantifying the heat to be evacuated from the building during space cooling [59] and preventing overheating during space heating [60].

Though building envelope design is a crucial aspect of energy flexibility, it is a difficult job due to a wide range of efficiency measures. Quantifying the energy flexibility from various building optimization schemes using the conventional approach is challenging. The researchers have coupled building simulation tools like Ecotect, EnergyPlus, Doe-2, and TRNSYS (Transient Systems Simulation Program) with optimization algorithms to determine energy-efficient solutions[12,61]. Optimization algorithms assess design options for required outcomes and make it possible to tradeoff between objective functions simultaneously while considering the design constraints [62].

Previous studies have shown that metaheuristic algorithms are adequate tools to prompt energy flexibility by optimizing envelope design. Penna et al. [63] conducted a tri-objective optimization on a single-family household in two cities in Italy having different climates using TRNSYS and NSGA-II. The objectives were minimizing the cost, discomfort hours, and energy use by improving the envelope insulation, window glazing, and HVAC equipment. Both cities achieved more than 57 % energy savings in the cost-optimum scenario. Rabani et al. [64] developed an optimization scheme to mechanize the selection of best-suited windows' configuration, envelope parameters, shading system, and service system for a Norwegian office building. Ascione et al. [65] simulated the thermal load of a residential building in four cities having Mediterranean climate in Energy Plus and optimized the building architecture using NSGA-II. The type of windows, walls, and roofs were determined by reaching a trade-off between heating and cooling demands. Ferrara et al. [66] optimized the energy use, energy cost, and acoustic performance of a nearly zero energy building in GenOpt using the particle swarm

optimization (PSO) algorithm. The energy system model of a French home was co-simulated with a MATLAB-based acoustic performance model. A previous study coupled IDA-ICE with GenOpt and optimized the energy consumption by 77% using NSGA-II. The optimal shading control based on solar radiations and zone temperature was the most influential design parameter for optimization. Chang et al. [67] optimized multiple design parameters of four households in Tokyo using a flexible MOO scheme. The optimum retrofit area of the building envelope was determined for improved energy performance, higher thermal comfort, and lower GHG emissions. As the MOO generates a series of Pareto fronts (PFs), the choice of the most appropriate solution is complicated. Multi-criteria decision-making (MCDM) is an established technique to order the Pareto solutions and select the optimum. The MCDM method is explained along with related literature in section 3.5.

The review of past literature emphasizes that the climate needs to be considered at the preliminary design phase to get an idea of energy flexibility potential. Zhao & Du [68] applied the MOO technique to an office building to reduce energy use and increase thermal comfort in China's four climates, from extreme cold to hot. Optimizing building orientation, windows layout, and shading in those locations revealed that envelope design depended on the local conditions to achieve energy efficiency. In the optimum solution, the window type and overhang length differed in hot and cold regions. A study investigated different passive design options for a household in twenty-five different climate regions [69]. The authors examined the effect of window shades during daylight and air change rate (ACH) of 1 and 1.5 for passive cooling. Under five scenarios, they varied the thermal transmittance of windows and walls, window area, and windows glazing type. The thermal transmittance of external walls and roof were 0.2 W/m^2K and 0.6 W/m^2K in extreme cold and hot regions, respectively. The optimal window-to-wall ratio (WWR) was up to 0.8 in cold climates ensuring higher solar gains during heating. Natural ventilation remarkably reduced the cooling load in hot regions and prevented overheating in cold regions.

Naji et al. [70] simulated a double-story detached house of 214 m^2 using TRNSYS and EnergyPlus and minimized the life-cycle costs by employing a genetic algorithm. The authors conducted case studies in eight cities representing Australia's tropical, temperate, and continental climates. It was observed that tropical, hot desert, and humid subtropical climate zones require smaller WWR, whereas the oceanic clime zone was characterized by larger WWR. Furthermore, the optimal solutions showed that low-level insulation was needed in the

tropical climate. In contrast, high-level insulation was feasible in oceanic climate. In addition, the shading effect was more prominent in tropical and hot deserts than in cold climates.

To evaluate the energy-saving potential of a zero-energy building, Harkouss et al. [71] designed a co-simulation platform of the MOO tool and EnergyPlus. Multi-story residential buildings were investigated in different locations in France and Lebanon. The design variables were envelope insulation, WWR, window shading, window glazing, and temperature set points for heating and cooling. The results established that it is imperative to use passive techniques and a high-insulated envelope to reduce the building's thermal load. The optimization framework reduced the thermal load between 6.7% to 33.1% in different locations. Delgarm et al. [72] coupled EnergyPlus and a genetic algorithm to determine the optimal orientation, WWR, and window shading fraction of a thermal zone in Iran's four climate zones (cold to hot). The optimization resulted in a 23.8% to 42.2% decrease in final energy use in those locations. The optimum values of WWR were 0.26 and 0.08 in heating-dominant and cooling-dominant climates, respectively. The building orientation and overhang length did not show much variation in optimal solutions of investigated climates.

2.1.2 Building energy system

Building energy system is another critical aspect of improving energy flexibility in buildings and is ranked at 3rd for energy flexibility potential, as evident in Table 2-2. BES can be categorized into two subsystems: energy supply mix and building service system. An optimal energy supply mix can provide generation flexibility, and the building service system is responsible for the system flexibility. According to the previous studies on energy flexibility (c.f. Table 2-3), regarding energy supply, grid supply is the mandatory element, and other supply options may include photovoltaic (PV) generation, solar thermal collectors, micro-wind, CCHP, fuel cell, etc. At the same time, the HVAC system is an essential component of services, with the auxiliary system being a combination of structural thermal energy storage, thermal storage tank, and electric storage.

Very few studies exist that compare the energy flexibility of service systems in residential buildings concerning the HVAC system [36,48,50,52,54,55], as evident from Table 2-3. However, the scope of energy flexibility is firmly established by the results of those studies. A comparison of underfloor heating and radiator showed that the floor heating system stored more energy for a longer duration due to low energy losses. In contrast, the shifting efficiency of the radiator was high due to the lower thermal inertia. Both systems could provide thermal comfort

in the building with negligible variation [50]. In another study [55], the comparison of floor heating and a conventional radiator showed that the storage efficiency of the floor heating system was above 90% in various building topologies, which varied between 65 – 91% for radiator heating. Similarly, Johra et al. [45] investigated the performance of floor heating and radiator heating in buildings having different structural properties. The floor heating had better performance in building with medium and heavy structures. Moreover, replacing the radiator with a floor heating system resulted in an 8% improvement in energy flexibility in highly-insulated buildings. Clauß et al. [52] individually analyzed an air-source heat pump (ASHP) and a direct electric heater for flexibility potential against different control strategies. It was observed that scheduled base control substantially decreased energy use and cost during peak hours. Since the electricity consumption of the reference case was higher than the ASHP for direct heating, the direct heating system showed comparatively higher energy flexibility potential. A study calculated the energy flexibility for replacing existing service systems (traditional boiler/heat pump/electric water heater/air conditioner) with efficient systems (condensing boiler/A+++ class heat pump/heat pump for water heating/A+++ class air conditioner) [53]. The upgraded system reduced the primary energy consumption and local CO_2 emissions. Also, the flexible loads and renewable use were significantly increased when replacing the gas-fired system with a heat pump. Regarding the energy supply, Ma et al. [43] evaluated the energy flexibility of integrating wind generators in building power system. It was found that the flexibility of the power system increased with the increasing share of wind generator output in the electricity supply.

2.1.2.1 Selection of optimal energy system

Climate, occupancy rate, internal heat gains, natural ventilation, and building service technologies are some of the factors that determine energy use in a building [31]. The operational characteristics of BES, such as efficiency, power demand, and operating cost, vary with the changing climates. Additionally, various HVAC alternatives can be installed in the same building for heating and cooling[10,26,73]. Although there are energy-efficient and financially feasible HVAC and energy supply systems for households, choosing the most suitable BES for a particular climate zone involves an integrated strategy. Traditionally, the HVAC system is selected based on the building's final energy use and thermal load. Nevertheless, evaluating additional performance measures such as environmental impacts, capital and operating costs, energy costs, and thermal comfort is essential while selecting a BES. Also, the financial benefits, renewable energy share, and environmental effects need to

be assessed for the installed renewable energy technologies. MCDM methods compute the aggregated impact of these contradictory indicators and rank the possible solutions according to the provided criterion [74].

Solar, wind, and geothermal are feasible energy source options. Whereas PV, solar thermal, gas or oil boiler, (reversible) air source heat pump (ASHP), (reversible) water-source heat pump (WSHP), (reversible) ground-source heat pump (GSHP), vapor compression chiller, and absorption chiller are the most common HVAC systems and energy converters in buildings [8,26,73,75,76]. There are several MCDM methods and various performance indicators that can be used for the evaluation of building energy systems. Table 2-4 summarizes different MCDM methods and evaluation criteria used to select building energy systems in recent years.

Table 2-4: Application areas and performance indicators of MCDM for building energy system

MCDM method/ building type	Energy system under evaluation	Performance Indicators	Application/ Criteria evaluation methods	Reference
Elimination and Choice Translating Reality (Electre) III (Office)	- Heating: gas-fired boiler, oil-fired boiler - Cooling: split air conditioner, air-cooled chiller	Net present cost, energy consumption, thermal comfort, indoor air quality, CO_2 emissions	- Selection of best HVAC system in an office building. - Simulation (TRNSYS) + computation	[77]
Analytic hierarchy process (AHP) (Commercial)	- different sizes of the internal combustion engine, boiler, PV/PVT, absorption chiller, electric chiller	annual operation cost ratio, primary energy saving ratio, carbon emission reduction ratio	- Integration of combined heating, cooling, and power system in a commercial building using renewable and non-renewable sources. - Computation	[11]
Weighting: entropy method + geometric mean method + additive combination weighting method *Ranking:* Technique for Order of Preference by Similarity to Ideal Solution (TOPSIS) (Office)	- air-cooled chiller with gas boiler - absorption chiller with gas boiler - combined heat and power with a hot water absorption chiller - ground coupled heat pump	energy consumption, thermal comfort, indoor air quality, initial cost, operational cost, CO_2 emissions	- Multi-climate study to develop a decision-making tool for the HVAC&R system, including primary and secondary components of the system. - Simulation (TRNSYS) + computation	[10]
Stochastic multicriteria acceptability analysis (SMAA) (District heating)	- coal-fired combine heat and power - gas-fired boiler - oil-fired boiler - coal-fired boiler - solar energy heat pump - water-source heat pump - ground-source heat pump	cost per unit area, GHG emissions, qualitative criteria	- Selection of sustainable district heating system considering the uncertainties of criteria. - Computation	[78]
Preference Assessment by Imprecise Ratio Statements method (PAIRS) (Residential)	- district heating - geothermal heating - electric heating - air heat pump - solar heating - oil heating - solar oil heating - natural gas heating - natural gas heating with fuel cell	Life-cycle costs, CO_2 emissions, SO_2 emissions	- Comparison of micro-CHP (micro-cogeneration) heating with traditional heating systems for financial and environmental impacts. - Computation	[79]
AHP + Preference Ranking Organization Method for Enrichment Evaluation (PROMETHEE) (Residential)	- Grid + AC + boiler - Grid + PV + AC + boiler - Grid + PV + Battery + AC + boiler - Grid + wind turbine + AC + boiler Grid + wind turbine + PV + AC + boiler - Grid + gas engine + AC	investment cost, running cost, CO_2 emissions, primary energy consumption	- Evaluation of conventional and renewable energy systems by combing linear programming and MCDM. - Computation	[80]

MCDM method/ building type	Energy system under evaluation	Performance Indicators	Application/ Criteria evaluation methods	Reference
	- Grid + fuel cell + AC			
SMAA (Residential)	- electric heating - District heating with biomass fuel - GSHP - Pallet boiler heating - solar heating - fireplace	investment cost, operating cost, CO_2 emissions, particulate emissions	- Multicriteria decision support for planning new sustainable residential area - Measured data + computation	[81]
AHP + Weighted Additive Sum Product Assessment (WASPAS) (Residential)	- Energy supply options: wood, pallets, natural gas, PV, solar thermal, grid supply - heating /DHW options: Boiler, air-water heat pump, ground-water heat pump	energy consumption, CO_2 emissions, total cost, thermal comfort, maintenance, and operation	- integrated assessment model of an energy supply system considering different envelope combinations and technological solutions. - Simulation (DesignBuilder, Polysun) + computation	[82]
AHP + TOPSIS (Residential)	- wood pallet boiler - solar thermal heating system - air-to-air HP - air-to-water HP - water-to-water HP,	investment cost, running cost, payback period, equipment performance, GHG emissions, renewable energy share	- Investigation of the drivers for decision makers for selecting different renewable heating technologies. - Computation	[83]
Electre III (Residential)	- evacuated tube solar collector + flat plate solar collector + absorption chiller + PV + wind turbine - GSHP + PV + wind turbine - flat plate collector + ASHP + PV + wind turbine - flat plate collector + GSHP + PV + wind turbine	Life-cycle cost, CO_2 emissions, total energy consumption, grid interaction index	- Optimization of Renewable energy solution sets for net zero energy building in different climates. - Simulation (TRNSYS) + computation	[84]
criteria importance through intercriteria correlation (CRITIC) + TOPSIS (Community)	- PV + wind turbine + diesel generator + battery - PV + diesel generator + battery - Wind turbine + diesel generator + battery - diesel generator + battery - PV + battery	Unmet load, Excess electricity, total electricity production, Renewable fraction, life-cycle costs, cost of energy	- evaluate the techno-economic performance of six PV/wind/battery/diesel generator energy system alternatives. - Simulation (HOMER) + computation	[85]
CRITIC + TOPSIS (Community)	- PV + diesel generator - wind turbine + diesel generator - PV+ diesel generator + battery - wind turbine + diesel generator + battery - PV+ wind turbine + diesel generator - PV+ wind turbine + diesel generator + battery - PV + battery, wind turbine + battery - PV+ wind turbine + battery	initial cost, operating cost, cost of energy, CO_2 emissions, Excess electricity, Unmet electric load, Capacity shortage, Renewable fraction	- Identification of the best hybrid. Renewable energy system for a specific load of electricity and hydrogen. - Simulation (HOMER) + computation	[86]

In previous literature, MCDM methods have been implemented for performance assessment of BES from a single component to large systems and an individual building to the whole district. The researchers have not set certain criteria for applying a specific MCDM technique for building types and energy systems. Choosing an MCDM technique and assessment criterion is problem specific. Nevertheless, energy use, costs, and environmental impacts are three performance indicators generally used for aggregated evaluation of energy systems. For district heating application, H. Wang & Lahdelma [78] investigated a coal-fired combined heat and power (CHP) boiler with various fuels and HVAC technologies. The authors applied the

stochastic multicriteria acceptability analysis (SMAA) technique to identify the appropriate energy supply and HVAC systems, considering uncertainties of energy cost, carbon emissions, and qualitative indicators. Alanne et al. [79] used preference assessment by imprecise ratio statements method (PAIRS) method with life-cycle costs and GHG emissions as performance criteria for comparison of micro-CHP and conventional heating systems. The decision-making results showed that micro-CHP was the preferable system for economic and environmental benefits. Ren et al. [80] studied the combination of photovoltaic, wind power, gas-fired engine, conventional boiler, and grid supply in a residential building for air conditioning service. The analytical hierarchy process (AHP) and preference ranking organization method for enrichment evaluation (PROMETHEE) approaches were applied to capital cost, operating cost, carbon emissions, and primary energy consumption to determine the optimal energy mix. Kontu et al. [81] performed a multi-criteria assessment of various heating systems for a household using the SMAA method. The performance indicators were initial and operating costs and GHG emissions. The optimal choice was district heating with biomass regarding the capital cost and environmental impacts, whereas GSHP was a suitable option to reduce the operating cost. Džiugaitė-Tumėnienė et al. [82] developed a unified model to assess the flexibility of combinations of energy supply technologies for various heating systems. AHP and weighted additive sum product assessment (WASPAS) were applied to calculate the weights of energy consumption, carbon emissions, investment cost, operational cost, and thermal comfort. AHP and the Technique for Order of Preference by Similarity to Ideal Solution (TOPSIS) approaches were used in a study [83] to examine the performance of the traditional boiler, solar heating, air-to-air heat pump (A/AHP), air-to-water heat pump (A/WHP), and water-to-water heat pump (W/WHP). The performance criteria were energy supply from renewable energy sources, costs, payback period, GHG emissions, and equipment efficiency. Harkouss et al. [84] designed various BES combinations of photovoltaic, thermal collectors, wind turbines, absorption chiller, GSHP, and ASHP. Elimination and Choice Translating Reality (Electre) III was employed to rank BESs based on energy use, environmental impacts, costs, and grid utilization. Babatunde & Ighravwe [85] and Salameh et al. [86] used combinations of PV, wind turbine, diesel generator, and battery storage for the energy supply system of a household. They used criteria importance through intercriteria correlation (CRITIC) weighing and TOPSIS ranking to identify the best energy system. Both studies used costs, renewable fraction, excess electricity, and unmet load to assess energy systems.

2.1.3 Building control system

HVAC system has a major share in building energy consumption. The HVAC system also has promising potential for demand flexibility through optimum control. The building control system can be categorized into two types, local controller and supervisory controller. The function of the local controller is to assure the continuous operation of subsystems by passing set points, on/off signals, and a base for determining parameters like flow rates. The Control system is designed to formulate the demand response measures into a control strategy in the supervisory controller. The supervisory controller communicates with local controllers and is responsible for the smooth operation of the whole system. The supervisory control receives information from the building and gets the time-varying parameters like weather conditions, price of energy, and occupancy rate [87]. In a supervisory controller, an explicit method is used to decide control signals and passes them to the local controllers to operate building components to achieve the control objective. The control objective depends on the problem delimitation. The typical control objectives are minimizing energy use, reducing energy cost, maximizing thermal comfort, peak shaving, peak shifting, and minimizing emissions. Two control strategies are generally employed in buildings (c.f. Table 2-3): rule-based control (RBC) and model predictive control (MPC).

Rule-based control: RBC is a simplified strategy for controlling the subsystem of an energy system. Rule-based controllers are easy to integrate into dynamic simulation tools and determine the state of a system component based on the user-specified decision rules (using "if-then" statements). The rule-based controller can improve energy flexibility with one of the control objectives mentioned earlier by adjusting the set points of the indoor environment or thermal energy storage (TES). However, since RBCs are designed to control a specific component of BES, they cannot optimize the operation of the whole energy system[88].

Model predictive control: In MPC, the optimal control signals are determined iteratively over a specified time horizon by using the information from the system model being controlled and uncertainties. This task is accomplished by performing optimization processes at each time step based on the current state of the energy system. The optimization problem tends to maximize or minimize a control objective subject to the given constraints. As a result, MPC can predict the building response to variations of parameters like weather conditions, energy use, energy prices, and occupancy rates and make decisions about system operation to achieve the control objective [89].

Figure 2-1 shows the basic principle of MPC. Numerous studies have shown that MPC can deliver better energy efficiency and cost savings and gained growing interest in recent years. A review of the literature on MPC in buildings reveals that MPC can be applied to a wide range of building systems and is recognized as a suitable choice for energy flexibility [90]. An effective HVAC controller should consider time-varying uncertainties like climate, internal gains, and comfort constraints. MPC can address these uncertainties of building and HVAC

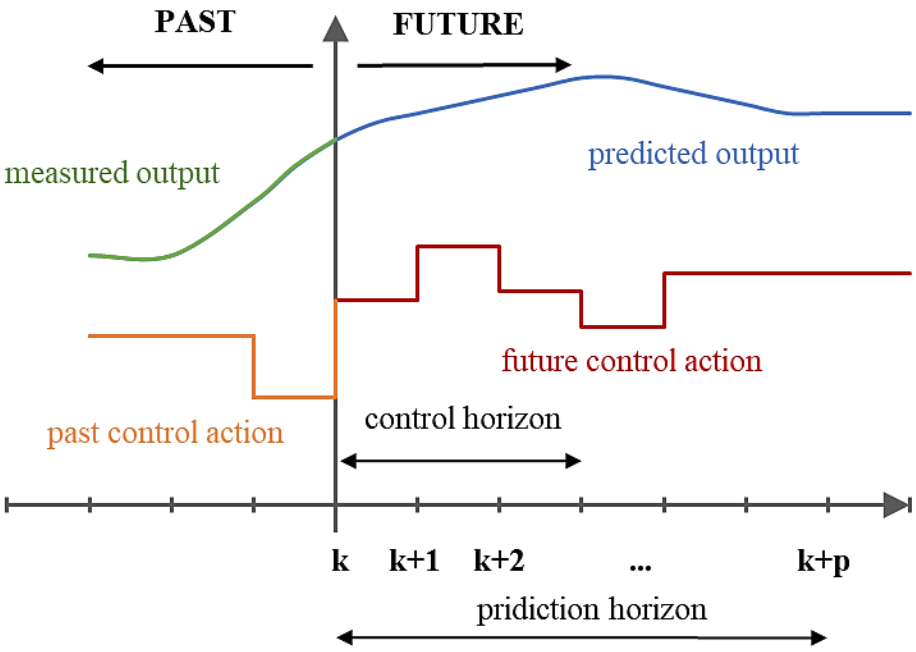

Figure 2-1: Basic principle of model predictive control

systems.

In some cases, control strategies have been applied for generation flexibility (PV supply) [34] and system flexibility (battery power, volume of storage tank) [51]. However, the literature review reveals that researchers mainly focused on activating demand flexibility through modulation of temperature set point or heat pump's power [32,45,52,55]. For example, by applying the MPC technique, Péan et al. [32] reduced the energy use, costs, and emissions of a residential building in a Mediterranean climate. The system states were zone temperature, the internal surface temperature of the wall, and TES temperature. Weather data, internal gains, and occupancy rates were uncertainties of the control problem. To minimize the cost functions, the supervisory controller manipulated the heat pump load and TES load for a prediction horizon of 24 hours. The MPC strategy reduced costs (13 – 29%) and emissions (19 – 29%) during heating and cooling services. A study used MPCs as part of a home energy management system [34]. MPC contributed to the energy flexibility for generation, system, and demand.

The control objectives were minimizing electricity cost, discomfort, and battery degradation. The controller obtained system states of indoor temperature, the temperature in a water heater, and battery state of charge and external data of weather conditions, price of electricity, PV generation profile, and user preferences. The system calculated the net house load, indoor temperature, and battery cycles at each time step of the simulation based on the control inputs of temperature set points, PV power, battery power, and water heat duty cycle. Similarly, the MPC-based optimal control of underfloor heating resulted in 300 kWh saving in electricity consumption in a year [91]. The control input, temperature set point, was manipulated to minimize the energy use with outdoor temperature as a disturbance. The system outputs were indoor temperature and heat flux density. The minimum and maximum heat flux were fixed as constraints of the optimization problem. In another study[49], a comparison of RBC and MPC was performed for thermostatic control of the HVAC system. The controllers modulated the heating set temperature for four hours of heating service in the morning and evening, intending to minimize energy costs. The limits of indoor temperature were set as constraints, and power demand, energy price, and indoor temperature were forwarded to a supervisory controller at each time step. The findings of the comparative analysis showed that MPC provided twice higher energy flexibility as the RBC. However, the flexibility efficiency was higher in the RBC strategy.

2.2 Quantification of energy flexibility

The fundamental goal of energy flexibility is to reduce the net energy use of BES. The energy flexibility is achieved by adjusting the building load profile, as shown in Figure 2-2.

The following strategies can manipulate the energy demand from local energy networks:

- improving envelope parameters (load conservation) [45,46]
- integration of renewable energy supply (generation) [43]
- using efficient building service system (load conservation) [53]
- moving the demand in time (load shifting) [92]
- reducing the peak demand (load shaving) [92]
- increasing the load for financial incentives for a limited time (valley filling) [92]

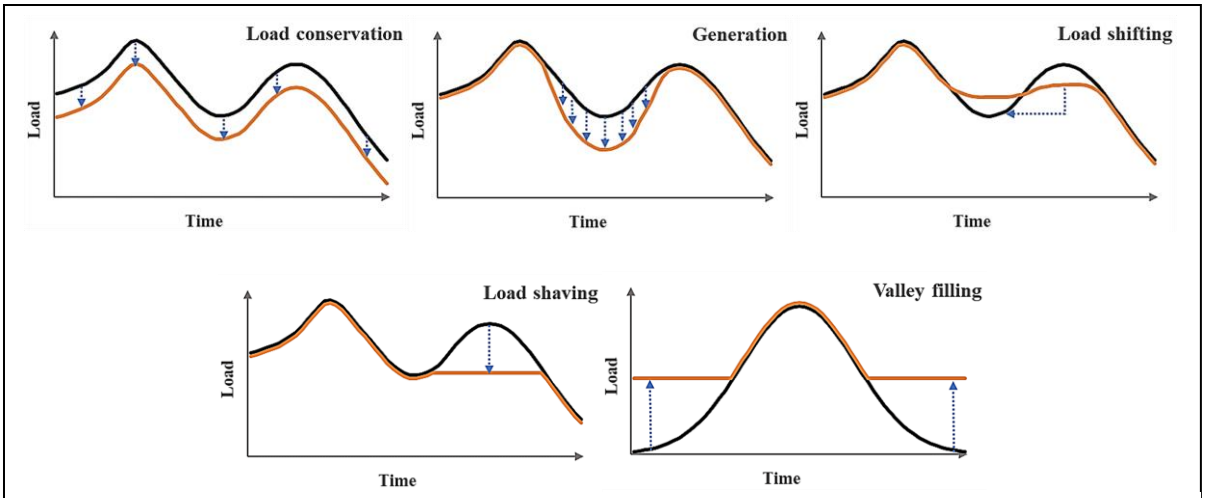

Figure 2-2: Load management techniques

The quantification of energy flexibility from the load shaping techniques can be expressed as the energy conserved (kWh), load covered by renewable energy sources, and power (kW) or energy (kWh) shifted or shed. The energy flexibility indicators (EFI) can be further classified into potential and performance indicators[12].

Potential indicators: The potential indicators quantify the amount or the expected amount of energy conserved or shifted by implementing a flexibility strategy. It should be noted that potential indicators typically quantify the energy flexibility of a building subsystem during the DRE.

Performance indicators: The performance indicators quantify the targeted benefit of applying energy flexibility to an energy system. The potential target of energy flexibility could be thermal comfort, emission reduction, grid independence, or cost reduction. Furthermore, the scope of performance indicators is not limited to building subsystems or DREs. It can quantify the energy flexibility of a building service component to the whole building.

The potential indicators are only a function of the flexibility strategy, but performance indicators depend on the price of energy networks, the type of fuel used, and renewable energy potential. Table 2-3 shows different potential and performance indicators used to quantify energy flexibility. The generation energy flexibility can be characterized by self-consumption (potential indicator) and load cover factor (performance indicator). The energy flexibility from envelope improvements can be quantified by peak shaving and flexible load as potential indicators and primary energy consumption and CO_2 emissions as performance indicators. Similarly, the energy flexibility from system upgradation is expressed as flexible energy (a potential indicator) and primary energy consumption, cost of heating/cooling, and CO_2

emissions (performance indicators). Storage capacity and efficiency are potential indicators, while energy cost and CO_2 emissions are performance indicators for thermal energy storage. The typical potential indicators of demand response strategies are flexible energy, flexible power, flexibility factor, and flexibility index. The performance indicators of demand flexibility include the cost of energy and CO_2 emissions. Table 2-5 provides an overview of different flexibility indicators used in the literature in different domains of energy flexibility.

Table 2-5: Overview of flexibility indicators for various flexibility sources

Indicators	Unit	Description	Sources	Reference
		Potential Indicators		
Self-consumption	[-]	The degree to which the building directly consumes the on-site generation.	Onsite generation	[54,93]
On-site Energy Ratio	[-]	The ratio between annual energy supply from local renewable sources and annual energy demand.		[92]
Flexible thermal load	kWh	The decrease in the thermal load by improving envelope parameters.	Envelope parameters	[32]
Flexible peak power	kW	The peak power reduced by improving envelope parameters.		
Flexible energy	kWh	The reduction in energy consumption by upgrading the service system	Service system	[50,52]
Storage capacity	kWh	The reduction in energy consumption due to energy storage during an active DRE.	energy storage	[33,50,52,54,92]
Storage efficiency[1]	%	The efficiency of energy storage for active DRE.		[33,54,55,92]
Flexible energy	kWh	The reduced energy consumption during DREs.	Demand response	[13,14,92]
Residual load	kWh	The load covered by grid supply after DREs.		[12]
Flexibility factor	[-]	It indicates the capability of exploiting energy, cost, or emissions during DREs.		[40,51,92]
Flexibility index	[-]	The ratio between the energy cost of flexible operation and reference operation.		[45,94]
		Performance Indicators		
PER	kWh	The reduction in primary energy consumption.	Generation/ System/ Demand	[32,34,43,47,52,53]
Flexibility cost	€	Flexibility in terms of decrease in the cost of electricity by modulation load profile.		
Flexibility emissions	$kgCO_2eq.$	The reduction in CO_2 emissions by a flexibility strategy.		

[1] the storage efficiency is calculated for independent DREs only, not for continuous modulation.

3 Methodology of optimization framework

This research has developed a system optimization framework for improving energy flexibility in buildings. The framework can be applied at the design stage of building envelope and/or building service system for improving energy flexibility. Further, it provides an optimal control strategy for the service system for demand flexibility. A household building was selected to assess energy flexibility potential by employing the proposed framework. The optimization framework comprised four flexibility strategies, as shown in Figure 3-1. The first step towards energy flexibility was the upgradation of the building's passive design to minimize the heating/cooling demand. In the next phase, a BES was identified, which could maintain thermal comfort in the building while also improving renewable energy production, reducing CO_2 emissions, and operating an energy system at a lower cost. Next, a steady-state multi-objective optimization was performed to optimize different parameters of the building service system for energy flexibility. Finally, the dynamic control was applied using MPC to minimize the energy consumption of BES while maintaining the required thermal comfort. Sections 3.1-3.6 describe the optimization process in detail.

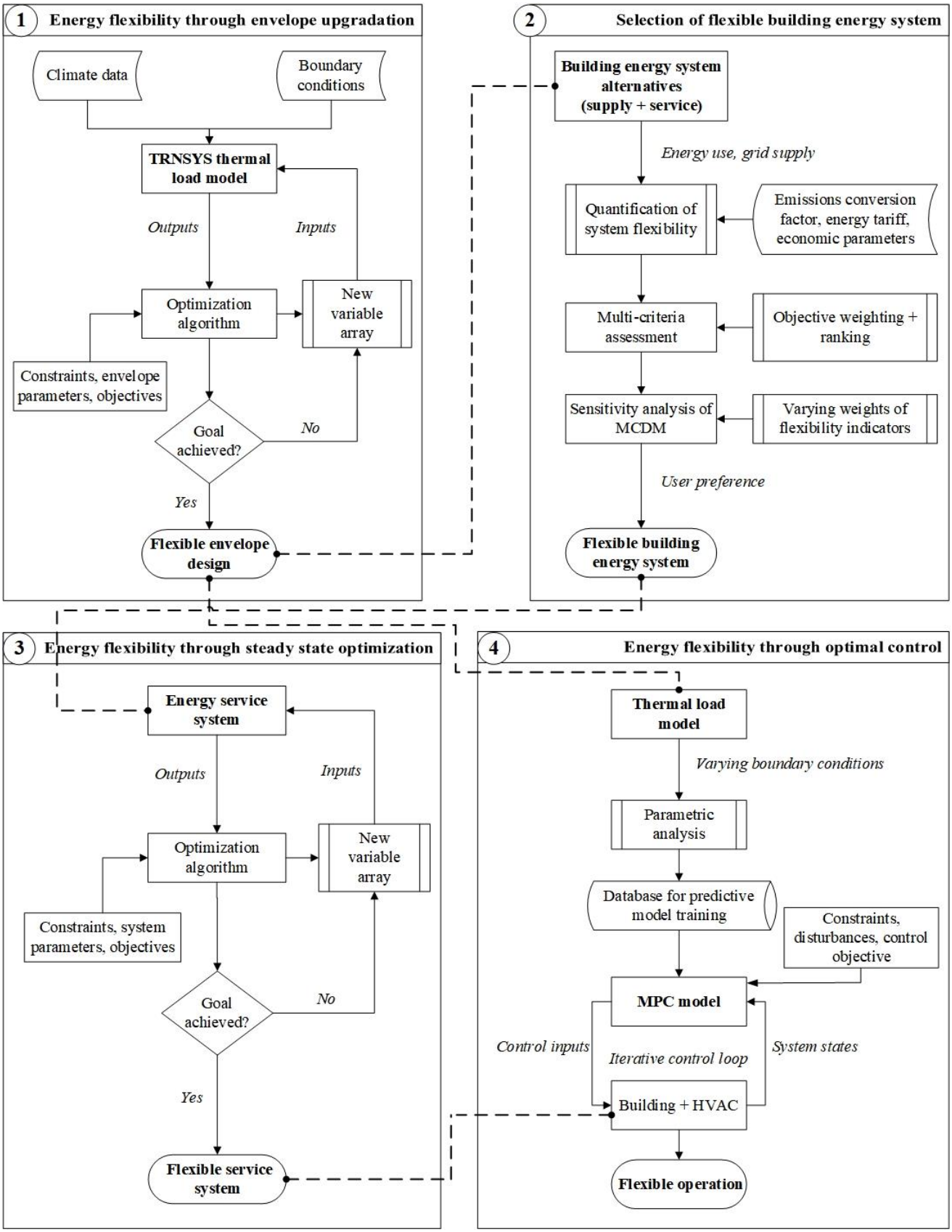

Figure 3-1: Optimization framework for improving energy flexibility

3.1 Reference building

The reference building was a double-story household with boundary conditions and architecture from International Energy Agency (IEA), Solar Heating and Cooling (SHC) Task 44/Annex 38 [95]. The building had a 70m^2 floor area for each story, a total surface area of 216 m^2 for external walls, and an external surface area of 81 m^2 for the roof. Figure 3-2 shows the geometry and orientation of the building. The representative building was modeled and simulated as a single thermal zone in TRNSYS. To incorporate the capacity of the internal building structure, the internal walls (200 m^2) and the floor area of the second story (70 m^2) were also added in TRNBuild.

The thermal properties of the building were given according to the energy codes in the investigated location [96–112]. These standards provided the references for the thermal transmittance (U-value) of walls and windows. Table 3-1 and Table 3-2 describe the construction and thermal properties of the building envelope. Expanded polystyrene (EPS) and rockwool insulation were used as an insulation layer for external walls and roofs, respectively. In each location, the insulation level was specified such that the thermal transmittance of the walls and roof met the criteria of regional building standards. Double-glazed windows, having 4/16/4 geometry (4 mm inner pane, 16mm space bar, and 4mm outer pane), U-value of 1.4 W/m^{2}K, and g-value of 0.622, were used for all facades.

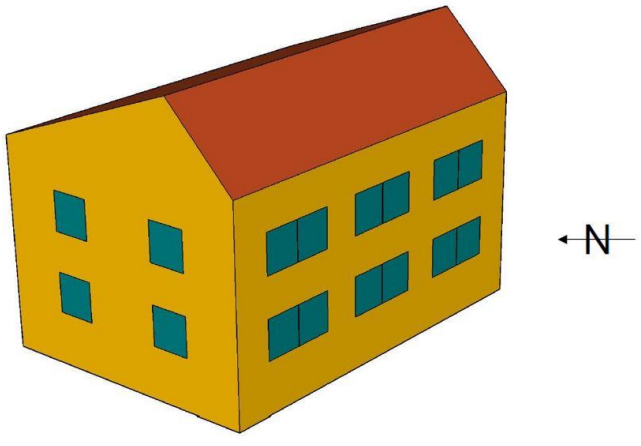

Figure 3-2. Geometry of base case building

Table 3-1: Construction and thermal properties of opaque elements

Element	Layer	Thickness (m)	Density (kg/m^3)	Conductivity (W/mK)	U-value (W/m^{2}K)
External wall	plaster inside	0.015	1200	0.60	0.18[1]
	brick	0.210	1380	0.70	0.16[2]
	plaster outside	0.003	1800	0.70	0.20[3]
	EPS (expanded polystyrene)	0.200[1] 0.230[2] 0.180[3] 0.135[4] 0.120[5]	17	0.04	0.26[4] 0.30[5]
Floor	wood	0.015	600	0.15	0.649
	plaster floor	0.080	2000	1.40	
	sound insulation	0.040	80	0.04	
	concrete	0.150	2000	1.33	
Roof ceiling	gypsum board	0.025	900	0.21	0.13[1]
	plywood	0.015	300	0.08	0.17[2]
	plywood	0.015	300	0.08	0.15[3]
	rockwool	0.250[1] 0.190[2] 0.215[3] 0.140[4] 0.160[5]	60	0.03	0.22[4] 0.20[5]
Internal wall	clinker	0.200	650	0.230	0.885

[1] Ostersund and Stockholm, [2] Saarbrücken, [3] Strasbourg, [4] Milan, [5] All investigated locations other than those mentioned earlier.

Table 3-2: Construction and thermal properties of windows

Windows	Construction (mm)	Height (m)	Width (m)	Windows area (m^2)	U-value (W/m^{2}K)	g-value
North	(4,16,4)	1.0	1.0	3.0	1.4	0.622
South				12.0		
East				4.0		
West				4.0		

3.1.1 Energy consumption by end-use

Building energy consumption by end use may be divided into four categories: space heating load, space cooling load, domestic hot water (DHW) load, and electricity load of appliances and lighting. The heating and cooling loads depend on the location's boundary and climate conditions. The annual simulations of the BES were carried out to determine the power demand of the HVAC system.

Since household electricity consumption also changes depending on the climate, hourly load profiles of twelve months were formulated from previous literature and surveys [113–127] for

investigated locations. The load profiles did not include the electricity consumption for heating, cooling, and DHW. Further, the reference building model had the same area and geometry for performance evaluation and thermal load in all climates. Therefore, load curves were modified, if required, for a household of 140 m^2 floor area to realize the actual heat gain of household appliances. Kuusela et al. modeled common home appliances' electricity use as a floor area function. The relation between the electricity consumption (relative to 140 m^2 floor area) and floor area is shown in Figure 3-3 and mathematically represented in Eq. 3.1 [128].

$$\boldsymbol{y = -0.44\ ln(x) + 3.19} \qquad \textbf{3.1}$$

The hot water was supplied at 45 °C with an average daily demand of 140 liters per day [129], consuming 5.845 kWh/d for cold-water inlet temperature at 10 °C. Using Eq. 3.2, the local energy demand of DHW ($Q_{dhw,loc}$) was modeled as a function of outdoor temperature while keeping the hot water supply at 45 °C.

$$Q_{dhw,loc} = Q_{dhw,std} \cdot \left(\frac{T_{dhw,set} - T_{amb,avg}}{T_{dhw,set} - 10} \right) \qquad 3.2$$

Where $Q_{dhw,std}$ represents the energy required for warm water supply at 45 °C. $T_{dhw,set}$ and $T_{amb,avg}$ represent DHW water and annual average outdoor temperatures, respectively.

3.1.2 Internal gains

The reference building was a household for four people. The occupancy rate was defined from ASHRAE [130] as shown in Figure 3-4, and the same profile was used throughout the week. According to ASHRAE standards, each occupant produces 115 W of heat such that 70W is generated as the sensible gain, and 45 W is the latent gain [131]. The sensible heat was released by radiation (42 W) and convection (28 W). The latent heat gain was defined in TRNBuild by including a humidity rate of 0.059 kg/h. Electrical equipment also generates waste heat causing thermal gains in the building. It was assumed that 58% of the building's electric energy was retained as thermal gain. The hourly profiles for occupancy and electric heat gains were given as text files to the building model in TRNSYS.

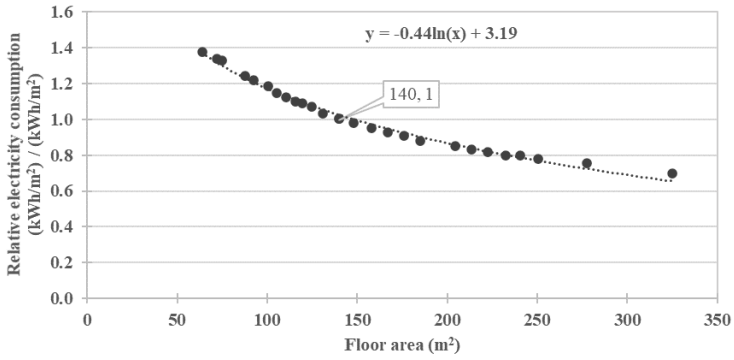

Figure 3-3. Relative electricity consumption as a function of area

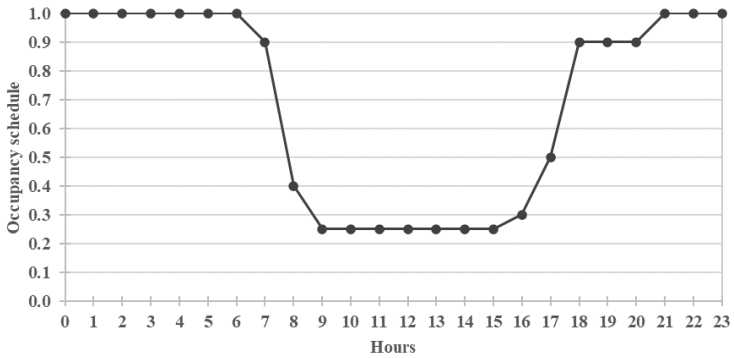

Figure 3-4. Occupancy schedule of a day from ASHRAE

3.2 Energy system alternatives

This work considered fourteen alternative energy systems for the reference building with different energy supply and HVAC systems. It should be noted here that the building envelope was upgraded for energy system simulations according to the results of MOO in Phase 1 of the optimization framework. The energy flow of BESs under evaluation is shown in Figure 3-5. This investigation regarded the grid power supply as a conventional energy source. The building was equipped with solar PV, FPCs, and a vertical borehole heat exchanger (BHX) to utilize the available solar and geothermal energy. A storage tank was used for thermal energy storage having capacities of 250 L, 500 L, or 1800 L according to the requirement of the BES alternative. Thermal energy storage (TES) could receive thermal energy from three sources: an auxiliary electric heater, hot fluid from FPCs, and hot water from the heat pump (HP).

Table 3-3 provides the combinations of energy systems for the base case and alternative. The auxiliary heater of TES supplied the energy for DHW in the base case and A6. Furthermore, as HPs provided chilled water to cooling coils for space cooling in summer, the electric heater in TES was turned on for water heating in the alternatives A1, A2, A10, and A11 during cooling hours. Alternatives A3, A4, A5, A12, and A13, on the other hand, did not require auxiliary

heater DHW since FPCs provided the necessary energy to TES during summer. The hot water in TES circulated in a heat exchanger for DHW supply and a radiator or hot water coils for room heating. Five HVAC technologies were assessed for providing thermal comfort in the reference building: brine-to-air heat pump (B/AHP), A/AHP, A/WHP, B/WHP, and single-stage hot water-fired absorption chiller. The base case energy system comprised an A/AHP for space heating/cooling and an electric heater for DHW. The energy demand in the base case was met by grid networks only. A vertical BHX, B/WHP, TES, and PV supply were integral components in alternatives A1, A2, A3, and A4. Water coils provided the cooling service using the chiller water from HPs. At the same time, heating was accomplished by emissions heating through the radiator (A1 and A3) or ventilation heating through water coils (A2 and A4). Alternatives A3 and A4 were also equipped with FPCs to provide heat to TES. B/WHP was a primary component in alternatives A5 and A6, and other components were the PV system, TES, and BHX. FPCs in A6 supplied heat to TES through the heat exchanger.

In alternatives A7 and A8, the absorption chiller produced the chilled water, and flat plate collectors supplied the energy to the TES. Alternatives A7 and A8 were also equipped with PV panels and a battery bank. The alternative A9 has the same energy system configuration as the base case, with the PV and FPCs as additional components. The alternatives A10, A11, A12, and A13 were equipped with A/AHP, TES, and PV as integral components. FPCs were also part of BESs in alternatives A12 and A13. Moreover, alternatives A10 and A11 used a radiator for heating, whereas alternatives A11 and A13 used water coils for this service.

PV capacity: The performance characteristics of the PV array and FPCs were specified according to findings of a validated photovoltaic- TRNSYS model [132,133] and thermal collector model in IEA Task 32[134], respectively. The electricity load of the building was used to calculate the required PV capacity using the relation in Eq. 3.3 [17].

$$P_{PV} = P_{el,avg}/(\eta_{overall} \times ESH) \quad 3.3$$

Where $P_{el,avg}$ represents the electricity load per day. ESH is the estimated solar hours, equivalent to global horizontal solar radiation per day. P_{PV} represents the power required by the PV array, and $\eta_{overall}$ is the overall efficiency of the inverter, battery, and cables.

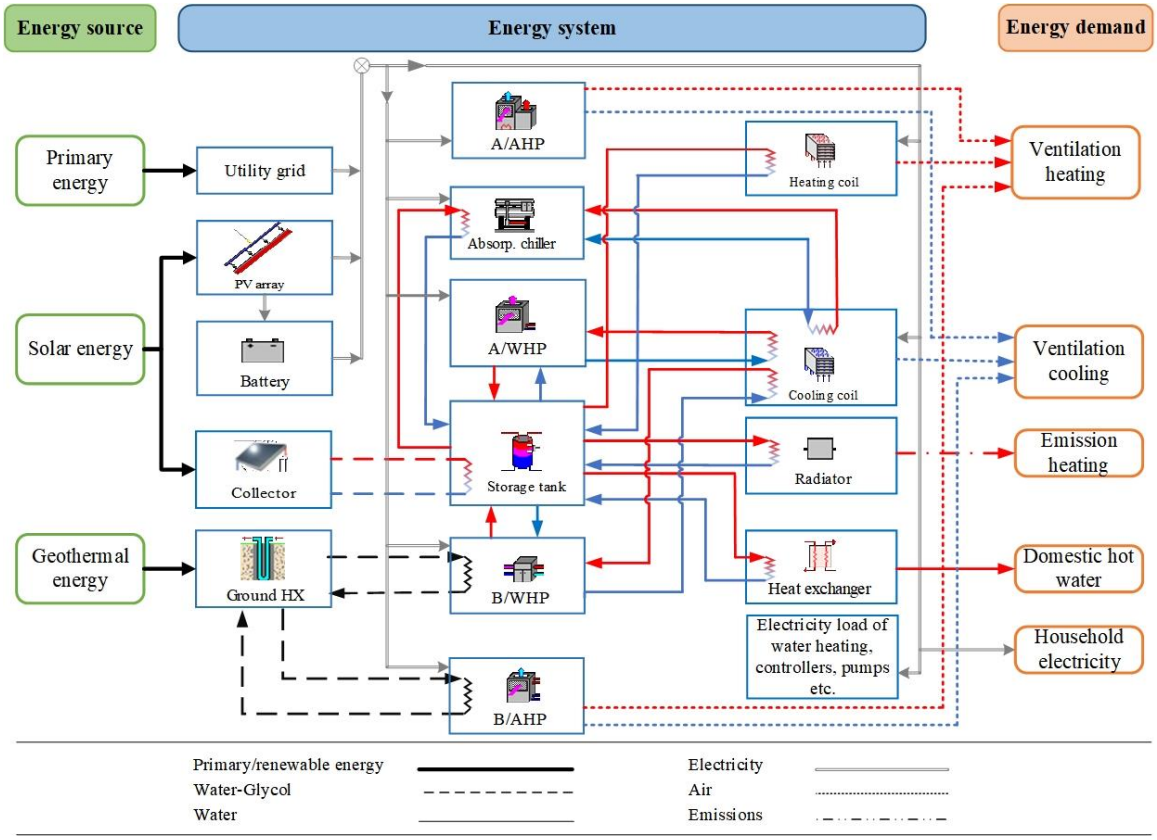

Figure 3-5: Building energy supply and HVAC options

Table 3-3: Energy system configurations for the base case and alternatives

Energy system	GHX	FPC	PV	TES	B/WHP	B/AHP	A/AHP	A/WHP	Absorp. chiller	Radiator	Heating coil	Cooling coil	Electric water heating
Base case				×			×						×
A1	×		×	×	×					×		×	×
A 2	×		×	×	×						×	×	×
A 3	×	×	×	×	×					×		×	
A 4	×	×	×	×	×						×	×	
A 5	×	×	×	×		×							
A 6	×		×	×		×							×
A 7*		×	×	×					×	×		×	
A 8*		×	×	×					×		×	×	
A 9		×	×	×			×						
A 10			×	×				×		×		×	×
A 11			×	×				×			×	×	×
A 12		×	×	×				×		×		×	
A 13		×	×	×				×			×	×	

* Alternatives (A7 and A8) with hot water-fired absorption chiller are evaluated only in cooling dominant locations, i.e., QTA and JKT.

Borehole heat exchanger sizing: The fluid in a vertical U-tube BHX extracted heat from or released heat to the ground during heating or cooling modes. The heat transfer fluid (HTF) in the U-tube heat exchanger was a mixture of water and ethylene glycol, an antifreeze agent with a concentration of 20%. The HTF was pumped to the evaporator (heating mode) or condenser (cooling mode) of the heat pump, where the heat transfer occurred between the refrigerant and HTF. The borehole lengths for cooling mode L_c and heating mode L_h were calculated using the ASHRAE method [135] described in Eqs. 3.4 & 3.5.

$$L_c = \frac{q_a\, R_{ga} + q_{cond}(R_b + PLF_m R_{gm} + R_{gd} F_{SC})}{t_g - \frac{t_{wt} + t_{wo}}{2} - t_p} \quad 3.4$$

$$L_h = \frac{q_a\, R_{ga} + q_{evap}(R_b + PLF_m R_{gm} + R_{gd} F_{SC})}{t_g - \frac{t_{wt} + t_{wo}}{2} - t_p} \quad 3.5$$

Where, *Fsc* is short-circuit heat loss factor, L_c is the required bore length for cooling (m), L_h is the required bore length for heating (m), PLF_m is a part-load factor during design month, q_a is the net annual average heat transfer to the ground (W), q_{cond} is the heat rejection rate of heat pump condenser to the ground (W), q_{evap} is the heat extraction rate of heat pump evaporator from the ground (W), R_{ga} is the effective thermal resistance of ground (annual pulse) ((m·K)/W), R_{gd} is the effective thermal resistance of ground (peak daily pulse:1 h ((m·K)/W), R_{gm} is the effective thermal resistance of ground (monthly pulse) (m·K)/W), R_b is the thermal resistance of bore ((m·K)/W), t_g is undisturbed ground temperature (°C), t_p is temperature penalty for the interference of adjacent bores (°C), t_{wi} is the liquid temperature at heat pump inlet (°C), t_{wo} is the liquid temperature at heat pump outlet or the BHX inlet temperature (°C). These parameters were calculated according to the guidelines of the ASHRAE method for each location. The undistributed ground temperature is a function of the time of the year, ambient temperature, and depth. That is calculated using the ground-coupling heat losses model from IEA SHC Task 44/Annex 38 [136].

HVAC options: In this study, ventilation heating or emission heating was used to meet the demand for space heating, while ventilation cooling was used for space cooling service. PID controllers generated control signals (0 to 1) based on the difference between room temperature and the reference set temperature. The instantaneous flow rates of water and ventilation air were set by multiplying the design flow rates with control signals from PID controllers.

Although there are various HVAC technologies, the commercially available and domestic-applicable options: GSHPs (B/WHP and B/AHP), ASHPs (A/AHP and A/WHP), and absorption chiller, were evaluated in this study. In addition, the heating and cooling capacities of the HVAC system were given according to the location's peak heating/cooling demand.

3.3 Energy flexibility assessment

A novel set of flexibility indicators were employed from the findings of the extensive literature review for energy flexibility assessment of envelope upgradation, multiple energy systems, SSO of service system, and optimal control of service system. The selected flexibility indicators

were categorized as potential indicators and performance indicators. Further, the flexibility assessment was not limited to the single unit of BES, but this work quantified the energy flexibility of the energy system from an integrative perspective. Also, the performance indicators' assessment was extended to the life cycle of BESs. Table 3-4 shows the EFIs used to assess flexibility potential for the employed strategies. The following sections describe the potential and performance indicators used in this study.

Table 3-4: The indicators for quantifying the energy flexibility from four different strategies

Flexibility strategies	Energy flexibility indicators
Optimization of envelope parameters	- Flexible thermal load (ΔQf_{lex})
Selection of flexible BES	- Load cover factor (γ_{load}) - Non-renewable energy savings ($f_{sav,NRE}$) - Life-cycle CO2 emissions ($LCEs$) - Thermal comfort - Net present value (NPV_{25}) - Levelized costs of energy ($LCOEs$)
Steady-state optimization of the service system	- Storage capacity (C_{DR}) - Flexible energy (ΔE_{flex}) - Residual Load (l_{res}) - Flexibility emissions (ΔEmi_{flex}) - Flexibility cost ($Cost_{flex}$)
MPC-based dynamic optimization	- Storage capacity (C_{DR}) - Flexible energy (ΔE_{flex}) - Residual Load (l_{res}) - Flexibility emissions (ΔEmi_{flex}) - Flexibility cost ($Cost_{flex}$)

3.3.1 Potential indicators

Flexible thermal load: The energy flexibility from upgrading envelope parameters was quantified by the flexible thermal load. Flexible thermal load is the difference between the building thermal load before and after the upgradation of the building envelope and is mathematically described as follows:

$$\Delta Q_{flex} = Q_{flex} - Q_{ref} \quad 3.6$$

Q_{flex} is the thermal of the building with an improved envelope, and Q_{ref} is the thermal load of the reference building.

On-site Energy Ratio/Load cover factor: On-site energy ratio, also referred to as load cover ratio, was used to quantify generation flexibility from PV power. This EFI computes the fraction of the electricity load covered by the on-site electricity generation by renewable energy sources. It can be calculated using Eq. 3.7 as follows [137]:

$$\gamma_{load} = \frac{\int_{T1}^{T2} min[g(t) - S(t) - \zeta(t), l(t)].\, dt}{\int_{T1}^{T2} l(t)\,.\, dt} \quad 3.7$$

Where *g(t)*, *S(t)*, *ζ(t)*, and *l(t)* represent the electricity from renewable energy sources, energy storage balance of battery bank, energy losses, and electricity load during the period of *dt*, respectively. T_1 is the start of the evaluation period, and T_2 is the end of the evaluation period. The excessive electricity is either exported to the grid or considered a loss. So, the maximum value of γ_{load} is always 1.

Storage capacity: The storage capacity is defined as the amount of energy added to (up-flex) or curtailed from (down-flex) from the energy storage component. In the case of up-flex, the upward temperature modulation is activated, or storage capacity is increased to store the energy, which could be later discharged in post-DRE hours. In down-flex, the downward temperature modulation is activated, or storage capacity is decreased to save the energy supply from a service system. The storage capacity for both cases can be calculated using Eqs. 3.8 & 3.9. This EFI was used to evaluate the energy flexibility by optimal sizing of thermal energy storage in SSO and temperature modulation in MPC-based dynamic optimization of building service systems.

$$C_{DF} = \int_0^{t_{DR}} \left|(P_{h,flex} - P_{h,ref})\right|\, dt \quad 3.8$$

$$C_{UF} = \int_0^{t_{DR}} (P_{h,flex} - P_{h,ref})\, dt \quad 3.9$$

Where C_{DF} and C_{UF} are down-flex and up-flex storage capacities, respectively. $P_{h,flex}$ and $P_{h,ref}$ represent the heating power demands during the DRE and reference scenarios, respectively. t_{DR} is the duration of DRE.

Flexible energy: The energy consumption reduction during the DREs is characterized as flexible energy and can be determined using Eq. 3.10.

$$\Delta E_{flex} = \int_0^{t_N} (P_{flex}(t) - P_{ref}(t))\ dt \quad 3.10$$

Where P_{flex} is the power consumed during DRE and P_{ref} is the power consumed in reference operation. t_N represents the total number of demand response events.

Residual Load: This EFI measures grid energy networks' utility after implementing the energy flexibility strategies. It is donated by the difference between the building load (P_{bui}) and the energy supply from renewable sources (P_{RE}), as given in Eq. 3.11.

$$l_{res} = \int_0^{t_N} (P_{bui}(t) - P_{RE}(t))\ dt \quad 3.11$$

3.3.2 Performance indicators

Non-renewable energy savings: This EFI is calculated based on the primary energy ratio of non-renewable sources (PER_{NRE}). The primary energy ratio of the reference system (base case) ($PER_{NRE,ref}$) is compared with BES alternatives ($PER_{NRE,i}$) to calculate $f_{sav,NRE}$. As the share of non-renewable energy in the energy supply decreases, the value of PER_{NRE} increases, and ultimately $f_{sav,NRE}$ becomes closer to 1. If $f_{sav,NRE}$ has a value of 1, renewable energy sources completely meet the building energy demand. PER_{NRE} and $f_{sav,NRE}$ are calculated using Eqs. 3.12 & 3.13 [73].

$$PER_{NRE} = \frac{\sum Q_{out}}{\sum \left({Qel_{in}}/{\in_{el}} + {Q_{in}}/{\in_{in}} \right)} \quad 3.12$$

$$f_{sav,NRE} = 1 - \frac{PER_{NRE\_ref}}{PER_{NRE\_i}} \quad 3.13$$

Where Q_{out} is the energy acquired for heating, cooling, and DHW. Qel_{in} and Q_{in} represent the grid electricity and other non-renewable energy networks like boilers. These energy inputs are converted to primary energy using the conversion factors $\in_{el}$ = 0.4 and $\in_{in}$ = 0.85 (boiler) [73].

Life-cycle CO_2 emissions: Life cycle assessment (LCA) can be used to evaluate the environmental impacts of various BESs over the life cycle. LCA considers CO_2eq emissions from raw materials to manufacturing, transportation, installation, operation, and disposal of each element of the energy system. The CO_2eq emissions for electricity generation depend on the local power plant technologies in a country. For case studies in this research, the grid utility

emissions are taken as 0.012 kgCO_2eq/kWh, 0.350 kgCO_2eq/kWh [138], 0.707 kgCO_2eq/kWh [139], and 0.734 kgCO_2eq/kWh [140] in Stockholm (STK), Saarbrücken (SBK), Quetta (QTA), and Jakarta (JKT), respectively. The LCEs of energy system components, excluding the emissions during operation, are summarized in Table 3-5. The emissions during the operation were computed by multiplying the emissions factor and total electricity from the grid for one year and extrapolated for 25 years of operation.

Table 3-5: Life-cycle emissions (excluding operation) of components of building energy system

Equipment	Unit	GHG emissions	Reference
GHX	(kg CO_2eq/m)	4.59	[141]
ASHP	(kg CO_2eq/kW)	193	[142]
WSHP	(kg CO_2eq/kW)	171	[142]
Absorp. Chiller	(kg CO_2eq/kW)	127.08	[143]
Cooling Tower	(kg CO_2eq/kW)	4.41	[143]
Collector	(kg CO_2eq/m^2)	110	[143]
PV + BOS	(kg CO_2eq/kWh)	0.04	[144]
Batteries	(kg CO_2eq/Wh)	0.0729	[145]
Storage Tank	(kg CO_2eq/2000 liter)	780.9	[143]
Radiator	(kg CO_2eq)	12.62	[146]
Heating Coil	(kg CO_2eq)	97	[147]
Cooling Coil	(kg CO_2eq)	97	[147]
Pumps	(kg CO_2eq)	66	[143]
Heat Exchanger	(kg CO_2eq)	32.4	[148]

Flexibility emissions: The flexibility in emissions is defined as the difference in CO_2 emissions between the flexible operation ($Emis_{flex}$) and regular operation ($Emis_{ref}$) of BES. It can be mathematically described as in Eq. 3.14.

$$\Delta Emis_{flex} = Emis_{flex} - Emis_{ref} \quad 3.14$$

Thermal comfort: Thermal comfort is evaluated in terms of Predicted mean vote (*PMV*) and Predicted percentage dissatisfied (*PPD*). *PMV* is a function of occupant activity, clothing, air temperature, mean radiant temperature, air speed, and relative air humidity. The relation between thermal sensation and *PMV* is described in Table 3-6. *PPD* is the level of satisfaction of the occupants and is defined according to the PMV values. The count of hours when *PMV* fall between -0.5 and +0.5 or *PPD* is less than 10% is also calculated to measure thermal comfort hours (TCH) in a year. The average value of *PPD* was taken as the flexibility indicator for thermal comfort for a metabolic rate of 1.2, clothing factor of 1 in winter and 0.5 in summer, and average air speed of 0.12 m/s.

Table 3-6: Thermal sensation scale

Assessment Criteria		
$-0.5 \leq PMV \geq +0.5$	$PPD \leq 10\%$	Slightly cool to slightly warm
$-1 \leq PMV < -0.5 / +0.5 < PMV \geq +1$	$10\% < PPD \leq 25\%$	Cool to warm
$PMV < -1 / PMV > +1$	$PPD > 25\%$	Cold to hot

Life-cycle costs (LCCs): The life cycle cost analysis (LCCA) is an effective technique for the economic evaluation of building energy systems. The net present cost (NPC), computed from Eq. 3.15 [17], is used to conduct the LCCA. The real discount rate (r_d) and net annual cash flows (CF_n) are the inputs of NPC. The net cash flow is the sum of investment, operation and maintenance, and local electricity tariff-based annual electricity costs. The electricity tariffs of 0.183 €/kWh in STK [149], 0.303 €/kWh in SBK [149], 0.10 €/kWh in QTA [150], and 0.085 €/kWh in JKT [151] were used in LCCA. The costs of BES's components for LCCA were acquired from the market survey and the articles of economic investigation of energy system components [152–159]. Table 3-7 presents the assumptions of economic analysis used in this study.

$$NPC_n = capital\ cost + \sum_{1}^{n} CF_n \left[\left(\frac{1}{1+r_d}\right)^n\right] \quad 3.15$$

Table 3-7: Assumption in life cycle cost analysis

LCCA assumptions
Twenty-five years life cycle is considered in LCCA.
Real discount rate (r_d) is 3.5 % [160,161].
PV cells' degradation rate is 0.5% per year.
A feed-in strategy is not implemented.
Installation costs of the energy system are not considered in the investment cost.
The costs of the main components of HES like HPs, absorption chiller, GHX, heat exchanger, radiator, water coils, storage tank, pumps, and solar systems are considered for investment cost.
Maintenance cost is 2.5% of the investment cost per year.
The battery bank is replaced every 6.5 years during the life cycle.
The LCCs do not include the costs of household construction, household appliances, and household maintenance.

PV system degradation was considered in the LCCA assessment such that the power supply from the PV system was 0.5% less than the previous year. The grid utilities filled this gap in the power supply.

Levelized costs of energy: The LCCs are inadequate for providing a complete picture of the building's energy costs. The levelized cost of energy is another indicator for comparing the flexibility of BESs. For this purpose, Eqs. 3.16 & 3.17 are also used in this work to determine the LCOE for electricity and thermal energy. The average cost per kWh of electricity throughout the life cycle is regarded as the levelized cost of electricity ($LCOE_{el}$). The electricity consumption of appliances and HVAC were considered in the computation of $LCOE_{el.}$ The cost of heating and cooling can also be calculated using the same method [162]. Thus, the $LCOE_{th}$ measures the average cost per kWh_{th} of heating, cooling, and DHW loads.

$$LCOE_{el} = \frac{total\ annualized\ cost\ of\ the\ system\ [€/yr]}{total\ electrical\ load\ served\ [kWh/yr]} \quad 3.16$$

$$LCOE_{th} = \frac{total\ annualized\ cost\ of\ the\ system\ [€/yr]}{total\ thermel\ load\ served\ [kWh_{th}/yr]} \quad 3.17$$

The costs associated with a solar PV system were considered for calculating $LCOE_{el}$, and the costs of HVAC equipment, FPCs, and GHX were used to compute the total annualized cost in $LCOE_{th}$. The electric load served included household electricity load and electricity consumption of the HVAC system. The thermal load was the sum of space heating, cooling, and DHW demands.

Flexibility cost: This indicator is a function of grid tariff. It defines how much electricity cost is saved after modulation of the electricity load profile by flexible operation, as formulated in Eq. 3.18.

$$Cost_{flex} = \int_0^T (P_{flex} - P_{ref})\, pc_{tariff}\, dt \quad 3.18$$

P_{flex} and P_{ref} are grid power demands during flexible and regular operation. T is the total duration of energy system operation, and pc_{tariff} is the grid electricity tariff.

3.4 Multi-objective optimization

Genetic algorithms are commonly applied techniques for optimizing the energy performance of buildings[163–170]. To achieve the desired optimization objectives, a population-based metaheuristic genetic algorithm modifies the following population according to the intuitive rule of survival of the fittest. When improving the building performance, a genetic algorithm can handle the non-linearity of design variables. They also investigate the global optimum solution and do not just focus on local optimal solutions [171].

TRNSYS is a building simulation tool that investigates the building's thermal load and evaluates the performance of transient systems. The design parameters and system inputs are given as text files to the TRNSYS model. After simulating the model, TRNSYS produces the specified outputs as a text file. Python code created an interface between TRNSYS and NSGA-III to employ the MOO. This study applied NSGA-II in an optimization scheme using an object-oriented Python-based framework, jMetalPy [172]. The Python script extracted the design variables from the TRNSYS input file and passed it on to the optimization algorithm. Next, the script read the simulation results output file to get objective function values. Based on the values of the objectives in the previous simulation, jMetalPy produced a revised set of design parameters for the next simulation. Following that, Python updated these parameters in the input files, and TRNSYS simulated the energy system model to evaluate the objective function for the revised design parameters. Pareto front (PF), a non-dominated solution set produced by MOO, is the only viable option to improve one objective without sacrificing the second. An MCDM technique was applied to the Pareto points to select the best solution. Figure 3-6 illustrates the generalized optimization flow for the TRNSY-Python co-simulation platform.

3.4.1 Non-dominated sorting genetic algorithm (NSGA-III)

NSGA-III, a basic evolutionary MOO algorithm, is an expansion of NSGA-II. It uses equally spaced reference points to select non-dominated solutions for the new generation [173]. Hence, NSGA-III resolves the problem of non-diversity in NSGA-II while predicting the succeeding populations. The structure of NSGA-III is identical to basic GA, and the concept behind the GA is to execute the natural evolution process. Every design variable in the optimization problem is a genetic factor that combines to characterize a chromosome. The initial population is a random selection, but the next population is generated through selection, mutation, and crossover and comprises the individuals suitable for the environment. The population continues to reproduce and eventually evolve into the best individuals for the environment [68].

Envelope optimization: In this work, the envelope parameters were optimized in two steps. Initially, the Python-TRNSYS co-simulation platform generated PFs between the cost of insulation and the thermal load of the reference building using NSGA-III. In the second step, the weights of the objective functions were assigned using the CRITIC technique, and the Pareto-optimal solution was identified using the TOPSIS methodology. The multi-criteria assessment method is described in the later section.

Service system optimization: A multi-objective optimization process was conducted to maximize the primary energy ratio and minimize the electricity demand of the building service system. The genetic algorithm NSGA-III was implemented with constraints of thermal comfort level and fractional state of charge (FSOC) of battery storage. In the case of service system optimization, the multi-criteria assessment was not required because the minimum energy consumption also characterized the Pareto solution of maximum PER.

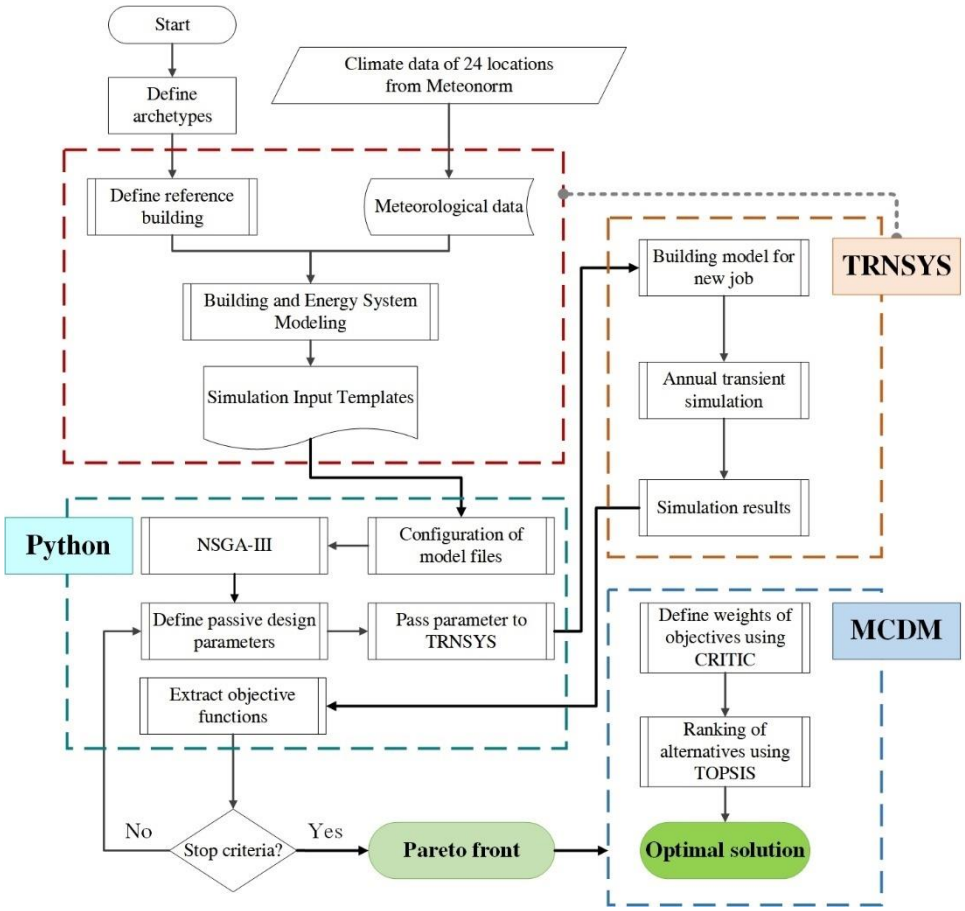

Figure 3-6: Python-based optimization scheme

3.5 Multi-criteria assessment

The first step in the MCDM process is assigning the weights of performance indicators. Two weighing methods are usually applied, subjective weighting and objective weighting. The experts perform a pairwise comparison of the performance criteria in the subjective weighing method. In contrast, objective weighing techniques such as mean weight, entropy method, standard deviation, and CRITIC allocate weights based on the diversity of the objectives in Pareto solutions [174]. Some studies in the literature employed CRITIC for weighing the attributes and TOPSIS for ranking the energy system alternatives. The schematic of the hybrid MCDM process used in this study is presented in Figure 3-7.

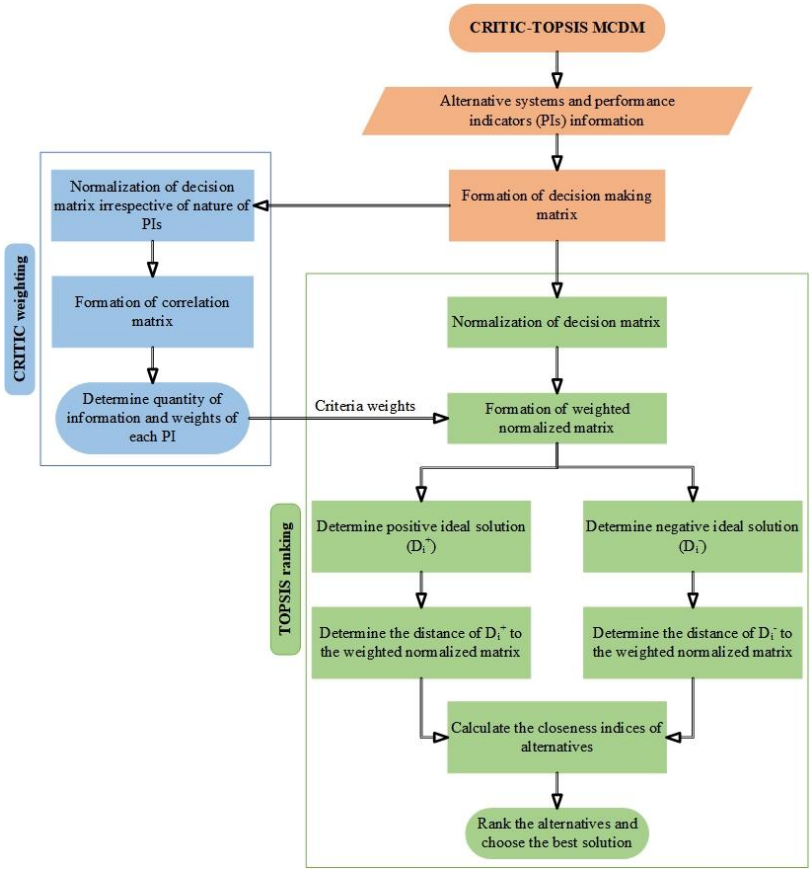

Figure 3-7: Schematic of CRITIC-TOPSIS MCDM process

CRITIC method: The CRITIC method uses standard deviation to assess the variation of performance indicators in alternative systems. The performance indicator with the maximum variation is assigned the highest weight in this technique. Next, the data is normalized to formulate a correlation matrix, which calculates the quantity of the information and the significance of each indicator (Eqs. 3.19–3.22).

$$r_{ij} = \begin{cases} \dfrac{x_{ij} - x_j^{min}}{x_j^{max} - x_j^{min}} & if\ criteria\ is\ benefit - based \\ \dfrac{x_j^{max} - x_{ij}}{x_j^{max} - x_j^{min}} & if\ criteria\ is\ cost - based \end{cases} \quad 3.19$$

$$r_{jk} = \frac{\sum_{i=1}^{m}(r_{ij} - \overline{r_j}).(r_{ik} - \overline{r_k})}{\sqrt{\sum_{i=1}^{m}(r_{ij} - \overline{r_j})^2.\sum(r_{ik} - \overline{r_k})^2}} \quad 3.20$$

$$c_j = \sigma_j \sum_{k=1}^{k} 1 - r_{jk} \quad 3.21$$

$$w_j = \frac{c_j}{\sum_{j=1}^{n} c_j} \quad 3.22$$

Where r_{ij} represents the normalized value of *ith* alternative on *jth* EFI. r_{jk} indicates the correlation coefficient between *j x k* EFIs matrix. σ_j, c_j, and w_j represent the standard deviation, the quantity of information contained, and the weight of the *jth* EFI.

TOPSIS method: In the TOPSIS method, the alternative systems are ranked according to their geometrical distance from ideal and worst solutions (Eq. 3.23–3.27). First, the decision matrix is normalized for each EFI (Eq. 3.23). Then a weighted normalized matrix is created using the weights determined by the CRITIC technique (Eq. 3.24). Next, the distance of each alternative to the ideal and non-ideal solutions is calculated (Eq. 3.25 & 3.26). Finally, Eq. 3.27 is used to determine the relative closeness of alternatives. The BES with the maximum score was chosen as the most flexible option.

$$n_{ij} = \frac{x_{ij}}{\sqrt{\sum_{j=1}^{n} x_{ij}^2}} \quad 3.23$$

$$v_{ij} = \overline{n_{ij}}.w_j \quad 3.24$$

$$D_i^+ = \sqrt{\sum_{j=1}^{n} \left(v_{ij} - v_j^+\right)^2} \quad 3.25$$

$$D_i^- = \sqrt{\sum_{j=1}^{n} \left(v_{ij} - v_j^-\right)^2} \quad 3.26$$

$$D_i = \frac{D_i^-}{D_i^+ + D_i^-} \quad 3.27$$

Where n_{ij} denotes the normalized value of *jth* EFI for *ith* alternative. *wj* is the weight of the *jth* EFI, and v_{ij} represents the weighted normalized value of *jth* EFI for the *ith* alternative. v_j^+ and v_j^- stand for the best and the worst values of the *jth* EFI, respectively. D_i^+ and D_i^- represent the ideal and non-ideal distances for the *ith* alternative, respectively, and D_i refers to the measure of relative closeness of the *ith* alternative to the ideal solution.

3.6 MPC-based optimization

The MPC-based optimization was subdivided into two steps, as shown in Figure 3-8. In the first step, the building thermal load and boundary conditions dataset was used to develop a predictive model, which was employed on the service system with similar boundary conditions in the second phase for improving energy flexibility. A TRNSYS model calculated the building

demand for heating and cooling in the first phase. Then, a parametric analysis was performed with a time step of 30 minutes with the concerned parameters of BES. The dataset obtained from the parametric analysis contained information on weather conditions, internal gains, indoor conditions, and respective thermal comfort and demand for ranges of underlying parameters. The prediction models were developed for each month of the year using the RandomForestRegressor (RF) algorithm. RandomForestRegressor, an ensemble method, is a supervisory machine learning algorithm of scikit-learn, a Python library for predictive analysis [175]. The RF algorithm has been used in the literature for predicting building energy use [176]. Some studies showed that the RF algorithm depicted better prediction accuracy than other regression-based algorithms [177,178]. The ensemble algorithm builds decision trees and uses the bootstrap aggregation (bagging) technique over multiple decision trees. The decision trees are trained on different data sets extracted from the original data set. The final decision is reached using the average of individual trees' outcomes.

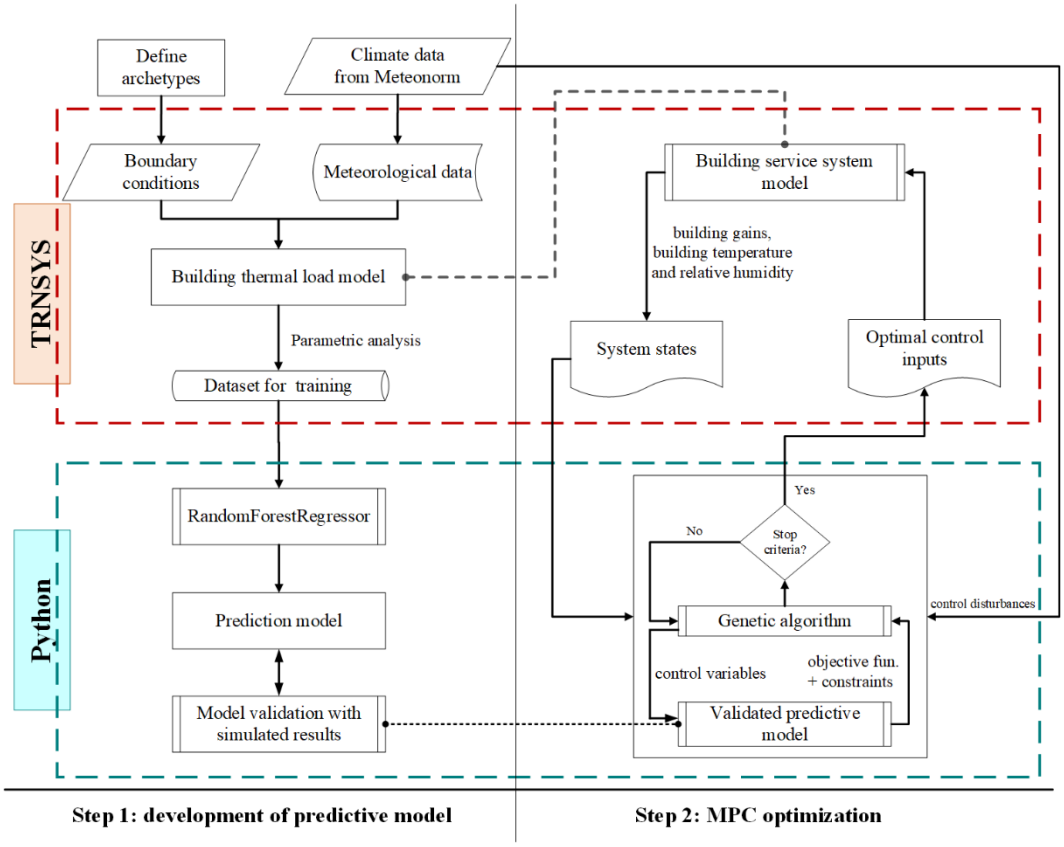

Figure 3-8: MPC-based optimization scheme

The second step applied the control optimization strategy to the building service system. The MPC-based supervisory controller, developed in Python, passed control signals to local controllers in TRNSYS. The supervisory controller had a predictive model and a genetic algorithm (GA). The predictive model fetched the control disturbances and BES states at the

start of each time step. The predictive model and GA operated in a loop for the current time step. The GA passed the control variable to the predictive model and retrieved the control objective and constraints from the predictive model until the termination criterion was reached. Finally, the MPC identified the control inputs of the predictive model for which the control objective was minimized or maximized, and control constraints were fulfilled. This process was repeated for each time step during the TRNSYS simulation. The mathematical formulation of a general MPC problem is described in Eq. 3.28 [179].

$$\min_{u_i} \sum_{k=0}^{P-1} J_k\,(x_k, u_k, y_k) \tag{3.28}$$

Subject to:

$$x_0 = x \tag{3.29}$$

$$x_{k+1} = f(x_k, u_k, d_k) \tag{3.30}$$

$$y_k = g(x_k, u_k, d_k) \tag{3.31}$$

$$y_{i,k} = h(x_k, u_k, d_k) \geq 0 \tag{3.34}$$

$$u_{min} \leq u_k \leq u_{max}$$

Where *k* is the simulation time step, *P* is the prediction horizon, and J_k is the objective function of the control problem. $y_{i,k}$ is the inequality constraint of *ith* system output. The vectors *x*, *y*, *u*, and *d* are system states, system outputs, control inputs, and disturbances, respectively.

The MPC receive system states *x* containing information about the building and energy system like zone temperature, energy supply, gains, etc. The controller runs the optimization process at each time step and decides the control inputs *u* considering the constraints and disturbances. The constraints are generally problem-specific, like thermal comfort in climate control, power of a heating system, and fractional state of charge of the battery. The common disturbances are weather conditions in building automation problems. The control inputs could be temperature set points for zone or water storage, chiller or heating system flow rates, air handling unit speed, etc. The model determines outputs y for the current time step with given control inputs. Energy consumption, energy cost, zone temperature, thermal comfort, and emissions are system outputs used in building control problems.

3.7 Assumptions and limitations

The scope of this study was to establish a methodology to select the best-suited envelope design, energy supply mix, and energy service system and devise a generic dynamic control scheme for

the service system. There were a few assumptions and limitations implied during the case studies of the proposed framework as follows:

- A typical household building was used for the case study in all investigated locations. The occupancy rate was the same in all locations and adopted from ASHRAE. However, the boundary conditions such as DHW load, household electricity load profile, and thermal load were modified for each location.
- The area of PV and thermal collectors was limited by the available rooftop area of the building.
- While calculating the life-cycle costs, the real discount rate (r_d) was fixed at 3.5 % in all locations. Moreover, the maintenance cost of BES was assumed to be 2.5% of the capital cost.
- The capital cost of BES only included costs of main components like the heat pump, BHX, TES, water coils, heat exchanger, PV system, etc. Moreover, the costs of building construction, maintenance, and appliances were constant for all energy system configurations and excluded during the cost analysis.
- A constant grid tariff was assumed for each location throughout the year.
- The average thermal conductivity and thermal capacity were considered for designing BHX and the operation of GSHP.
- Since energy flexibility was evaluated for the whole building, those EFI were calculated, which provided information on an integrative prospect.
- Since the grid tariff was constant, the tariff-based or incentive-based control strategies were excluded from the analysis.

4 Modeling and simulation

Two programs were used to conduct the simulations in this study: TRNSYS for simulating building and energy systems behavior and Python programming language for the interface between optimization algorithms/MPC and TRNSYS. The building and energy systems were modeled in TRNSYS using the built-in standard components and individual components from TRNSYS distributors. The genetic algorithms and MPC were developed in Python using the jMetalPy, a metaheuristics optimization library, and scikit-learn, a predictive analysis library. The Python code also established the TRNSYS-Python co-simulation scheme for optimization.

4.1 Thermal load model

TRNSYS simulated the reference building's space heating and cooling loads using the TRNSY component for multi-zone building (Type 56). Type 56 imported the text file containing the information on the geometry, envelope properties, and the descriptions of building gains/losses, which were specified in TRNBuild. Yearly simulations were conducted with a five-minute timestep to compute building thermal load. Figure 4-1 shows the building thermal load model in the TRNSYS environment. The mathematical models for the system components are derived from ordinary differential or algebraic equations in the TRNSYS program. These models are made commercially available from TRNSYS after validation and are extensively used in building energy systems. The main components of the TRNSYS model are the following:

- *Type 56* – Multi-zone building
- *Type 75b* – Natural ventilation/infiltration
- *Type 109* – Weather data processor
- *Type 2b* – ON/OFF differential controller
- *Type 14h* – Time-dependent forcing function
- *Type 358* – infiltration through the tilted window
- *Type 985* – Undistributed ground temperature
- *Type 9c* – Data reader for external file
- *Equation* – define new variables as algebraic functions of constants, previously defined variables, and outputs from other components

The occupancy rate and internal gains were given as external files, described in sections 3.1.1-3.1.2. The envelope properties were defined in TRNBuild as listed in Table 3-1 and Table 3-2.

The control schemes of tilted window ventilation and shading are explained in sections 4.1.1 and 4.1.2.

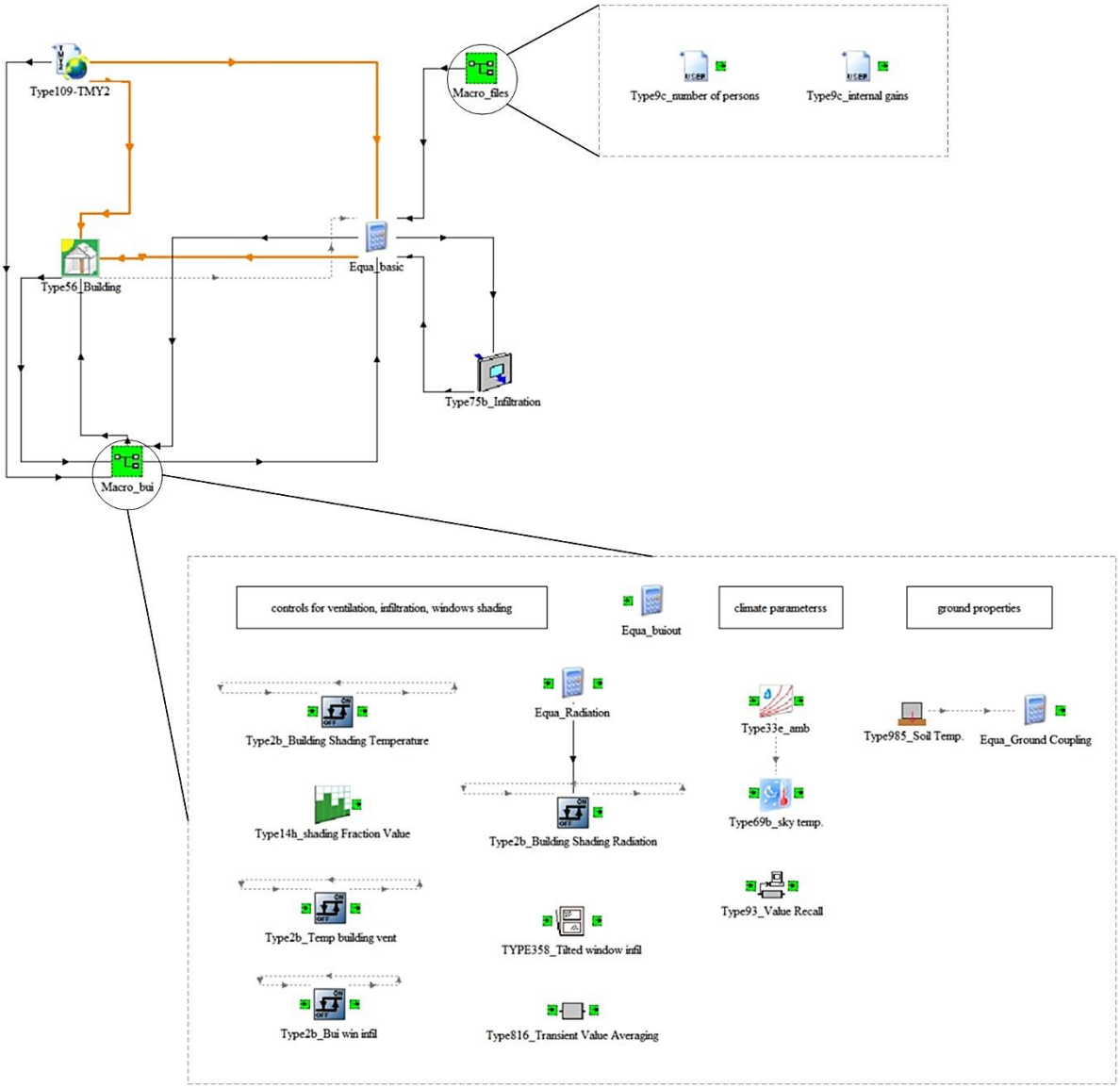

Figure 4-1: TRNSYS model for thermal load simulation

4.1.1 Ventilation load

Thermal load simulations considered two ventilation loads resulting from the airflow through cracks in the building envelope and window's aperture. The infiltration rate (Q_{inf} [m^3/s]) was computed using the Sherman Grimsrud model for a single zone, defined by Eq. 4.1 in ASHRAE fundamentals 1997 [180].

$$Q_{inf} = (A_L/1000).\sqrt{C_s\Delta T + C_w V^2} \qquad 4.1$$

Where A_L and C_s represent the effective area of envelope cracks [cm^2] and stack coefficient [$(L/s)^2/(cm^4K)$]. ΔT denotes the difference between indoor and outdoor temperature for the time interval of investigation [K]. C_w and V are wind coefficient [$(L/s)^2/[cm^4\ (m/s)^2]$] and average wind speed (m/s). The value of C_s depends on the total number of floors in the building. For instance, its values are 0.000145 for single-story, 0.00029 for double-story, and 0.000435 for triple-story buildings. The wind coefficient C_w depends on the height of the building and local shielding from surrounding objects. The values of these coefficients were assigned according to the guidelines in ASHRAE fundamentals 1997.

The passive cooling was activated through window openings based on the zone and outdoor temperature at night (21:00 to 08:00 hrs.). The average temperature of the last twenty-four hours ($T_{avg}24$) was used to decide the heating and cooling seasons. The climate data show that $T_{avg}24$ falls below 12 °C in the winter, and the building does not need to be cooled. In summer, passive cooling started when the zone temperature exceeded 24 °C and the outdoor temperature was at least two degrees lower than the zone temperature. On the other hand, active cooling started when the zone temperature exceeded 25 °C. The gap of one degree before activating the active cooling was given to save energy through passive cooling. Windows were closed after the room temperature dropped to 23 °C. Hence, passive cooling was realized between zone temperatures of 23 °C and 25 °C. When all the conditions mentioned in Figure 4-2 were satisfied, windows tilted to start passive ventilation. The building's total ventilation load was a total of heat gains and/or losses from two air exchange rates.

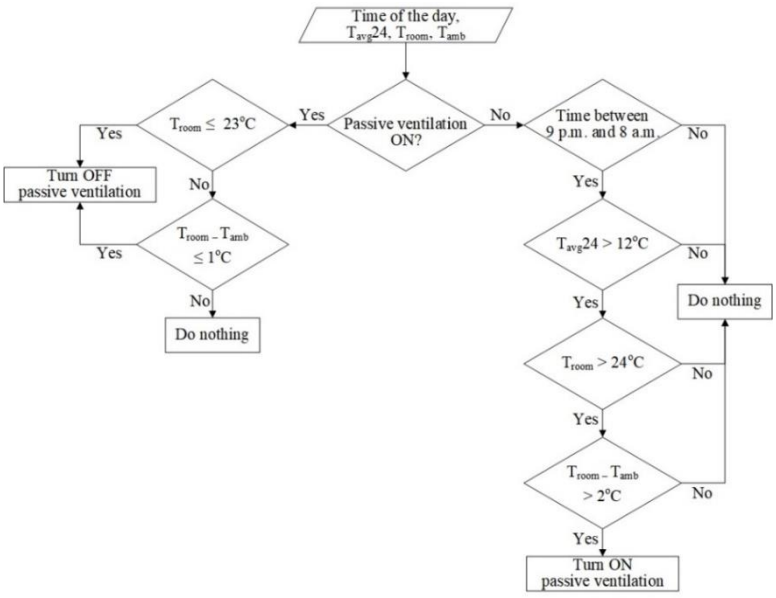

Figure 4-2. Temperature-based control of passive ventilation through windows

4.1.2 Solar gain

Windows in the building had shading blinds to reduce the cooling demand by controller solar gain and preventing overheating in the winter. The current study planned a monthly schedule of the window shading fraction in the building model such that the shading fraction in each month was a function of the lowest value during the year. A study concluded that the average value of the optimum shading during winter was approximately 23%, and the lowest value during the day was 10% [181]. In the summer, window shading can range from 25% to 100% for the optimization process [182]. Thus, the base-case building model fixed the minimum shading fraction of 0.11 for December. Figure 4-3 shows the variation in the shading for other months of the year relative to December.

In addition, a control strategy was also realized to activate the window shading based on the outdoor temperature, zone temperature, and global horizontal solar radiations (IT_H). The control scheme for shading on/off is shown in Figure 4-4. The active cooling was functioning at a zone temperature above 25 °C. The window shading was activated at 23.8 °C [95] to avoid further increase in zone temperature from solar gains. Hence, the gap of 1.2 °C delayed the active cooling in the building. Though a higher margin could be set to save energy, it would also increase the lighting loads and heat gain. Therefore, the window shading was deactivated at 22.8 °C, i.e., one degree below the shading-on temperature, to allow sunlight into the building and prevent a further drop in the zone temperature during summer. The second element that affected solar gains was the WWR. Each façade had a different WWR (c.f. Table 3-2). However, the South façade had a value of 0.2 for WW in the base case. According to the recommendation of ASHRAE standard 90.1-2019[183], the maximum WWR was set to 0.4 (residential building) in the optimization process.

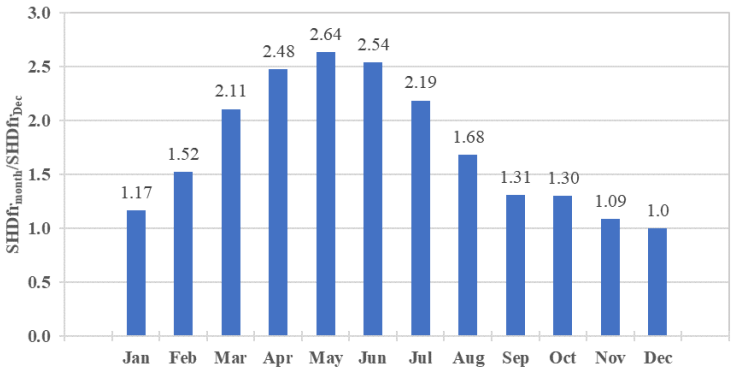

Figure 4-3: Relative shading fraction during the year

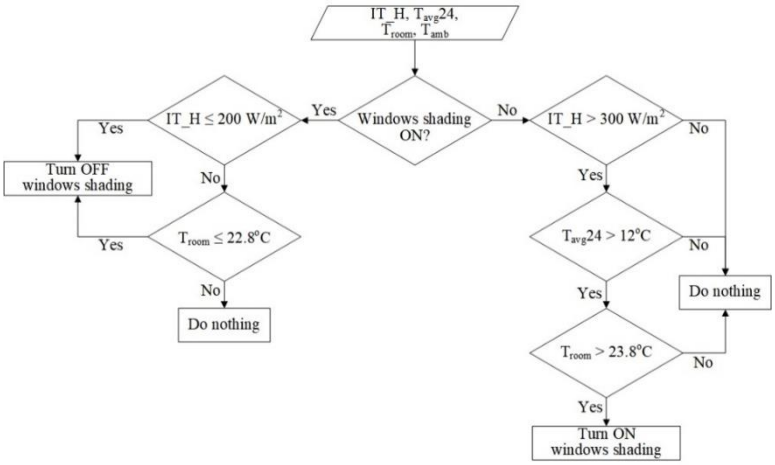

Figure 4-4: Solar radiation-based control of window shading

4.2 Energy system models

TRNSYS simulated the behavior of building and energy system alternatives having different energy supply and service system configurations. The envelope design, building geometry, climate data, and schedules of occupants and residential appliances were identical for all BESs in a location, as obtained from MOO of envelope parameters in phase 1. The year-round simulations were performed for each energy system alternative in the investigated climates. Figure 4-5 shows the TRNSYS model of the energy hub. The BES was divided into subsystems; GSHPs, ASHPs, absorption chiller, solar energy system, and energy system control. The heat exchanger of the DHW and a TES were integral components in all BES configurations. The space heating service was realized by emission heating or ventilation heating using a radiator or hot water coils. At the same time, a chilled water coil provided the ventilation air for space cooling. A subsystem was activated according to the configuration of BESs under evaluation. The components of BES's subsystems are displayed in Figure 4-6 to Figure 4-9. Table 4-1 presents the types used and connectivity of the main components in the TRNSYS model.

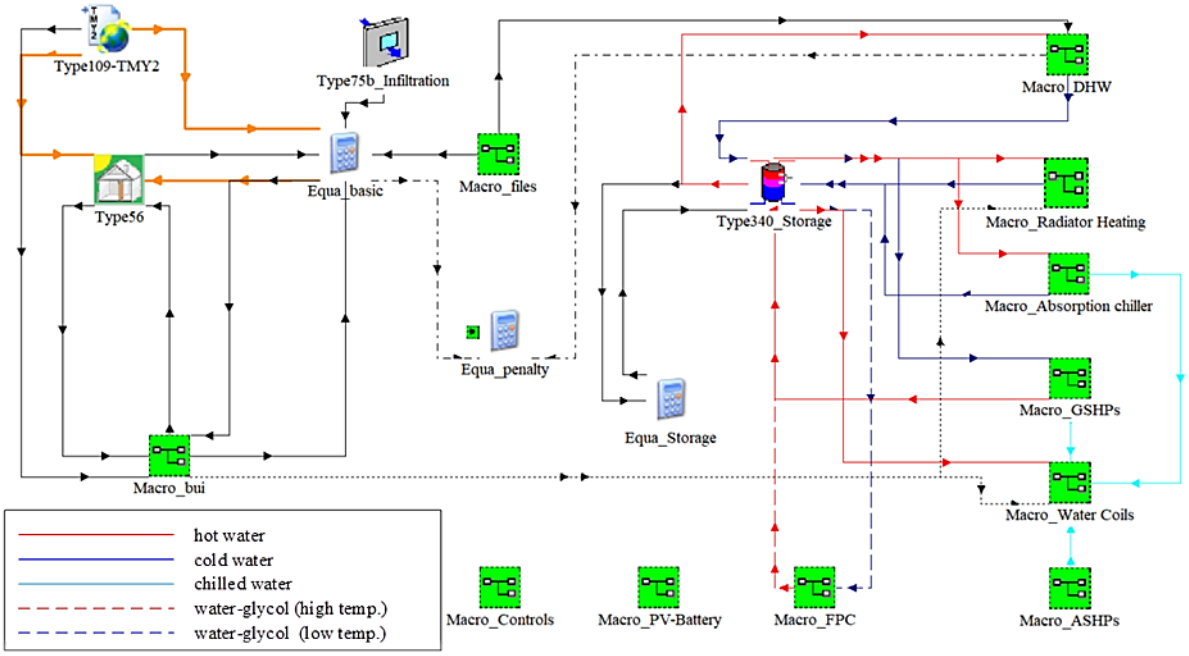

Figure 4-5: TRNSYS model for simulation of BESs

The GSHPs system had a borehole heat exchanger, B/WHP, and B/AHP. The additional components were adiabatic pipe for short-term thermal capacity effects, horizontal ground heat exchangers for buried pipes, pumps, equation blocks, and liquid flow control valves. The HTF on the source side of GSHPs absorbed heat from or released heat to the borehole in heating and cooling seasons, respectively. The HTF released the absorbed heat to the load side liquid in B/WHP and air in B/AHP during the heating service. In contrast, during the cooling service, the HTF absorbed the heat from the load-side liquid stream in B/WHP and the air stream in B/AHP. The ASHPs system was comprised of A/AHP and A/WHP. The air stream was the source-side fluid to heat or cool the air and water on the source side in A/AHP and A/WHP, respectively. The hot/cool air was directly supplied to the building for HPs having an air stream at the load side.

For HPs having water at the load side, the hot water was supplied to the TES, which was further used for space heating and DHW supply. Regarding space cooling, the chilled water was supplied to the water coils for air conditioning. In the case of the absorption chiller system, a single-stage absorption chiller produced the chilled water by using the heat of hot water from TES. A cooling tower cooled down the cooling water stream of the absorption chiller through natural convection. The chilled water was used in water coils for air conditioning.

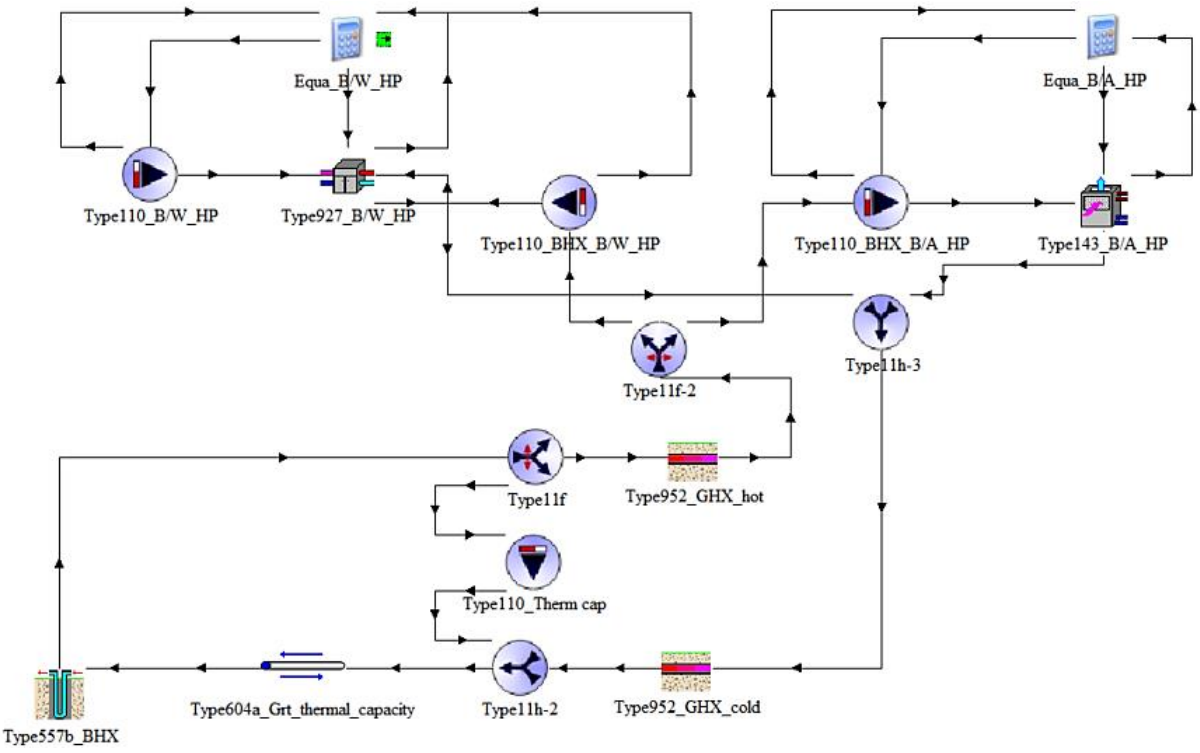

Figure 4-6: TRNSYS subsystem model for GSHPs

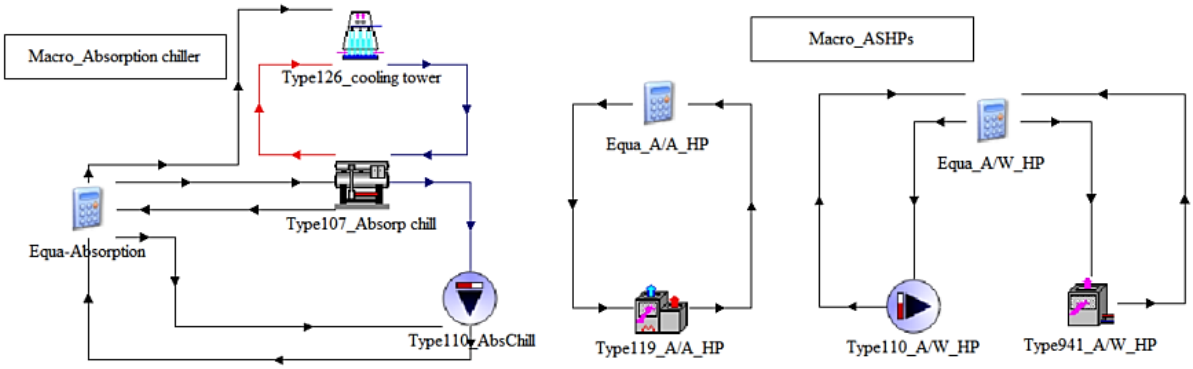

Figure 4-7: TRNSYS subsystem model for ASHPs

The PV array supplied electricity to the building through an inverter or stored in the battery bank. The stored electricity was drawn later when solar radiations dropped below a certain level until the lower limit FSOC reached. The grid supply provided the PV-unmet electricity load of the building. FPCs absorbed solar energy in water-glycol fluid and transferred that energy to the water in TES through a heat exchanger, which was used for hot water supply to the radiator/hot water coils for space heating, absorption chiller for space cooling, and/or to the heat exchanger for DHW supply. A flow rate of 35 kg/h.m^2 was given for the HTF in FPCs.

The control system components were equation blocks, differential controllers, and PID controllers. The equation performed an algebraic function on the inputs from the differential controller to define the ON/OFF signals for the heating or cooling season, heating or cooling

mode of HPs, and electricity supply from the PV array or battery storage. For PV supply, the priority was assigned to the building electricity demand over battery charging. Only excess electricity, if available after covering the building electricity demand, was stored in the battery. The heating season was active if the average outdoor temperature in the last twenty-four hours was below 12 °C. The cooling season was activated if the twenty-four hours average outdoor temperature was above 20 °C. The upper and lower limit of the battery's FSOC was 0.9 and 0.25, respectively. The PID controllers set the zone temperature to be achieved by the service system and generated the control signals (0 to 1) for ventilation and water flow rates in the radiator and water coils. The B/W and A/W HPs were active in the heating season whenever there was DHW demand and/or heating demand and the temperature of TES was below 55 °C. In the cooling season, the chilled water was supplied by the B/WHP, A/WHP, or absorption chiller when the zone temperature elevated from the set point. Similarly, B/A and A/A HPs were activated when the zone temperature dropped below or raised above the set point during the heating and cooling seasons, respectively.

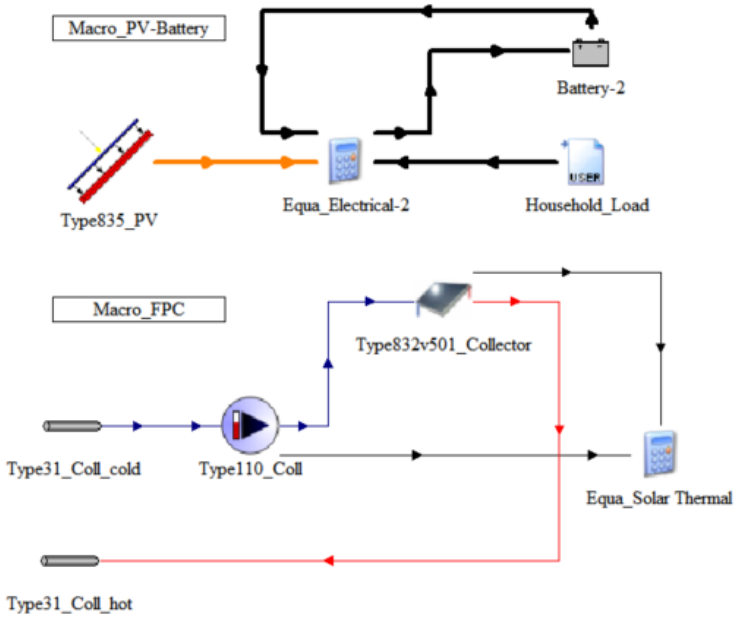

Figure 4-8: TRNSYS subsystem model for PV supply and FPCs

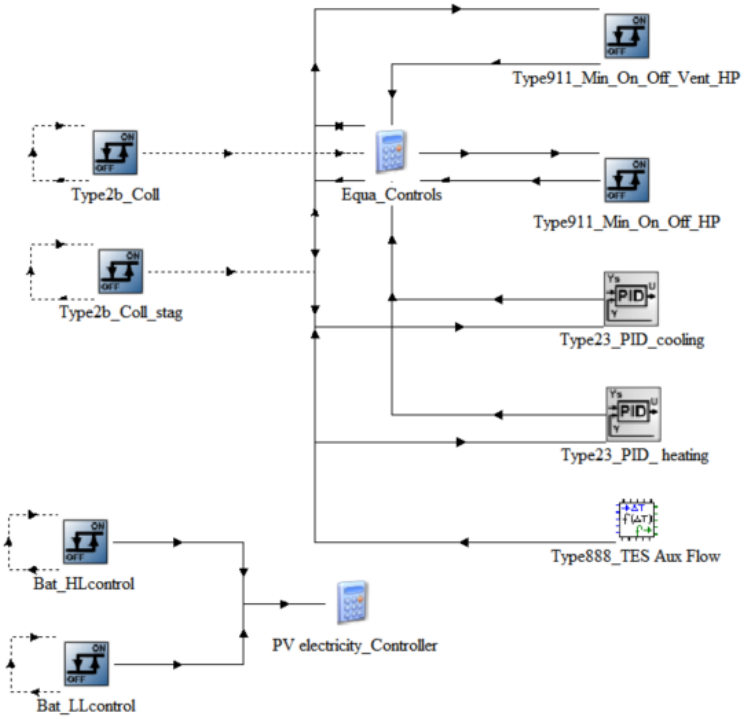

Figure 4-9: TRNSYS subsystem model for control strategies

Table 4-1: TRNSYS types and connectivity of main components of TRNSYS simulation models

Energy system component	TRNSYS type	Connectivity
Building	Type 56	Weather data, Internal gains, convective and radiative gains, and ventilation air were input from other model components.
Thermal energy storage	Type 340	Heat gain from the hot fluid stream of FPCs through heat exchangers and inlet/outlet ports for water circulation with DHW circuit, B/WHP, A/WHP, and absorption chiller.
Borehole heat exchanger	Type 557b	A vertical U-tube heat exchanger extracted heat from or released heat to a circulating water-glycol mixture from GSHPs.
Adiabatic nodded pipe	Type 604a	To model the short-term behavior of the BHX.
PV panel	Type 835 [184]	Generated electricity was supplied to the building via an inverter or the excess electricity was stored in the battery (Type 47).
FPC	Type 832	The water-glycol mixture circulated between FPCs and TES to transfer the absorbed solar energy to the water.
B/WHP	Type 927	Hot water supply to the storage tank in heating mode by absorbing heat from the source-side water-glycol mixture or chilled water supply to cooling coils by rejecting heat to the source-side liquid stream.
B/AHP	Type 143	Conditioned air stream to the building by absorbing heat from (heating mode) or rejecting heat to (cooling mode) the source-side water-glycol mixture.
A/WHP	Type 941	Hot water supply to TES in heating mode by absorbing heat from source-side outside air or chilled water supply to cooling coils in cooling mode by rejecting heat to the outside air.

Energy system component	TRNSYS type	Connectivity
A/AHP	Type 119	Conditioned air stream to the building by absorbing heat from (heating mode) or rejecting heat to (cooling mode) the outside air stream.
Absorption chiller	Type 107	To supply chilled water to the cooling coils in cooling mode by using TES-supplied hot water energy in the generator.
DHW heat exchanger	Type 805	Counter flow heat exchanger for heating the utility water to the set point by using hot water from the storage tank on the primary side.
Radiator	Type 362	Space heating through convection and radiation using the heat of liquid stream from the storage tank.
Cooling coils	Type 124	Conditioned air stream to the building by rejecting heat to the chilled water flowing inside the tube.
Heating coils	Type 140	Conditioned air stream to the building by absorbing heat from hot water flowing inside the tubes.

4.2.1 Performance mapping of HVAC equipment

The performance catalog of commercial equipment characterized the performance of HPs and the absorption system. The performance data contained information on power consumption, cooling capacity, and/or heating capacity at various flow rates and fluid stream temperatures. B/WHP, A/WHP, and absorption chiller needed normalized power consumption, heating/cooling capacity, and flow rates to predict the performance. The reference equipment for performance mapping of HVAC systems are described below, and complete performance data files are available online [185] for reference.

Ground source HPs: The water or air was heated or cooled in brine-to-water HP and brine-to-air HP, respectively, using a borehole heat exchanger. The performance attributes of geothermal HP were defined by the performance characteristics of YORK® HPs based on the peak heating and cooling demands for each climate [186]. The performance data of YAWS series heat pumps were used to parameterize brine-to-water HP. The HP's normalized capacity and power at entering temperatures and normalized flow rates of the fluid were calculated in the performance file. Likewise, the performance file of brine-to-air HP was created using YAFS series HPs. The normalized capacity and power of the heat pump (relative to the peak loads) at different entering temperatures and normalized flow rates of the working fluid were attributes of the performance file. Similarly, YAFS series residential heat pumps parameterized the performance of brine-to-air HPs. As a limitation of available data, the available minimum cooling load's performance characteristics were assumed when the performance mapping was unknown at very low cooling rates. The performance file contained the heating or cooling capacity with the power demand

of HP at specific airflows, flow rates, and working fluid temperatures. Reversible valves controlled the refrigerant flow in both the cooling and heating modes of the reversible GSHPs.

Air source HPs: The performance of ASHPs was also defined by the peak heating/cooling demand in the investigated locations. The HP's heating or cooling capacity and power demand at various airflows and ambient and return air temperatures were used to simulate the performance of air-to-air HPs. The performance parameters of Bosch® IDS HPs were used to parameterize the performance of air-to-air HP [187]. The performance file defined the air-to-water HP's fractional capacity and power demand at varying water and air input temperatures. The performance mapping of low temperature ERLQ HP from DAIKIN Altherma [188] was used to parametrize air-to-water HP. Both ASHPs were reversible, with the capacity to divert the refrigerant flow to switch between heating and cooling modes.

Absorption chiller: This work investigated a lithium bromide (LiBr) single-effect absorption chiller powered by hot water in a temperate range of 70 °C to 95 °C. This investigation used the WFC-SC5 absorption chiller's performance attributes to calculate the normalized cooling capacity and the required energy at various cooling load fractions, chilled water, and cooling water temperatures [189]. In cooling-dominant climates, such as QTA and JKT, the BES included an absorption chiller and a cooling tower of 3 kW and 7.2 kW, respectively. The generator of the absorption system was powered by hot water from TES.

4.3 MPC-based dynamic control

MPC-based dynamic control used a predictive model for predicting the system's future behavior over the prediction horizon of thirty minutes. Initially, a correlation was computed between the control variables and outputs of the predictive model to determine the potential variables for the MPC model. Then, based on MPC model prediction and control variables, the optimal control inputs were determined for a control objective of minimizing the thermal load of the building subject to a constraint of thermal comfort. Finally, the control scheme was employed on the flexible BES, identified from the multi-criteria assessment process, for three representative months: January (cold), June (warm), and October (mild). The dynamic control problem was formulated as given below.

$$\boldsymbol{J_e = min} \sum_{k=0}^{P-1} \boldsymbol{Q}_k \left(x_k, u_k, y_k\right) \qquad 4.2$$

Where k is the simulation time step, P is the prediction horizon, and J_e is the objective function for minimizing the thermal load (Q_k). The thermal load of the building is a function of system states (x), system outputs (y), control inputs (u), and disturbances (d).

System states: MPC model received the solar gains through windows and heating or cooling mode of the HVAC system as the system states at the current time step of the simulation.

Control inputs: The reference set points of PID controllers for the heating and cooling operation were control inputs of MPC. The upper and lower limits of the reference set point were specified in the control problem. For heating mode, the upper and lower limits of the temperature set point were 22 °C and 18 °C, respectively. Similarly, 26 °C and 24 °C were given as upper and lower temperature set point limits in cooling mode, respectively. Additionally, the window shading fraction was the second control input in the cooling season, with a range of 0 to 1.

Control disturbances: The outdoor temperature, relative humidity, and total horizontal solar radiations were control disturbances of the control problem.

System outputs: The model predicted the zone temperature and relative humidity, heating or cooling load, and PPD based on the control variables at the current time step. Thermal comfort was specified as a control constraint such that the optimal control inputs were defined for a PPD value not higher than 10%. According to ASHRAE standards 55 [190] for thermal environmental conditions for human occupancy, PPD is a quantitative indicator of the percentage of thermally dissatisfied occupants. The allowable range of PPD is 10%, above which the occupants feel warm or cool.

A TRNSYS component, type163, was used to co-simulate TRNSYS and Python. Type 163 forwarded the control variables in a text file to the MPC model in Python. The path of the Python script needed to be specified in type 163. The MPC model created a text file containing the optimal control inputs, which were retrieved by type 163. This information exchange loop was executed iteratively during the TRNSYS-Python co-simulation.

5 Case studies

The optimization framework, described in chapter 3, was tested on reference building for different climate conditions. Three case studies were conducted to validate the effectiveness of the devised methodology for improving energy flexibility. Firstly, the energy flexibility potential of the building envelope was evaluated in major climate zones worldwide. Then, a flexible energy system was identified by computing a comprehensive set of EFIs in severe cold, cold, mild, and hot climates. Finally, the steady-state and dynamic optimization strategies were employed on the flexible BES in a cold climate to further improve the energy flexibility of the underlying residential building.

5.1 Building architecture flexibility

Multi-objective optimization strategy was implemented on the reference building in four major climate zones; A: Tropical, B: Dry, C: Temperate, and D: Continental, according to Köppen-Geiger climates classification [191] (first letter). These climate zones are subdivided based on the annual variation in ambient temperature and precipitation. The precipitation level (second letter) is defined as f (no dry season), m (Monsoon), s (dry summer), w (dry winter), S (semi-arid), W (desert). Similarly, the temperature level (third letter) is categorized as a (hot summer), b (warm summer), c (cold summer), d (very cold winter), h (hot), k (cold). Table 5-1 describes the average temperature (T_{avg}), cooling degree days (CDD), and heating degree days (HDD) for twenty selected climates in twenty-four locations. Meteonorm tool was used to generate the meteorological data for these locations. The CDD_{10} and HDD_{18} are defined as follows:

$$HDD_{18} = \sum_{t=1}^{365} (T_{base} - T_a) \quad 5.1$$

$$CDD_{10} = \sum_{t=1}^{365} (T_a - T_{base}) \quad 5.2$$

Where T_{base} is 18 °C for HDD and 10 °C for CDD, T_a is the average temperature of the day, and degree days are the yearly sum of the daily temperature differences.

Table 5-1: Climate characteristics and electric gains of investigated locations

SN	Country	Location	Köppen Climate	IECC Climate	T_{avg} (°C)	HDD_{18}	CDD_{10}	Electricity consumption (kWh/m²a)	Electric gains (kWh_{th}/m^2a)
1	Sweden	Ostersund	Dfc	7 A	3.9	5468	429	30.20 [113]	17.52
2	Sweden	Stockholm	Dfb	5 A	7.4	3922	841	30.20 [113]	17.52
3	Austria	Bischofshofen	Dfb	5 A	8.3	3660	994	23.87 [114]	13.85
4	China	Daocheng	Dwb	6 A	5.9	4434	378	11.67 [115]	6.77
5	Iran	Sarab	Dsb	5 C	9.1	3496	1305	32.51 [116]	18.85
6	Japan	Sapporo	Dfa	5 A	9.3	3523	1430	28.80 [117]	16.71
7	China	Beijing	Dwa	4 B	12.8	2875	2470	11.67 [115]	6.77
8	Iran	Arak	Dsa	4 B	14.4	2320	2523	32.51 [116]	18.85
9	Denmark	Odense	Cfb	5 C	8.9	3364	835	26.77 [118]	15.53
10	Germany	Saarbrücken	Cfb	5 A	9.8	3119	1074	34.36 [114]	19.93
11	UK	Birmingham	Cfb	5 C	10.8	3679	930	37.34 [119]	21.66
12	France	Strasbourg	Cfb	4 A	12.1	2470	1533	30.00 [114]	17.40
13	China	Kunming	Cwb	3 C	15.7	1137	2204	11.67 [115]	6.77
14	Spain	Vigo	Csb	3 A	15.4	1282	2042	19.92 [120]	11.55
15	Italy	Milan	Cfa	4 A	13.9	2099	2115	21.81 [121]	12.65
16	China	Hanzhong	Cwa	3 A	15.4	1853	2589	11.67 [115]	6.77
17	Portugal	Evora	Csa	3 A	16.1	1404	2397	27.15 [122]	15.75
18	Iran	Birjand	BWk	3 B	17.0	1693	3052	32.51 [116]	18.85
19	Pakistan	Quetta	BSk	3 A	17.9	1182	3312	22.19 [123]	12.87
20	Pakistan	Lahore	Bsh	1 B	24.7	348	5382	22.19 [123]	12.87
21	UAE	Dubai	Bwh	0 B	28.9	0	6910	39.93 [124]	23.16
22	Singapore	Singapore	Af	0 A	28.6	0	6782	28.04 [125]	16.26
23	India	Mumbai	Aw	0 A	28.1	0	6594	22.92 [126]	13.30
24	Indonesia	Jakarta	Am	1 A	26.6	0	6045	18.40 [127]	10.67

5.1.1 Optimization scheme

The optimization goal was to identify a flexible envelope design for the building at the preliminary design stage according to the climate conditions. At this point, the absolute thermal load of the building was calculated instead of the energy consumption of HVAC equipment for attaining thermal comfort in the building.

The heating and cooling set points were 20 °C and 25 °C, respectively, with a relative humidity level of 50% in both cases. The predicted mean vote (PMV) and predicted percentage discomfort (PPD) values quantified the thermal comfort in the zone.

The NSGA-III performed 5000 simulations with a population size of 100 for every run to complete the optimization process. Table 5-2 provides the attributes of the MOO problem in this study. The optimization algorithm produced PFs of 100 non-dominated envelope design options for each location. Finally, an MCDM method was applied using the CRITIC and TOPSIS techniques to identify the optimum option from the Pareto solutions.

Table 5-2: Inputs of genetic algorithm

NSGA-III attributes	Value
Population size	100
No of variables	7
No of objectives	2
Maximum evaluations	5000
Mutation method	Polynomial
Mutation probability	0.15
Crossover method	Simulated binary crossover
Crossover probability	0.8
Termination criteria	Max evaluations

5.1.1.1 Design variables

Solar gains, infiltration gains/losses through cracks, and transmission gains/losses through opaque building parts are the decisive variables of a building's thermal load. Thus, the passive design parameters were chosen as design variables of the optimization problem according to their impact on heat gains and/or losses. The design variables for this study were building orientation, WWR, window shading fraction, minimum solar radiation to turn on window shading, and the insulation thickness of the external walls and roof. Table 5-3 provides information on the selected design variables.

Table 5-3: Design variables and their optimization bounds

Building element	Variable	Lower bound	Upper bound
External wall insulation	EPS thickness (EPS_{Thk}), m	0.10	0.25
Roof insulation	rockwool thickness ($Rockwool_{Thk}$), m	0.10	0.25
Window aperture	α (degrees)	5	20
South faced window	Window-to-Wall ratio (WWR)	0.2	0.4
Windows shading	Minimum horizontal solar radiation (IT_H) for shading on	250	500
Windows shading	Shading fraction in December (Shd_{Dec})	0.10	0.33
Building orientation	Orientation (N/S/E/W)	NA	NA

5.1.1.2 Objective functions

The optimization goal was minimizing the envelope insulation cost while employing passive design upgradation to minimize heating and cooling loads. The cost for insulation of the envelope was considered in the optimization problem because this study optimized the passive parameters only. TRNSYS estimated the yearly thermal load of the building using the boundary conditions specified in sections 3.1&4.1. TRNSYS model also computed the total cost of envelope insulation based on insulation thickness. The cost of insulating materials with identical thermal properties is about the same, according to a market assessment in the various regions under investigation. The same insulation materials were used in all locations at 139 € per cubic meter for EPS and 230 € per cubic meter for rockwool [192]. Concerning the cost of windows, it was assumed that the higher cost for large windows would balance the cost saved from constructing a smaller insulated wall. Finally, the TRNSYS model wrote text files containing values of the objective function. The following two objectives were selected for the bi-objective optimization.

Minimize annual thermal load (kWh_{th}/year): The annual thermal load was the sum of sensible and latent heating and cooling demands to maintain the comfort level in the building. This objective function was dependent on all design variables.

Minimize investment cost (€): This objective function only depended on the thickness of insulation materials and was calculated accordingly.

5.1.2 Optimization results

A MOO does not generate a solution that concurrently minimizes or maximizes the optimization objectives. However, it produces a Pareto optimal solution set such that each solution is independent of other solutions on PF. Also, improving an objective function is impossible without compromising at least another objective function. The bi-objective optimization in this investigation produced PFs for each location comprising about 100 solutions. Figure 5-1 presents the PFs of continental, temperate, dry, and tropical climate zones. The 2D PFs plots were constructed between the insulation cost and the annual thermal load. In all locations, the scatter plots were symmetric. Nevertheless, they were dispersed vertically because of the diversity in climate conditions.

The emplacement of PFs demonstrated that earlier, a little increase in the insulation cost led to a significant decrease in the thermal load. This trend was prominent in hot regions of tropical

and dry climates. In such regions, PFs had higher slopes but flattened out eventually as insulating costs increased. The CRITIC and TOPSIS techniques identified the best solution. In the optimal solution, good envelope insulation in all climate zones significantly reduced the thermal load. The optimal trade-off solution is highlighted in green on PFs. It is worth noting that, in each case, the best option was the solution with the lowest thermal load or the one close to it on PFs. The higher weight of the annual thermal load, assigned by the CRITIC weighing method, justified this phenomenon. The weight of the thermal load varied between 0.63 and 0.68 in cold climates but varied between 0.60 and 0.72 in cold climates.

Table 5-4 provides the values of design parameters, thermal transmittance of the external wall (U_w) and roof (U_r), and objective functions for the optimal solution in each location. A well-insulated envelope and windows with large shades were typical design requirements in optimal solutions. The WWR showed variation in different climates between lower and upper limits, i.e., 0.2 to 0.4. In most cases, the solar radiation for turning on the window shading was around 250 W. The window aperture angle ranged from 5 to 20 degrees depending on climate, with an average value of 11.88 degrees. In areas with high demand for space heating or cooling, the U-value of external walls and roofs was around 0.15 W/m^2K. In mild conditions, it was comparatively greater. The optimization reduced the thermal transmittance of the envelope in all locations except for Ostersund and Stockholm. The roof's U-value was increased from 0.13 W/m^2K to 0.15 W/m^2K in those locations.

The diversity of envelope parameters in optimal solutions with changing climate conditions was characterized according to the degree days. The optimization results showed that the envelope parameters in optimal solutions were consistent for a specific range of degree days. The mean, standard deviation (STD), and ranges of design parameters are shown in Table 5-5 for various degree days. The U-value should be low in heating-dominant locations. The mean of U-value was minimum in locations with heating degree days higher than 3500. The average U-value was 0.153 for the wall and 0.165 for the roof in climate zones with cooling days greater than 3500. The WWR had a maximum mean value of 0.36 for climates with HDD_{18}>3500 and decreased to 0.2 for climates with CDD_{10}>3500. For HDD18>2000, the window aperture angle was approximately 11 degrees. The largest aperture angle of 14.77 was found in the regions of CDD10>3500. The mean value of the IT_H for activating the shading was highest in areas with HDD18>3500 and lowest in areas with CDD10>3500.

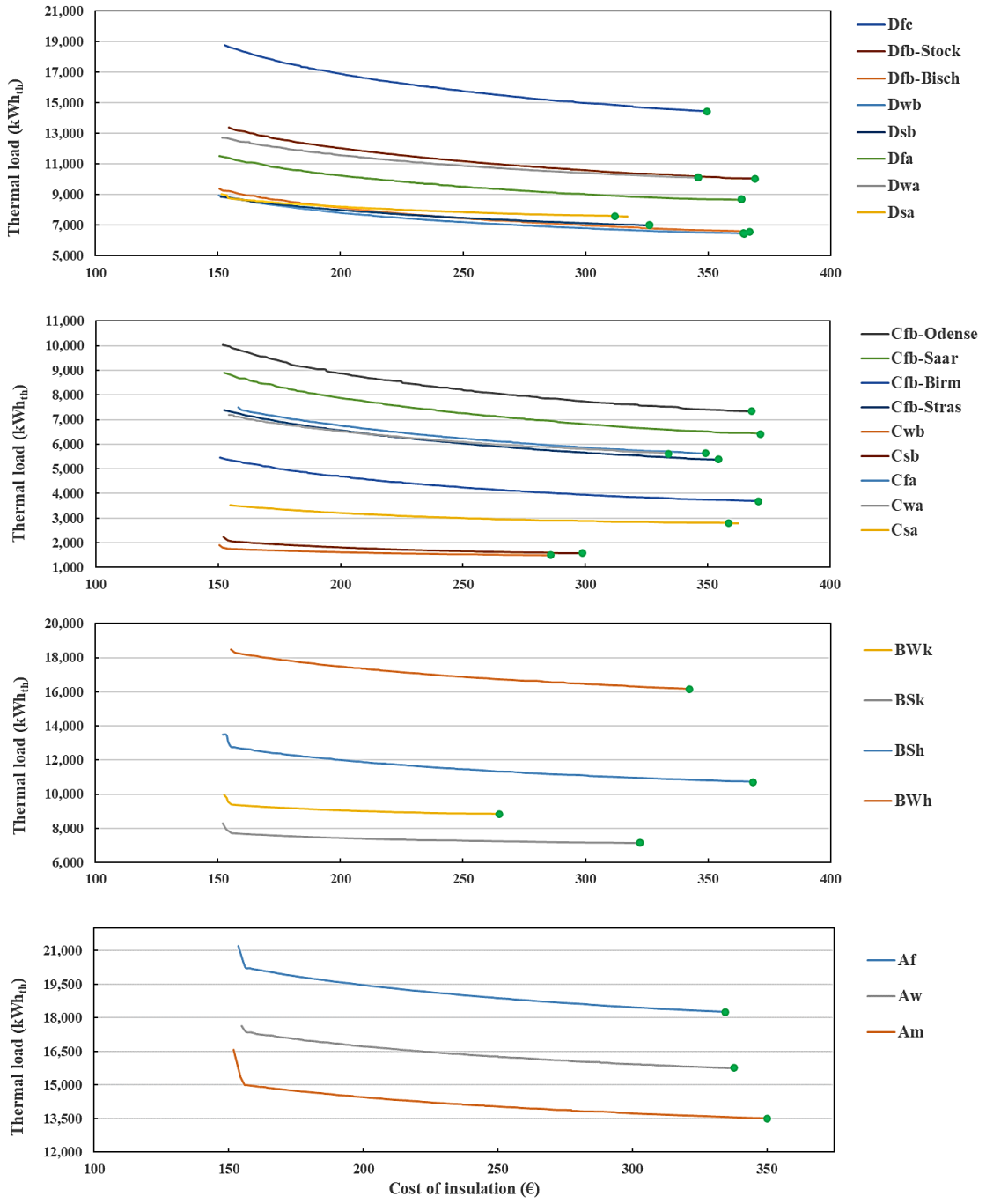

Figure 5-1: Pareto fronts of MOO in investigated climates

The STD was used to measure the spread of the solution set in different locations having similar climate conditions. The consistency of solution sets was justified by very low STD in each category for all design parameters, other than the aperture angle, which had a large spread and high STD value. A detailed analysis of variation in the design parameters for each climate zone is provided in Appendix A.

Table 5-4: Trade-off solution set in investigated climates

Climate	EPS_{Thk} (m)	$Rockwool_{Thk}$ (m)	α (degree)	WWR	IT_H (W)	Shd_{Dec}	Orientation	U_w (W/m²K)	U_r (W/m²K)	Thermal load (kW_{th}/a)	Cost of insulation (€)
Dfc (Ostersund)	0.247	0.211	9.8	0.37	279	0.330	North	0.150	0.154	14317	350
Dfb (Stockholm)	0.237	0.196	10.9	0.31	289	0.330	North	0.156	0.164	10426	335
Dfb (Bischofshofen)	0.247	0.240	12.7	0.39	256	0.328	North	0.150	0.137	6729	367
Dwb (Daocheng)	0.245	0.241	5.2	0.40	287	0.253	North	0.151	0.136	6546	365
Dsb (Sarab)	0.234	0.188	11.0	0.33	255	0.329	North	0.157	0.170	7159	326
Dfa (Sapporo)	0.246	0.237	15.4	0.40	277	0.330	North	0.150	0.138	8845	364
Dwa (Beijing)	0.240	0.218	16.1	0.40	251	0.330	North	0.154	0.149	10333	346
Dsa (Arak)	0.217	0.179	5.2	0.22	250	0.330	North	0.169	0.178	7757	317
Cfb (Odense)	0.246	0.237	10.0	0.34	304	0.328	North	0.150	0.138	7506	368
Cfb (Saarbrucken)	0.245	0.235	10.4	0.24	252	0.327	North	0.151	0.139	6595	372
Cfb (Birmingham)	0.240	0.249	13.1	0.32	279	0.329	North	0.154	0.132	3862	371
Cfb (Strasbourg)	0.244	0.214	12.3	0.28	260	0.330	North	0.151	0.152	5573	354
Cwb (Kunming)	0.160	0.219	7.3	0.22	250	0.330	North	0.222	0.148	1576	287
Csb (Vigo)	0.196	0.187	13.2	0.20	264	0.330	North	0.185	0.171	1674	298
Cfa (Milan)	0.231	0.223	16.1	0.28	251	0.330	North	0.159	0.146	5868	349
Cwa (Hanzhong)	0.232	0.203	8.4	0.32	255	0.328	North	0.159	0.159	5844	334
Csa (Evora)	0.235	0.224	19.2	0.20	261	0.330	North	0.157	0.145	2900	363
BWk (Birjand)	0.197	0.133	5.0	0.20	251	0.330	North	0.184	0.230	9000	265
BSk (Quetta)	0.223	0.185	12.0	0.20	250	0.330	North	0.165	0.173	7308	322
Bsh (Lahore)	0.249	0.219	16.3	0.20	256	0.330	South	0.149	0.148	10826	368
Bwh (Dubai)	0.232	0.203	20.0	0.20	250	0.330	South	0.159	0.159	16195	342
Af (Singapore)	0.250	0.167	13.4	0.20	251	0.330	South	0.148	0.189	17933	334
Aw (Mumbai)	0.247	0.176	19.2	0.20	253	0.330	South	0.150	0.180	15757	338
Am (Jakarta)	0.232	0.215	5.0	0.20	250	0.330	North	0.159	0.151	13503	350

Table 5-5: Comparison of design parameters based on degree days

Category		U_w (W/m²K)	U_r (W/m²K)	WWR	α (degree)	IT_H (W)
HDD_{18} >3500	Range	0.15-0.156	0.136-0.164	0.31-0.4	5.25-15.45	255-289
	Mean	0.152	0.144	0.362	11.192	278
	STD	0.003	0.013	0.040	3.505	11.90
3500> HDD_{18} >2000	Range	0.15-0.169	0.138-0.178	0.22-0.4	5.23-16.15	250-304
	Mean	0.156	0.153	0.297	11.599	261
	STD	0.007	0.015	0.061	3.789	19.62
3500> CDD_{10} >2000	Range	0.159-0.185	0.145-0.173	0.2-0.32	5.01-19.21	25-264
	Mean	0.179	0.171	0.224	10.859	255
	STD	0.024	0.031	0.048	5.083	6.04
CDD_{10} >3500	Range	0.149-0.159	0.148-0.189	0.2	5-20	250-256
	Mean	0.153	0.165	0.201	14.772	252
	STD	0.006	0.018	0.001	6.042	2.65

5.1.3 Effect of design optimization on energy flexibility

The optimized building envelope substantially improved energy flexibility by delivering flexible heating and cooling loads in cold and hot climate zones. The PMV index ranged between -0.5 and 0.5 throughout the year, or the PPD was below 10% for each case, which complied with the recommended thermal comfort level of ASHRAE standard 55. During MOO, design parameters were modified continuously for the subsequent evaluation until the desired outcome was achieved. Therefore, it could be challenging to explicitly predict how a particular design parameter influenced the objective functions. However, the combined impact of improved envelope design was evident by flexible thermal loads. Total building thermal load was the sum of infiltration losses/gains, transmission losses/gains, equipment gains, occupancy gains, solar gains, heating gains, and cooling losses. The passive design of the building was particularly effective for energy exchange through the envelope by infiltration, transmission, and solar radiation. Thus, this study evaluated the variation in those thermal loads in the investigated climates, as shown in Figure 5-2. The clustered columns represent the heat exchange through the building envelope for the base case and optimal envelope design of the household. While the scatter plots show the shift in those thermal loads after optimization on the secondary vertical axis. For transmissions and infiltration phenomena, the net effect for heat gain during summer and heat loss during winter in a location is plotted. The findings of the optimization strategy indicated that envelope insulation, window shading, and WWR were the most influential design parameters for household energy flexibility. On the contrary, solar radiation-based window shading control and window aperture (α) for passive ventilation did not significantly impact the flexible thermal load.

The optimal design increased the solar heat gains through windows (QSHG) in continental climates besides Dsa (Arak) and Dfb (Stockholm). Whereas in temperate climates, solar gains slightly increased or decreased depending upon the space cooling demand of the location. In the case of tropical and dry climates, the QSHG was always reduced after optimization. Furthermore, the optimal passive design decreased transmission losses during winter and transmission gains in summer. Thus, the net effect lowered the transmission heat exchange (Qtrans) after optimization in all locations. On the other hand, the change in heat exchange due to infiltration (Qinf) was insignificant in cold and hot climates. However, it avoided overheating in winter or lowered the cooling demand in summer to some extent through passive cooling. The following sections describe the energy flexibility of the architecture upgradation in the

household, computed using Eq. 3.6, in four major climate zones of the Köppen-Geiger classification.

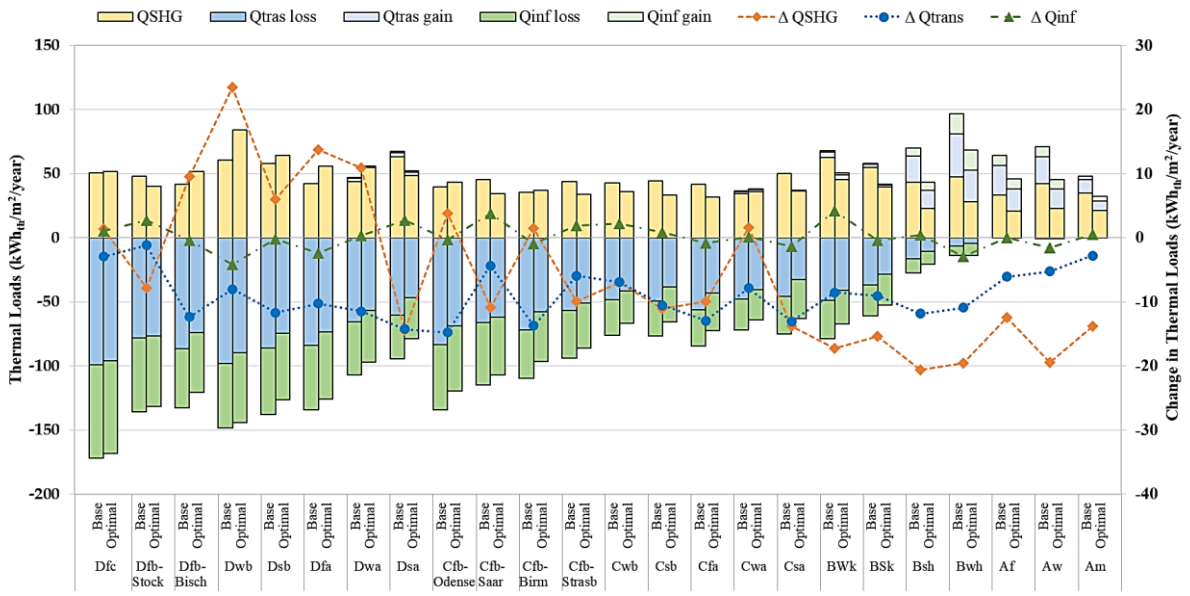

Figure 5-2: Household's thermal loads for the base case and energy-optimal scenarios

5.1.3.1 Continental climate

The continental climate has the temperature of the coldest month below 0 °C and the temperature of the hottest month greater than 10 °C. Therefore, the locations in this zone are heating-dominant besides the hot and dry summer continental climate (Dsa). Even though the cooling energy demand was very low, the optimization reduced it substantially. Figure 5-3 compares the reference and optimal household heating and cooling energy demands and illustrates the energy flexibility achieved through optimization. On average, the flexible thermal load was 2853 kWh_{th}/year in continental climate regions. The Daocheng (Dwb) was the location with a maximum flexible heating load of 3844 kWh_{th}/year. However, the optimization resulted in a negative flexible cooling load of -101 kWh_{th}/year. As a matter of fact, energy flexibility depends upon the current practices of building energy standards. For example, the optimization strategy did not depict significant flexibility potential in Dfc (Oestersund) and Dfb (Stockholm). This phenomenon was due to the energy-efficient envelope standards in those locations. On the other hand, the flexible heating load was quite prominent in locations with high heating demand. It can be observed that the flexible heating load decreased in Beijing (Dwa) and Arak (Dsa), but contrarily, the flexible cooling load was higher than in other locations. The maximum flexible load of 3921 kWh_{th}/year was achieved in Beijing (Dwa).

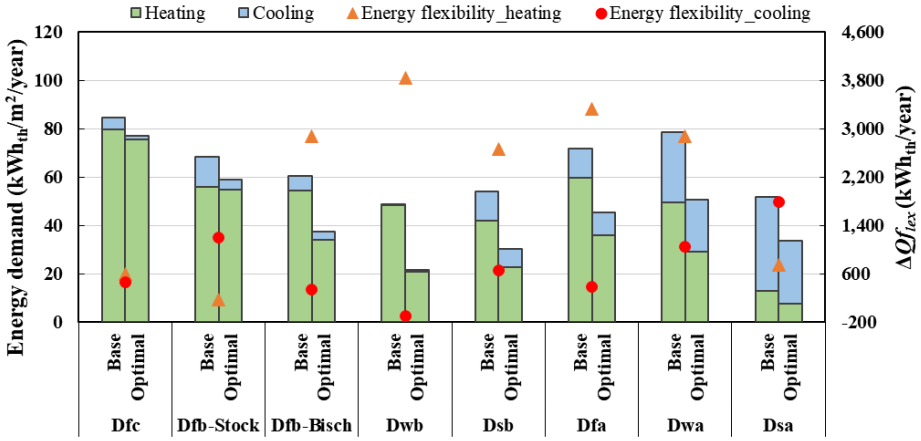

Figure 5-3. Heating and cooling loads and respective flexible thermal loads in continental climate

5.1.3.2 Temperate climate

The temperate climate is characterized by the coldest month's average temperature between 0 °C and 18 °C and at least one month's average above 10 °C. Figure 5-4 shows the energy demand of the reference building and the energy demand and flexible thermal loads after optimization. The investigated locations showed a mixed trend for space heating and cooling dominance. Contrary to the continental climate, the space cooling demand was relatively higher in temperate climates. The average flexible loads for space heating and cooling were 905 kWh_{th}/year and 1046 kWh_{th}/year, respectively. Similar to Dfc (Oestersund) and Dfb (Stockholm), the flexible heating load was small in Saarbrücken (Cfb) due to the well-insulated building envelope.

Further, the flexible thermal load was relatively small in locations having lower heating and cooling demands, as in the cases of Kunming (Cwb) and Vigo (Csb). Odense (Cfb) showed the highest flexible heating load of 2377 kWh_{th}/year, and the heating demand reduced to 42.59 kWh_{th}/m^2a after optimization. The maximum energy flexibility for cooling was achieved in Evora (Csa), having a flexible cooling load of 1918 kWhth/year and a cooling demand of 14.8 kWh_{th}/m^2a. The optimization strategy also showed that a higher flexible heating load was achieved in heating-dominant locations and a higher flexible cooling load in cooling-dominant locations. Milan (Cfa) was the location with a maximum flexible thermal load of 2714 kWh_{th}/year due to the poor envelope insulation in the reference building.

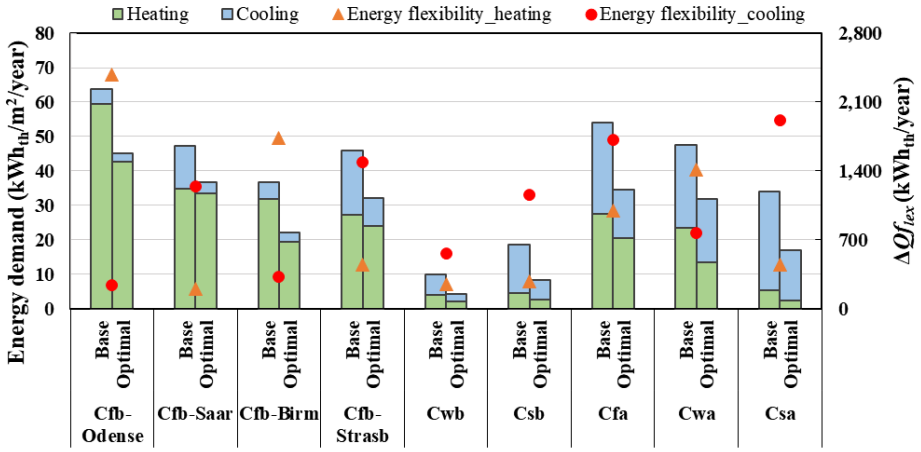

Figure 5-4. Heating and cooling loads and respective flexible thermal loads in temperate climate

5.1.3.3 Dry climate

The dry climate is defined by very little precipitation during the year. Moreover, it has two subgroups based on the mean average temperature, hot: MAT ≥ 18 °C and cold: MAT < 18 °C. Consequently, the locations in this zone have long summer and shortened winter seasons. The design optimization was equally effective in cooling-dominant climates, as shown in Figure 5-5. The flexible thermal load in dry climates was 3758 kWh_{th}/year on average for space cooling. The maximum cooling demand was 142.34 kW_{th}/m^2a in the hot desert climate of Dubai (BWh), which also had a maximum flexible thermal load of 5998 kWh_{th}/year. The energy flexibility for the heating load was not very significant in dry climates because these locations had only space cooling or very low space heating demand. However, the flexible cooling load increased with increasing cooling demand. Another factor for larger flexibility potential in these locations was the poorly-insulated envelope in reference cases.

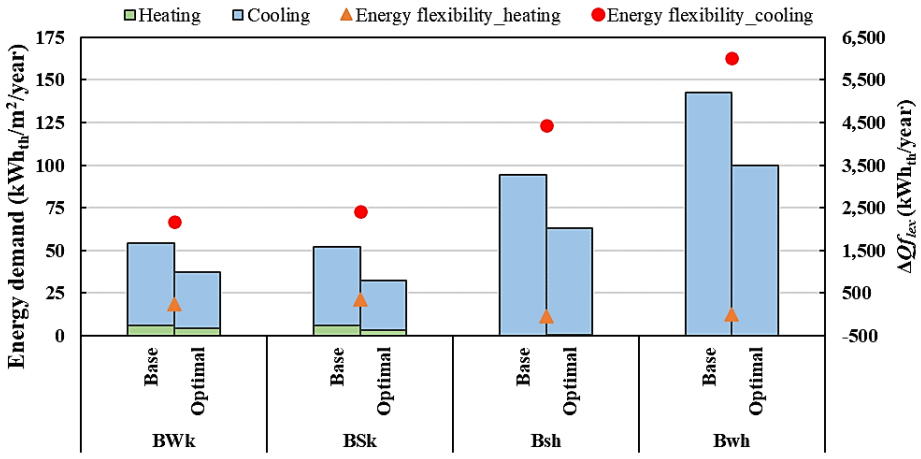

Figure 5-5. Heating and cooling loads and respective flexible thermal loads in dry climate

5.1.3.4 Tropical climate

In a tropical climate, the average temperature of every month is 18 °C or higher, with year around significant precipitation. High humidity throughout the year is another prominent feature of this climate. Therefore, there was no space heating load in this climate or such low to be negligible. Nevertheless, the space cooling load was very high, and the total thermal load was the largest of all investigated locations in the tropical climate. The space cooling loads for three representative tropical climates and energy flexibility through design optimization are presented in Figure 5-6. The space cooling demand in Jakarta's tropical-monsoon climate (Am) was the lowest due to the higher precipitation, resulting in a minimum flexible cooling load of 3490 kWh_{th}/year. The highest flexible load was 4870 kWh_{th}/year in Mumbai, a tropical savanna climate (Aw). The average flexible cooling load amounted to 3981 kWh_{th}/year, the maximum of all climate zones.

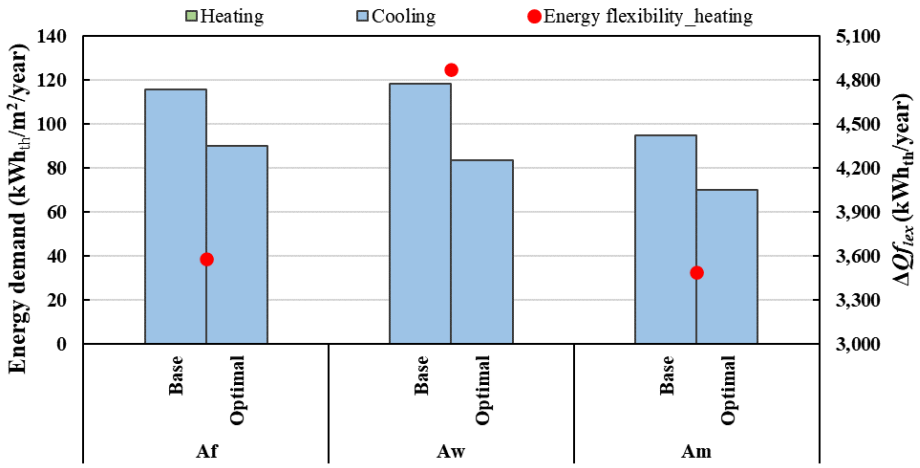

Figure 5-6. Heating and cooling loads and respective flexible thermal loads in tropical climate

5.1.4 Benchmarking of envelope parameters

The envelope optimization delivered flexible annual thermal loads in all investigated locations. Interestingly, building design optimization not only increased energy flexibility but also significantly reduced the operational cost of the building. Since the operating cost of a building depends upon the type of equipment, energy supply system, and local energy prices, the monetary savings from design optimization would vary in each location. Table 5-6 presents criteria for choosing the envelope parameters according to the degree days in various climate zones. Though this criterion was based on the investigation in twenty-four locations in major climate zones, its authenticity was justified by achieving the optimal solution from a large number of simulations, i.e., 5000, in each location. The design parameters are strongly related

to each other. Therefore, adopting an individual parameter to achieve a flexible thermal load is not advisable.

Table 5-6: Ranges of optimal design parameters and degree days in different climate zones

	Continental			**Temperate**		**Dry**		**Tropical**	
	cold	**warm summer**	**hot summer**	**warm summer**	**hot summer**	**cold**	**hot**	**Rainforest/ Savanna**	**monsoon**
HDD18	5468	3496 - 3922	2320 - 3523	1137 - 3364	1404 - 2099	1182 - 1693	0 -348	0	0
CDD10	429	378 - 1305	1430 - 2523	835 - 2204	2115 - 2589	3052 - 3312	5382 - 6910	6594 - 6782	6045
EPSThk (m)	0.247	0.234 - 0.247	0.216 - 0.245	0.160 - 0.246	0.231 - 0.238	0.197 - 0.223	0.232 - 0.249	0.247 - 0.25	0.232
RockwoolThk (m)	0.211	0.188 - 0.241	0.187 - 0.239	0.187 - 0.249	0.203 - 0.227	0.133 - 0.185	0.203 - 0.219	0.167 - 1.176	0.215
Uw (W/m2K)	0.15	0.150-0.157	0.150-0.169	0.150-0.222	0.157-0.159	0.165-0.184	0.149-0.159	0.148-0.150	0.159
Ur (W/m2K)	0.154	0.136-0.170	0.138-0.178	0.132-0.171	0.145-0.159	0.173-0.230	0.148-0.159	0.180-0.189	0.151
α (degree)	9.8	5.2 - 11	5.2 - 16.1	7.3 - 13.2	8.4 - 17	5 - 12	16.3 - 20	13.4 - 19.2	5
WWR	0.37	0.33 - 0.4	0.2 - 0.4	0.2 - 0.34	0.2 - 0.32	0.2	0.2	0.2	0.2
IT_H (W)	279	255 - 289	251 - 277	250 - 304	251 - 255	250 - 251	250 - 256	251 - 253	250
Shd_{Dec}	0.329	0.253 - 0.33	0.33	0.327 - 0.33	0.328 - 0.33	0.33	0.33	0.33	0.33
Orientation	North	North	North	North	North	North	South	South	North

The continental-cold climate was represented by maximum HDD. So, it needed high EPS thickness of 0.247 and a rockwool thickness of 0.211, resulting in a low thermal transmittance of 0.15 W/m^2K for the envelope. It was also characterized by large WWR, IT_H, and Shd_{Dec}. The continental-warm and continental-hot climates showed a similar pattern for design variables, but their ranges dropped with the decrease in HDD and increasing CDD. Furthermore, the window aperture angle needed to be increased from continental-cold to continental-hot climate. Regarding the orientation, the North faced household was the optimum choice in the continental climate zone.

The dominant thermal load in the temperate zone was space heating. Therefore, it also required a high level of insulation and, consequently, lower thermal transmittance of the envelope. Interestingly, the lower limits of insulation materials and U-values were higher in the temperate-hot summer zone than in the temperate-warm summer zone, and the upper limits were low. The reason was that the lower limit of HDD was high, but the upper limit of HDD was small in this climate zone. Also, the temperate-hot summer zone had higher CDD. Moreover, the design variables responsible for solar gains should be adjusted to minimize the solar heat gain, i.e., the ranges of WWR and IT_H decreased, and the Shd_{Dec} range increased in the temperate zone. The optimal orientation was North, the same as the continental climate zone.

In the dry-cold zone, neither cooling nor heating was the dominant thermal load. As a result, the HDD and CDD were in the same range and had relatively low values. The recommended

range of insulation materials was 0.197-0.223 m for EPS and 0.133-0.185 m for rockwool. Similarly, the U-values of the external wall and roof had relatively higher ranges of 0.165-0.184 W/m^{2}K and 0.173-0.230 W/m^{2}K, respectively. The window aperture angle was also smaller compared to the temperate climate. The WWR and IT_H needed to be kept at a minimum, and Shd_{Dec} was maximized to restrict the solar gains. The optimal orientation was North in the dry-cold zone. On the other hand, the dry-hot climate was represented by a higher cooling load and CDD. The optimal solution set was also quite different from a dry-cold climate. The recommended thermal transmittance of the envelope was lower than in dry-cold temperate climate zones, and the window aperture angle ranged to its upper limit. The optimal orientation also changed to the South in a dry-hot climate. Nevertheless, other design variables were the same as in the dry-cold climate.

The tropical zone consisted of cooling-dominant locations, and the CDD were above 3000. The values of WWR, IT_H, and Shd_{Dec} followed the same trend as in other cooling-dominant climates. In Af and Aw climate zones, the recommended EPS insulation was the maximum of all climates and thus had the minimum thermal transmittance range, i.e., 0.148-0.150 W/m^{2}K. However, the thermal transmittance of the roof required a comparatively higher range of 0.180-0.189 W/m^{2}K. The Am climate had lesser CDD than other tropical climates and required a relatively lower level of envelope insulation. The recommended U-value of the external wall was 0.159 W/m^{2}K, and it was 0.151 W/m^{2}K for the roof. The aperture angle was 5 degrees in Am climate due to higher humidity levels throughout the year. The households were South-faced in Af and Aw climates to attain a high flexible thermal load, whereas Am climate had an optimal orientation of North.

5.2 Flexible building energy system

As described in sections 3.2 & 4.2, fourteen BES configurations were modeled for year around simulations in four different climate conditions. These alternatives differed from each other w.r.t the share of RESs and heating/cooling service systems. MCDM was employed on energy system alternatives with $f_{sav,NRE}$, γ_{load}, *LCEs*, NPV_{25}, *PPD*, $LCOE_{el}$, and $LCOE_{th}$ as EFIs. The flexibility strategy was implemented in four locations: STK (severe cold), SBK (clod), QTA (mild), and JKT (hot and humid). The weather data and energy demand of the representative household are summarized in Table 5-7. At this, the envelope parameters were upgraded according to the findings of building architecture flexibility in section 5.1, as described in Table 5-8.

Table 5-7: weather conditions and energy demand in investigated locations

Country	Location	Köppen Climate	IECC Climate	$T_{amb,avg}$ (°C)	IT_H (kWh/m²a)	HDD_{18}	CDD_{10}	Electricity Consumption (kWh/m² a)	Sensible space heating load (kWh_{th}/m² a)	Sensible space cooling load (kWh_{th}/m² a)
Sweden	STK	Dfb	5 A	7.4	899.8	3922	841	30.20	54.63	3.47
Germany	SBK	Cfb	5 A	9.8	1141	3119	1074	34.36	33.36	4.18
Pakistan	QTA	BSk	3 A	17.9	2041.2	1182	3312	22.19	3.39	19.01
Indonesia	JKT	Am	1 A	26.6	1760.9	0	6045	18.40	0	69.87

Table 5-8: Thermo-physical properties of building envelope in investigated locations

Element	Layer	Stockholm (Dfb)		Saarbrucken (Cfb)		Quetta (BSk)		Jakarta (Am)	
		Thickness (m)	U-Value (W/m² K)	Thickness (m)	U-Value (W/m² K)	Thickness (m)	U-Value (W/m² K)	Thickness (m)	U-Value (W/m² K)
External wall	plaster inside	0.015	0.156	0.015	0.151	0.015	0.165	0.015	0.159
	Brick	0.210		0.210		0.210		0.210	
	EPS (expanded polystyrene)	0.237		0.245		0.223		0.232	
	plaster outside	0.003		0.003		0.003		0.003	
Floor	Wood	0.015	0.649	0.015	0.649	0.015	0.649	0.015	0.649
	plaster floor	0.080		0.080		0.080		0.080	
	sound insulation	0.040		0.040		0.040		0.040	
	Concrete	0.150		0.150		0.150		0.150	
Roof ceiling	gypsum board	0.025	0.164	0.025	0.139	0.025	0.173	0.025	0.151
	Plywood	0.015		0.015		0.015		0.015	
	Rockwool	0.196		0.235		0.185		0.215	
	Plywood	0.015		0.015		0.015		0.015	
Internal wall	Clinker	0.200	0.885	0.200	0.885	0.200	0.885	0.200	0.885
Window-to-wall ratio (South wall)	double glazed		0.31		0.24		0.20		0.20

5.2.1 Design parameters of BESs

The energy supply mixes were combinations of grid supply, PV generation with battery storage, FPC, and/or geothermal energy. The size of the PV system was calculated using Eq. 3.3, and it depended on the available solar radiation and rooftop area. The PV area and battery storage capacity were modified accordingly in alternatives having FPC. Since solar radiations were low in heating-dominant climates, the required PV power was 7.69 kW in STK and SBK, respectively. In contrast, solar radiations were substantially higher in QTA and JKT, which resulted in smaller installed PV power in those locations. Table 5-9 provides the installed PV system capacity and FPCs' area for different BESs in investigated climates.

Table 5-9: Installed capacity of PV system and FPCs in alternative energy systems

Location	Energy system alternative	P_{PV} (kW)	A_{PV} (m²)	Battery Capacity[1] (Wh)	A_{FPC} (m²)	Tilt angle (degree) [193]
STK	A3, A4, A5, A9, A12, A13	4.62_2	30	4320	20	41
	A1, A2, A6, A10, A11	7.69	50	5760	0	
SBK	A3, A4, A5, A9, A12, A13	4.62_2	30	4320	20	32
	A1, A2, A6, A10, A11	7.69	50	5760	0	
QTA	A3, A4, A5, A9, A12, A13	3.85	25	2880	20	30
	A1, A2, A6, A10, A11	3.85	25	2880	0	
	A7, A8	3.10_2	20	2880	30	

Location	Energy system alternative	P_{PV} (kW)	A_{PV} (m^2)	Battery Capacity[1] (Wh)	A_{FPC} (m^2)	Tilt angle (degree) [193]
JKT	A3, A4, A5, A9, A12, A13	4.62	30	4320	20	
	A1, A2, A6, A10, A11	4.62	30	4320	0	10
	A7, A8	2.31[2]	15	2880	35	

[1] The battery capacity is determined to keep the average FSOC of 0.45 by controlling the lower limit of discharge for the battery life of 6.5 years [159].

[2] The installed PV power is less than the required power due to the limitation of the available rooftop area.

The borehole lengths of GSHPs were computed using Eqs. 3.4&3.5 for peak cooling and heating load, respectively. The thermal properties of the ground soil were assumed to be the same in all locations. A specific heat capacity of 0.8 kJ/kgK, the ground thermal conductivity of 2 W/mK, and a thermal gradient of 0.025 K/m were used [129]. The larger of the two lengths was the required borehole length. The borehole lengths with respective design conditions and peak loads are presented in Table 5-10. STK was the location with the maximum peak load of space heating and was associated with a large borehole length of 99.29 m. The borehole length decreased to 66.46 m in SBK due to a smaller peak load. In cooling-dominant locations, though the peak load was much lower than STK and SBK, the borehole lengths were comparatively large due to the higher undisturbed ground temperature. In the case of JKT, the ground temperature was 27 °C, and the required borehole length (150 m) was the maximum of all locations.

Table 5-10: Length of borehole and design conditions of BHX

Location	L_c (m)	L_h (m)	t_g (°C)	$t_{wo,heating}$ (°C)	$t_{wo,cooling}$ (°C)	Flow rate heating (kg/h)	Flow rate cooling (kg/h)	Design load heating (kW)	Design load cooling (kW)
STK	29.59	99.29	7.84	-5	30	1590	681	5.43	1.88
SBK	35.62	66.46	10.14	-5	30	1136	681	4.55	1.94
QTA	89.53	20.42	18.27	-5	30	908	908	2.69	2.80
JKT	150	-	27	-	35	-	908	-	2.81

The heating and cooling capacities of HVAC systems were specified according to the peak loads in the location. The performance mapping of HVAC equipment was realized based on the flow rate and entering temperature of the fluid at the source and/or load sides of HPs at the peak load, as explained in section 4.2.1. According to the design load and performance ratings, the operating ranges in performance data files of HVAC systems are listed in Table 5-11.

Table 5-11: Design capacities and flowrates of HVAC systems

Location	Elements	Operational parameters
STK	• B/WHP	TH range: 3.44 – 7.68 kW, TC range: 1.18 – 2.56 kW, the flow rate of source and load sides: 680-1590 kg/h Performance rating (AHRI/ISO 13256-2): COP = 3.1, EER = 16.6
	• B/AHP	TH range: 3.86 – 8.09 kW at source flow rate: 684 – 1590 kg/h and airflow: 1047 – 1449 kg/h TC range: 2.31 – 3.05 kW, SC range: 1.55 – 2.08 kW at source flow rate: 454 – 908 kg/h and airflow: 624 – 840 kg/h Performance rating (AHRI/ISO 13256-1): COP = 3.8, EER = 18.6
	• A/WHP	TH range: 2.76 – 5.96 kW, TC range: 1.18 – 2.56 kW Performance rating: $COP_{heating}$ = 3.58 at Ta DB/WB 7ºC/6ºC - LWC 45ºC (dT = 5ºC), $COP_{cooling}$ = 2.32 at Ta 35ºC - LWE 7ºC (dT = 5ºC)
	• A/AHP	TH range: 2.39 – 5.63 kW at airflow: 819 – 1002 kg/h TC range: 1.85 – 3.02 kW, SC range: 1.030.8 – 2.27 kW, airflow: 455 – 553 kg/h Performance rating (AHRI 210/240): HSPF = 10.5, SEER = 20.5
SBK	• B/WHP	TH range: 3.44 – 7.68 kW, TC range: 1.18 – 2.56 kW, the flow rate of source and load sides: 680-1136 kg/h Performance rating (AHRI/ISO 13256-2): COP = 3.1, EER = 16.6
	• B/AHP	TH range: 3.86 – 8.09 kW at source flow rate: 684 – 1136 kg/h and airflow: 1047 – 1449 kg/h TC range: 2.31 – 3.05 kW, SC range: 1.55 – 2.08 kW at source flow rate: 454 – 908 kg/h and airflow: 624 – 840 kg/h Performance rating (AHRI/ISO 13256-1): COP = 3.8, EER = 18.6
	• A/WHP	TH range: 2.76 – 5.96 kW, TC range: 1.18 – 2.56 kW Performance rating: $COP_{heating}$ = 3.58 at Ta DB/WB 7ºC/6ºC - LWC 45ºC (dT = 5ºC), $COP_{cooling}$ = 2.32 at Ta 35ºC - LWE 7ºC (dT = 5ºC)
	• A/AHP	TH range: 2.39 – 5.63 kW at airflow: 819 – 1002 kg/h TC range: 1.85 – 3.02 kW, SC range: 1.030.8 – 2.27 kW, airflow: 455 – 553 kg/h Performance rating (AHRI 210/240): HSPF = 10.5, SEER = 20.5
QTA	• B/WHP	TH range: 1.72 – 3.84 kW, TC range: 1.56 – 3.4 kW, the flow rate of source and load sides: 454 – 908 kg/h Performance rating (AHRI/ISO 13256-2): COP = 3.1, EER = 16.6
	• B/AHP	TH range: 2.32 – 4.56 kW at source flow rate: 454 – 908 kg/h and airflow: 624 – 832 kg/h TC range: 2.31 – 3.05 kW, SC range: 1.55 – 2.08 kW at source flow rate: 454 – 908 kg/h and airflow: 624 – 840 kg/h Performance rating (AHRI/ISO 13256-1): COP = 3.8, EER = 18.6
	• A/WHP	TH range: 1.86 – 4.02 kW, TC range: 1.56 – 3.24 kW Performance rating: $COP_{heating}$ = 3.58 at Ta DB/WB 7ºC/6ºC - LWC 45ºC (dT = 5ºC), $COP_{cooling}$ = 2.32 at Ta 35ºC - LWE 7ºC (dT = 5ºC)
	• A/AHP	TH range: 1.33– 3.13 kW at airflow: 455 – 553 kg/h TC range: 1.85 – 3.02 kW, SC range: 1.030.8 – 2.27 kW, airflow: 455 – 553 kg/h Performance rating (AHRI 210/240): HSPF = 10.5, SEER = 20.5
	• Absorp. chiller	A capacity of 3 kW heat rejection from chilled water with a 7.2 kW cooling tower. Performance rating: COP = 0.7 at a hot water temperature of 90 °C
JKT	• B/WHP	TC range: 1.72 – 3.84 kW, the flow rate of source and load sides: 454 – 908 kg/h Performance rating (AHRI/ISO 13256-2): EER = 16.6
	• B/AHP	TC range: 2.31 – 3.05 kW, SC range: 1.55 – 2.08 kW at source flow rate: 454 – 908 kg/h and airflow: 624 – 840 kg/h Performance rating (AHRI/ISO 13256-1): EER = 18.3
	• A/WHP	TC range: 1.56 – 3.24 kW Performance rating: $COP_{cooling}$ = 2.32 at Ta 35ºC - LWE 7ºC (dT = 5ºC)
	• A/AHP	TC range: 1.85 – 3.02 kW, SC range: 1.030.8 – 2.27 kW, airflow: 455 – 553 kg/h Performance rating (AHRI 210/240): SEER = 20.5
	• Absorp. chiller	A capacity of 3 kW heat rejection from chilled water with a 7.2 kW cooling tower. Performance rating: COP = 0.7 at a hot water temperature of 90 °C

Note: TH is total heating, TC is total cooling, SC is sensible cooling, absorp. Chiller stands for absorption chiller, COP is coefficient of performance, Ta is air temperature, DB is the dry bulb, WB is the wet bulb, LWE is leaving water evaporator, and LWC is leaving water condenser. AHRI/ISO 13256-2: entering source at 25 °C and entering load at 12 °C for cooling, entering source at 0 °C and entering load at 40 °C for heating. AHRI/ISO 13256-1: entering source at 25 °C for cooling, entering source at 0 °C for heating. AHRI 210/240: 26.66 °C entering air temperature and 50% RH for cooling, 21.11 °C entering air temperature, and 50% RH for heating.

5.2.2 Energy flexibility assessment

5.2.2.1 Non-renewable energy savings

This EFI determined the alternatives' non-renewable primary energy ratio and non-renewable energy savings. Table 5-12 describes the energy output of BES and the grid's electricity supply for fourteen different BES in four locations. All alternative BESs fulfilled the energy demand for heating, cooling, and DHW supply. However, the electricity requirement from the grid was dependent on available solar potential, the size of the PV system and FPCs, and the power demand of HVAC equipment. The energy demand of BES was maximum for the base case because of the higher power demand of air-to-air HP and auxiliary water heating in TES. The alternatives with brine-to-water HP (A1-A4) required less grid electricity in cold climates. For the case of hot climates, the alternatives having an absorption chiller (A7&A8) utilized the least grid electricity. The same trend was observed for *PER* and $f_{sav,NRE}$, as evident in Figure 5-7. The alternative A3, an energy system having B/WHP and FPCs with radiator heating and ventilation cooling, achieved maximum flexibility with *PER* of 0.84 and $f_{sav,NRE}$ of 0.53 in STK. In SBK, the alternative A1 was the most flexible BES having *PER* and $f_{sav,NRE}$ as 0.82 of 0.57, respectively. Conversely, The BES with absorption chiller was a flexible option having maximum values of 0.80 and 0.82 for $f_{sav,NRE}$ in QTA and JKT, respectively. Since there was no space heating demand in JKT, the alternatives with radiator and hot water coils were treated the same. The alternative A7/8 attained the highest *PER*, 3.11, in JKT. The higher solar radiation and, consequently, higher power and heat supply from PV systems and FPCs in QTA and JKT relative to other locations resulted in a greater flexibility potential for *PER* and $f_{sav,NRE}$.

Table 5-12: Thermal energy output from energy system and grid electricity to building

	STK				SBK				QTA				JKT		
Alternatives	Q_{heat}	Q_{cool}	Q_{DHW}	Pel_{grid}	Q_{heat}	Q_{cool}	Q_{DHW}	Pel_{grid}	Q_{heat}	Q_{cool}	Q_{DHW}	Pel_{grid}	Q_{cool}	Q_{DHW}	Pel_{grid}
Base case	56.20	2.88	2030	10300	39.89	3.14	2001	10175	2.99	18.98	1458	6996	73.60	954	8255
A1	56.02	2.49	2139	4773	35.81	3.64	2011	3808	3.22	17.83	1458	2844	74.23	963	3516
A2	58.56	2.81	2138	5181	40.66	3.99	2011	4541	2.87	17.43	1486	2870			
A3	56.02	2.49	2146	4618	35.8	3.72	2021	4141	3.24	17.88	1576	1987	77.47	1101	2602
A4	58.42	2.81	2147	5130	40.62	4.07	2021	4691	2.74	17.45	1577	1964			
A5	56.97	3.06	2123	5920	36.46	3.82	1985	4824	3.04	20.9	1560	2178	77.60	1101	2546
A6	58.80	3.20	2047	6389	37.42	3.75	1996	5321	3.07	20.84	1590	3692	77.09	961	3444
A7	–	–	–	–	–	–	–		2.81	21.98	1503	1373	69.86	1101	1468
A8	–	–	–	–	–	–	–		3.22	21.98	1503	1452			
A9	56.73	2.88	2086	5875	37.64	4.03	1985	5810	2.97	19.4	1561	2176	73.67	1100	4124
A10	56.20	2.43	2143	5248	35.83	3.73	2014	4884	3.22	18.5	1499	3223	75.53	988	3733
A11	61.43	2.69	2139	5734	34.96	4.03	2007	5437	2.97	19.69	1499	3135			
A12	56.20	2.43	2148	5506	36.12	3.49	2020	5081	3.00	18.57	1577	2142	75.29	1096	2935

	STK				SBK				QTA				JKT		
Alternatives	Q_{heat}	Q_{cool}	Q_{DHW}	Pel_{grid}	Q_{heat}	Q_{cool}	Q_{DHW}	Pel_{grid}	Q_{heat}	Q_{cool}	Q_{DHW}	Pel_{grid}	Q_{cool}	Q_{DHW}	Pel_{grid}
A13	61.43	2.69	2150	6315	35.30	3.72	2020	5329	3.00	18.5	1577	2157			

Note: Q_{heat} (sensible heating load) and Q_{cool} (sensible cooling load) are given in kWh_{th}/m^2a, Q_{DHW} is given in kWh_{th}/a, and Pel_{grid} (grid electricity) is given in kWh/a

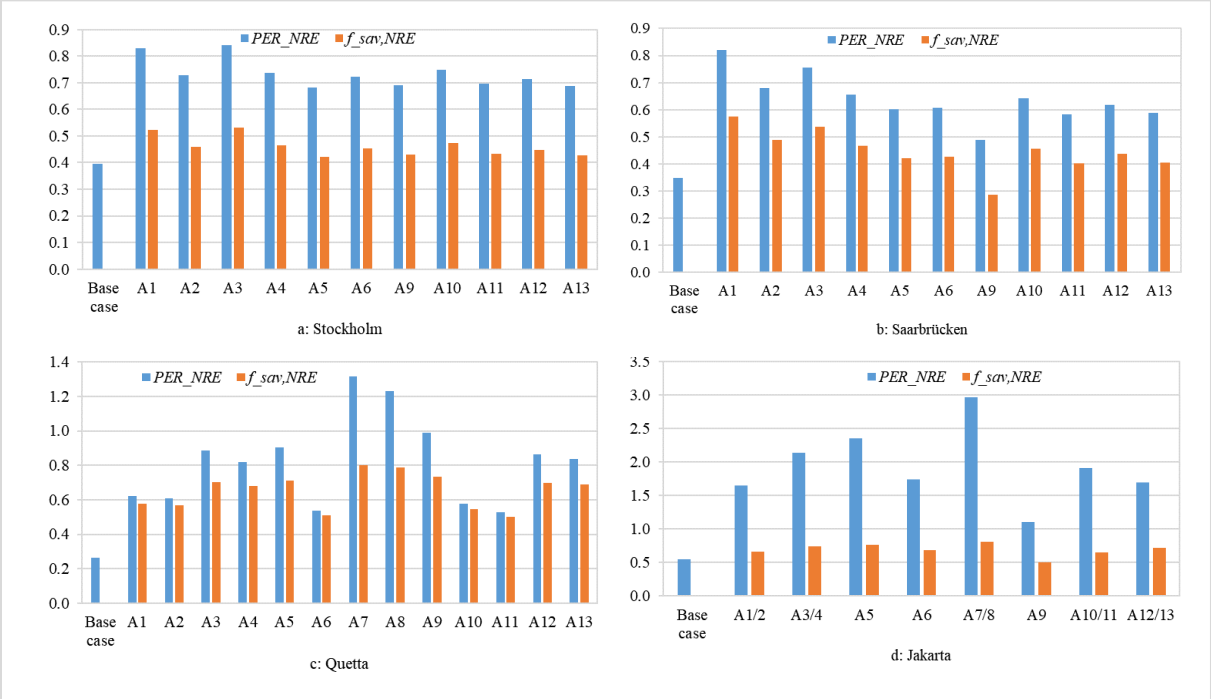

Figure 5-7: Primary energy ratio (PER_{NRE}) and Non-renewable energy saving ($f_{sav,NRE}$) of alternative energy systems. a) Stockholm, b) Saarbrücken, c) Quetta, d) Jakarta

5.2.2.2 Load cover factor

The load cover factor computed the fraction of electricity load covered by the on-site electricity generation. This indicator quantified the generation flexibility. The flexibility depended on the size of the PV system and the energy consumption of the building. The BESs with an electric heater like base case and A6 required more electricity to meet the energy demand. On the other hand, the brine-to-water HP utilized less electricity than other HVAC equipment, excluding the absorption chiller. As a result, the electricity consumption of the energy system was the lowest for BESs having brine-to-water HP in heating-dominant locations. However, the electricity load of BESs having brine-to-water HP increased in QTA. The fact was due to the electric heating in TES for DHW during the cooling hours. Moreover, the minimum electricity demand was noticed for energy systems with an absorption chiller in QTA and JKT. From Figure 5-8, it can be observed that the flexible energy system configurations were A1 (STK), A1 (SBK), A7 (QTA), and A7/8 (JKT), respectively, to reduce the dependence on grid networks. The load cover factor had a value of 0.44, 0.50, 0.65, and 0.66 in those four locations for the mentioned BES.

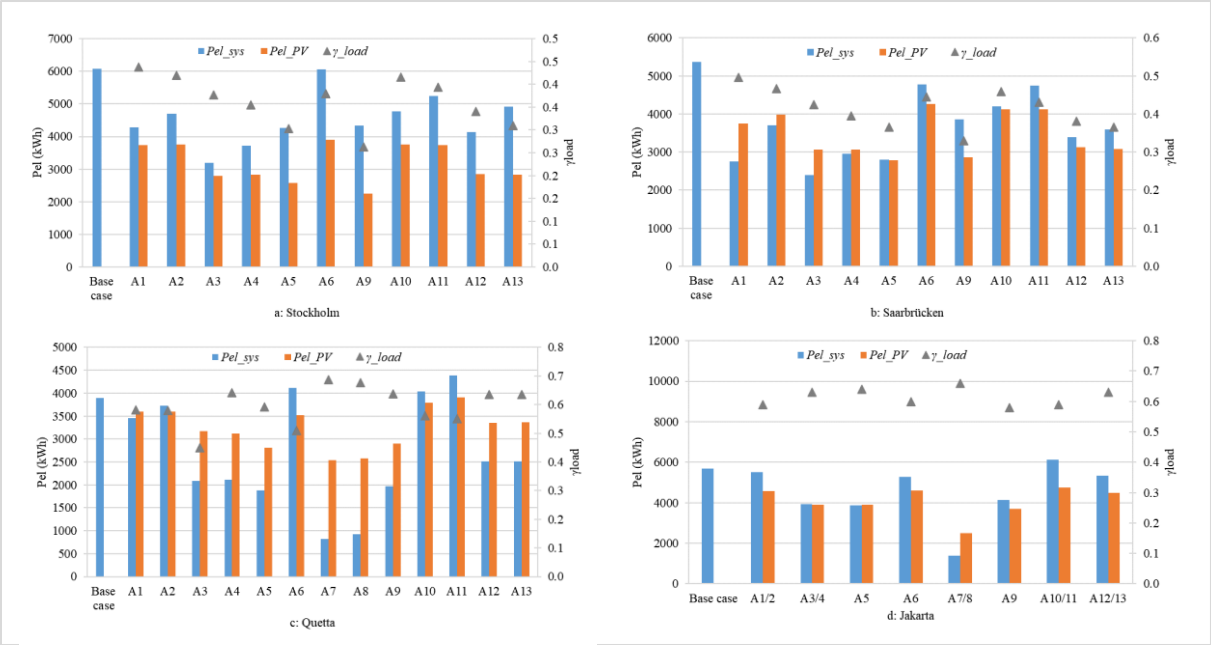

Figure 5-8: Electricity load (Pel_{sys}), PV supply (Pel_{PV}), and load cover factor (γ_{load}) of alternative energy systems. a) Stockholm, b) Saarbrücken, c) Quetta, d) Jakarta

5.2.2.3 Life-cycle emissions

The CO_2 emissions for the life cycle of each BES alternative are given in Table 5-13. The most critical elements in LCEs were the emissions from the utility grid and the emissions released during energy system manufacturing. In STK, the CO_2 emissions of the utility grid were much lower than in the other three cities. Hence, the LCEs were produced between 3000 kg CO_2eq and 4243 kg CO_2eq for various BESs. The LCEs reached 126457 kg CO_2eq for the base case in JKT due to higher electricity demand and CO_2 emissions. The LCEs ranged from 31809 kg CO_2eq to 80263 kgCO_2eq and 20205 kgCO_2eq to 99744 kgCO_2eq in SBK and QTA, respectively. In heating-dominant regions, the carbon emissions were minimum for BES having B/WHP during the operation (GHG_{oper}), but the emissions during manufacturing (GHG_{mfg}) were maximum due to the construction of the borehole heat exchanger. Conversely, BES having A/WHPs produced lower carbon emissions during the manufacturing and relatively higher emissions during the operation. Consequently, in STK, the alternative A10, A/WHP with a PV system and radiator heating, was the most flexible option due to the low CO_2eq emission of grid electricity. In contrast, alternative A1, B/WHP with a PV system and radiator heating, was the flexible choice in SBK due to higher CO_2 emission of grid electricity. BESs with absorption chiller had minimum environmental impacts in QTA and JKT due to the least CO_2 emissions during operation and relatively low CO_2 emissions during manufacturing.

Table 5-13: GHG emissions during manufacturing (GHG_{mfg}) and operation (GHG_{oper}) of energy systems and life-cycle emissions

	STK			SBK			QTA			JKT		
Alternatives	***GHG_{mfg}***	***GHG_{oper} per year***	***LCEs***	***GHG_{mfg}***	***GHG_{oper} per year***	***LCEs***	***GHG_{mfg}***	***GHG_{oper} per year***	***LCEs***	***GHG_{mfg}***	***GHG_{oper} per year***	***LCE***
Base case	1153	124	4243	1153	3164	80263	813	4947	99744	813	6282	126457
A1	2331	57	3782	2197	1184	31809	2024	2056	43140	2387	2676	55908
A2	2521	62	4073	2276	1412	37587	2096	2254	47180			
A3	2589	55	3977	2354	1288	34483	2188	1423	30656	2470	1981	42081
A4	2517	62	4060	2284	1459	38832	2115	1480	31724			
A5	1820	71	3596	1660	1500	39166	1476	1540	32276	1861	1938	40612
A6	1665	77	3582	1512	1655	42883	1297	2610	53502	1682	2621	52603
A7	–	–	–	–	–	–	781	971	20205	766	1117	23111
A8	–	–	–	–	–	–	853	1027	21391			
A9	1353	70	3116	1378	1807	46551	1040	1538	31808	1071	2282	46720
A10	1419	63	3000	1085	1519	39070	985	2329	47573	1101	3409	69287
A11	1490	69	3217	1556	1691	43442	1061	2477	50602			
A12	1496	66	3151	1164	1580	40671	1077	1570	32482	1200	2681	54816
A13	1567	76	3465	1235	1657	42673	1149	1587	32880			

Note: All values are given in kg CO_2eq.

5.2.2.4 Thermal comfort

The thermal comfort was investigated by calculating *PMV*, *PPD*, and the total number of comfortable hours when the *PPD* was ≤ 10% (-0.5 ≤ PMV ≤ 0.5). Table 5-14 summarizes the thermal comfort performance of BESs in the four investigated climates. Each BES alternative achieved thermal comfort in the building except base case & A9 with A/AHP and A5 & A6 with B/AHP in STK. The average PPD value was slightly above the recommended thermal comfort level in those cases. The choice of heat supply equipment, i.e., radiator or hot water coil, did not change the thermal comfort in the building. Moreover, the information in Table 5-14, lower *PPD* and higher *TCH* values in QTA and JKT, illustrates that the HVAC systems with the defined capacities were able to achieve a higher comfort level in climates having lower peak heating/cooling loads and fewer hours of higher heating and cooling demands.

Table 5-14: Average predicted percentage dissatisfied (PPD) and thermal comfort hours (TCH) of alternative energy systems

	STK		SBK		QTA		JKT	
Alternatives	**PPD (%)**	**TCH (%)**	**PPD (%)**	**TCH (%)**	**PPD (%)**	**TCH (%)**	**PPD (%)**	**TCH (%)**
Base case	11.06	84.3	9.11	88.7	6.23	99.2	7.33	98.2
A1	9.40	86.3	8.54	91.2	6.33	99.6	7.83	96.8
A2	9.23	87.5	8.48	91.4	6.41	99.4		
A3	9.39	86.3	8.53	91.2	6.33	99.6	7.86	96.6
A4	9.97	85.0	8.91	89.2	6.42	99.3		
A5	10.76	86.3	8.53	91.4	6.14	99.7	7.35	98.4

	STK		SBK		QTA		JKT	
Alternatives	**PPD (%)**	**TCH (%)**	**PPD (%)**	**TCH (%)**	**PPD (%)**	**TCH (%)**	**PPD (%)**	**TCH (%)**
A6	11.63	84.3	9.00	89.3	6.16	99.4	7.39	98.1
A7	–	–	–	–	6.28	99.5	7.11	98.2
A8	–	–	–	–	6.43	98.9		
A9	11.06	84.3	9.11	88.7	9.11	88.7	7.04	98.4
A10	9.22	87.9	8.41	92.1	6.26	99.5	7.33	96.9
A11	9.12	84.8	8.43	89.4	6.39	99.3		
A12	9.22	87.9	8.41	92.1	6.26	99.5	7.91	98.2
A13	9.05	85.1	8.41	89.6	6.39	99.3		

5.2.2.5 Net present cost

The cost analysis was conducted over a life cycle of twenty-five years by incorporating the major economic factors like capital cost, replacement costs, operating cost, and discount rate, along with the PV cell's degradation rate. Table 5-15 summarizes the investment costs, operating costs, and NPC_{25} of the fourteen BES in four locations. The base case required the lowest capital cost, but the operating cost was substantially higher than most alternatives because there was no on-site energy generation. Though the integration of PV, FPCs, and GHX in BESs reduced the cost of the utility grid, it also significantly increased the capital cost. The alternatives with GSHP required a large investment and, consequently, higher maintenance costs. In STK and SBK, the B/WHP (A1-A4) and A/WHP (A10-A13) systems had lower operating costs. In contrast, the energy systems having absorption chiller and ASHP reduced operating costs in QTA and JKT. Regarding flexibility, the minimum values of NPC_{25} were 33681 € for the base case in STK, 47833 € for A10 in SBK, 12056 € for the base case in QTA, and 12436 € for the base case in JKT. Regarding economic flexibility, GSHPs were the least feasible option in all locations. At this, it should be noted that national subsidies were not considered in the economic analysis.

5.2.2.6 Levelized costs of energy

The LCOE was the EFI to evaluate cost per unit of energy, considering all cost flows over the life cycle of the BES. LCOE was further categorized into $LCOE_{el}$ and $LCOE_{th}$ to explain the economic impacts of alternatives in terms of useful electricity and thermal energies, as presented in Figure 5-9. The LCOEs were calculated using the annualized cost of twenty-five years life cycle. The base case was the most flexible BES in STK, QTA, and JKT, having the lowest $LCOE_{el}$ values of 0.183 €/kWh, 0.105 €/kWh, and 0.080 €/kWh, respectively. This fact was due to the low local electricity prices, as there was no additional cost of on-site electricity generation. In contrast, the $LCOE_{el}$ was maximum (0.319 €/kWh) for the base case in SBK

because the grid electricity tariff was the highest of the investigated locations. This fact implied that the cost of electricity for a life cycle of twenty-five years for all BES would be lower than the grid electricity tariff in SBK. The minimum value of the $LCOE_{el}$ was 0.261 €/kWh for alternative A10, a BES having PV and A/WHP, in SBK. The BESs having ASHPs and solar energy systems were characterized by lower values of $LCOE_{th}$ in all locations. The flexible BES regarding $LCOE_{th}$ was A11 (A/WHP with PV generation), with values of 0.155 €/kWh$_{th}$ (STK), 0.261 €/kWh$_{th}$ (SBK), 0.167 €/kWh$_{th}$ (QTA), and 0.053 €/kWh$_{th}$ (JKT).

Table 5-15: Investment cost, operating cost, and net present cost (NPC_{25}) of alternative energy systems

Alternatives	STK			SBK			QTA			JKT		
	C_{invt} (€)	C_{oper} (€/year)	NPC_{25} (€)	C_{invt} (€)	C_{oper} (€/year)	NPC_{25} (€)	C_{invt} (€)	C_{oper} (€/year)	NPC_{25} (€)	C_{invt} (€)	C_{oper} (€/year)	NPC_{25} (€)
Base case	1852	1931	33681	1851	3133	53493	1558	739	12056	1558	765	12436
A1	22063	1425	49452	19409	1641	50722	17546	729	29415	20854	831	34968
A2	22251	1504	50951	18705	1845	53446	16842	740	28853			
A3	23890	1442	50589	21048	1783	53695	21442	737	33394	25232	860	39713
A4	24595	1554	53132	20343	1932	55452	22146	763	34448			
A5	20570	1598	49794	17561	1903	52117	18451	679	29584	25622	865	40169
A6	18520	1632	49349	15511	2002	52911	13440	705	24969	21244	817	35165
A7	–	–	–	–	–	–	16082	539	25287	15349	513	24172
A8	–	–	–	–	–	–	15377	530	24450			
A9	11949	1374	37437	10721	2031	48246	10593	482	19035	11655	555	21952
A10	14592	1325	40339	13487	1819	47833	9377	564	18987	8170	548	18426
A11	13887	1396	40807	12782	1969	49600	8672	567	18334			
A12	16231	1413	42461	15126	1920	50047	13977	572	23667	12548	572	23110
A13	15526	1544	43901	14421	1977	50283	13272	556	22751			

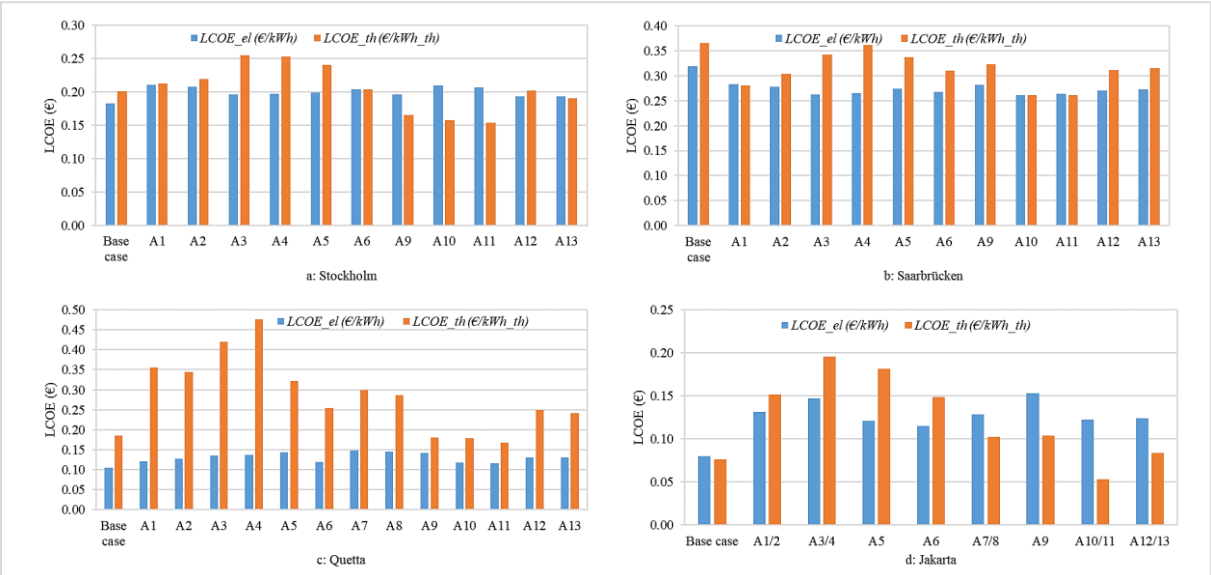

Figure 5-9: Levelized cost of electrical energy ($LCOE_{el}$) and levelized cost of thermal energy ($LCOE_{th}$) in alternative energy systems. a) Stockholm, b) Saarbrücken, c) Quetta, d) Jakarta

5.2.3 Multi-criteria assessment

5.2.3.1 Evaluation

The goal of the multi-criteria assessment was to identify the most flexible BES using the MCDM method. The multi-criteria assessment was completed in two steps. Initially, the CRITIC-TOPSIS scheme was applied to rank BESs according to the energy flexibility potential. Then MCDM was repeated with priority weights of EFIs in TOPSIS ranking to evaluate the certainty level of the multi-criteria assessment methodology.

Table 5-16 presents the weights of the EFIs, assigned by the CRITIC technique, for four locations. The significance score of an EFI varied in four different climates and from other EFIs in a specific climate. The EFIs with maximum weights were $LCOE_{el}$ (0.22) in STK, NPC_{25} (0.25) in SBK, $LCOE_{th}$ (0.19) in QTA, and NPC_{25} (0.16) in JKT. EFIs' weightage varied marginally, ranging from 0.12 to 0.16. On the other hand, the weights of EFIs in other three locations showed large variations. The NPC_{25} received the highest weightage of 0.25 and 0.16 in SBK and JKT, respectively, and the second highest weightage in STK and QTA with values of 0.16 and 0.18, respectively. LCEs and $f_{sav,NRE}$ ranged from 0.09 to 0.14 in investigated locations. The EFIs with the minimum weightage were $f_{sav,NRE}$ in STK, γ_{load} in SBK, and LCE in QTA and JKT.

TOPSIS technique assigned ranks to the BES based on the closeness coefficient to the best possible solution, as given in Table 5-17. The ranks of BESs, resulting from MCDM, were different as compared to individual EFI-based rankings. In the case of aggregated score-based ranking, it was determined how much energy flexibility could be delivered by a BES while providing thermal comfort with minimum grid interaction and environmental hazards. Hence, the base case was the least flexible BES in all locations except QTA. According to the findings of MCDM, the alternative A10, BES having A/WHP with PV generation and radiator heating, was the most flexible BES in STK, followed by A11, A12, and A1. This could be justified by the fact that the electricity tariff was significantly low, and the carbon emissions were the minimum of the investigated locations in STK. On the other hand, the higher initial costs and GHG_{mfg} emissions associated with GSHPs and FPCs resulted in a lower flexibility potential of the alternatives A1 to A6 in STK.

The GHG emissions and grid supply were relatively higher during operation for BESs having ASHPs. The electricity tariff was maximum in SBK as compared to other locations. Thus, the

flexibility of BESs having B/WHP was improved in SBK. At this, the most flexible BES was alternative A1 in SBK, followed by alternatives A10, A2, and A3.

In QTA, the grid electricity price was significantly lower than STK and SBK, and the output of the PV system and FPCs was relatively higher. Therefore, the BES having A/AHP with PV generation and FPCs (alternative A9) delivered maximum energy flexibility in QTA. The initial cost of alternative A9 was lower than most BESs, and the power demand of A/AHP was also not much higher than the GSHPs in QTA. Furthermore, in cooling-dominant climates of QTA and JKT, BESs having absorption chiller (A7 and A8) had the lowest electricity consumption and lowered costs compared to BESs having GSHP. Consequently, the EFIs of $f_{sav,NRE,}$ and GHG emissions were adequate for alternative A7/8. So, alternative A7/8 was the most flexible BES in JKT.

Table 5-16: Weights of EFIs in investigated locations

	$f_{sav,NRE}$	γ_{load}	*LCEs*	NPC_{25}	PPD_{avg}	$LCOE_{el}$	$LCOE_{th}$
STK	0.11	0.12	0.11	0.16	0.15	0.22	0.13
SBK	0.10	0.09	0.09	0.25	0.20	0.11	0.15
QTA	0.10	0.10	0.10	0.18	0.16	0.16	0.19
JKT	0.12	0.14	0.12	0.16	0.15	0.15	0.15

Table 5-17: Relative closeness (D_i) and ranking of alternative energy systems in investigated locations

	STK		SBK		QTA		JKT	
	D_i	*Rank*	D_i	*Rank*	D_i	*Rank*	D_i	*Rank*
Base case	0.278	12	0.111	12	0.497	12	0.430	9
A1	0.720	4	0.900	1	0.516	10	0.539	7
A2	0.682	8	0.798	3	0.490	13		
A3	0.650	9	0.763	4	0.498	11	0.512	8
A4	0.608	10	0.684	10	0.461	14		
A5	0.598	11	0.698	9	0.591	9	0.542	6
A6	0.698	6	0.728	7	0.615	8	0.675	4
A7	–	–			0.685	7	0.758	1
A8	–	–			0.700	6		
A9	0.712	5	0.585	11	0.820	1	0.653	5
A10	0.851	1	0.817	2	0.749	2	0.694	3
A11	0.819	2	0.749	5	0.740	3		
A12	0.736	3	0.741	6	0.717	5	0.717	2
A13	0.698	7	0.704	8	0.736	4		

5.2.3.2 Sensitivity analysis

A sensitivity analysis was conducted to examine the reliability of the multi-criteria assessment methodology. The approach for the sensitivity analysis was to analyze the ranks of BES with changing weights of EFIs. For this purpose, five scenarios were created by assigning equal weights to all EFIs and prioritizing the EFIs of energy efficiency ($f_{sav,NRE}$ & γ_{load}), economics

(NPC_{25}, $LCOE_{el}$, and $LCOE_{th}$), and other EFIs of GHG emissions and thermal comfort (*LCEs* & PPD_{avg}) by assigning a cumulative weightage of 50% one by one. Hence, the confidence of the MCDM method was verified under five scenarios, as summarized in Table 5-18. In addition, the flexibility ranking of BESs for these five scenarios is given in Table 5-19.

The findings of sensitivity analysis revealed that the base case was the least accepted BES in all scenarios except S1 in QTA and S5 in JKT. The ranks of BESs were consistent in five different scenarios. Particularly in STK, the BESs having A/WHP and the PV system were the alternatives (A10 and A11) with the maximum flexibility potential in all scenarios. The energy systems with B/WHP increased their rank in SBK for the energy efficiency-priority scenario (S3) because of the lower power demand of GSHP as compared to ASHPs. In SBK, the BESs having B/WHP (A1 and A2) were the flexible option. Since NPC_{25} received a higher weightage of 25% in S1, alternative A10 became the second-most flexible energy system in S1due to higher economic flexibility. Likewise, alternative A10 was the third most flexible BES for the economic-priority scenario (S5) in SBK. In the case of JKT, the alternative with an absorption chiller, PV, and FPCs (A7/8) was the most flexible BES for all scenarios, while the flexibility order of BES changed with varying weights of EFIs. Conversely, the ranks of BESs were sensitive to the variation in weights of EFIs in QTA. Although the flexibility order of BESs was different in all scenarios, the alternative A9, BES having A/AHP with PV and FPCs, was the preferred energy system in QTA with maximum energy flexibility except for scenario S4. The alternatives A7 and A8 were characterized by the lowest GHG emissions and electricity consumption in all alternative energy systems. Therefore, the alternative A8 was ranked first in scenario S4 and second in scenario S3 in QTA.

As presented in Table 5-19, the flexibility order of BESs changed by prioritizing the EFIs, which demonstrated that the weights of EFIs strongly influenced the ranks of BES and emphasized the importance of criteria weighting in MCDM. However, the most flexible BESs were the same in all scenarios except scenario S4 in QTA. Thus, it could be implied that the weights had little impact on the choice of the most flexible BES in the investigated locations, which verified the robustness of the CRITIC-TOPSIS scheme for MCDM in selecting the BESs with the employed EFIs.

Table 5-18: Weights of EFIs under five scenarios for sensitivity analysis of MCDM results

	Weights of EFIs						
	$f_{sav,NRE}$	γ_{load}	$LCEs$	NPC_{25}	PPD_{avg}	$LCOE_{el}$	$LCOE_{th}$
S1: Weights obtained from CRITIC method	weights from Critic method (c.f. Table 5-16)						
S2: Equal weightage to each EFI	0.14	0.14	0.14	0.14	0.14	0.14	0.14
S3: Prioritize EFIs of energy efficiency	0.25	0.25	0.10	0.10	0.10	0.10	0.10
S4: Prioritize EFIs of emission and comfort	0.10	0.10	0.25	0.10	0.25	0.10	0.10
S5: Prioritize economic EFIs	0.10	0.10	0.10	0.17	0.10	0.17	0.17

Table 5-19: The order of alternative energy systems under five scenarios in investigated locations

Scenario		Rank
STK	*S1*	A10 > A11 > A12 > A1 > A9 > A6 > A13 > A2 > A3 > A4 > A5 > Base case
	S2	A10 > A11 > A1 > A12 > A6 > A2 > A13 > A9 > A3 > A4 > A5 > Base case
	S3	A10 > A1 > A11 > A2 > A3 > A6 > A12 > A4 > A13 > A5 > A9 > Base case
	S4	A10 > A11 > A12 > A9 > A6 > A1 > A13 > A2 > A3 > A5 > A4 > Base case
	S5	A10 > A11 > A9 > A12 > A13 > A1 > A6 > A2 > A3 > A4 > A5 > Base case
SBK	*S1*	A1 > A10 > A2 > A3 > A11 > A12 > A6 > A13 > A5 > A4 > A9 > Base case
	S2	A1 > A2 > A3 > A10 > A6 > A12 > A4 > A11 > A5 > A13 > A9 > Base case
	S3	A1 > A2 > A3 > A10 > A6 > A4 > A11 > A12 > A5 > A13 > A9 > Base case
	S4	A1 > A3 > A2 > A10 > A4 > A5 > A12 > A6 > A11 > A13 > A9 > Base case
	S5	A1 > A2 > A10 > A3 > A11 > A6 > A12 > A13 > A5 > A4 > A9 > Base case
QTA	*S1*	A9 > A10 > A11 > A13 > A12 > A8 > A7 > A6 > A5 > A1 > A3 > Base case > A2 > A4
	S2	A9 > A8 > A13 > A7 > A12 > A10 > A5 > A11 > A3 > A6 > A1 > A4 > A2 > Base case
	S3	A9 > A8 > A7 > A13 > A12 > A5 > A3 > A4 > A10 > A1 > A11 > A6 > A2 > Base case
	S4	A8 > A7 > A9 > A13 > A12 > A5 > A3 > A4 > A10 > A1 > A11 > A2 > A6 > Base case
	S5	A9 > A13 > A10 > A11 > A12 > A8 > A7 > A6 > A5 > A1 > A3 > A2 > A4 > Base case
JKT	*S1*	A7/8 > A12/13 > A10/11 > A6 > A9 > A5 > A1/2 > A3/4 > Base case
	S2	A7/8 > A12/13 > A6 > A9 > A10/11 > A5 > A1/2 > A3/4 > Base case
	S3	A7/8 > A12/13 > A9 > A6 > A5 > A3/4 > A10/11 > A1/2 > Base case
	S4	A7/8 > A9 > A12/13 > A6 > A5 > A3/4 > A1/2 > A10/11 > Base case
	S5	A7/8 > A10/11 > A12/13 > A6 > A9 > Base case > A1/2 > A5 > A3/4

5.3 Building service system flexibility

In the previous section, the MCDM analysis of different BESs identified a feasible BES in each location. Two optimization methods, steady-state optimization and dynamic control, were further implemented to evaluate the energy flexibility potential of the building service system. The optimization scheme was implemented in a temperate oceanic climate (Cfb) of Saarbrücken for alternative A1 (energy system having brine-to-water heat pump with PV supply and

emission heating). The energy consumption profile of alternative A1 was taken as a reference scenario for assessing energy flexibility through steady-state or dynamic optimization of BES parameters.

5.3.1 Steady-state optimization

In SSO, fixed optimal values of selected design variables were evaluated by conducting annual simulations. The building architecture was defined according to the findings of section 5.1, and the energy system model of alternative A1 in Saarbrücken was used as a reference for this optimization problem. The capacity and performance characteristics of the heat pump, length of the borehole, properties of the soil, and control strategies were fixed in SSO. NSGA-III completed the bi-objective optimization task by conducting 5000 annual simulations with constraints of thermal comfort and FSOC and produced a PF to identify the optimal solution set.

Design variables: Table 5-20 describes the variables with their lower and upper bounds for the optimization scheme. Borehole radius and active energy storage, i.e., battery capacity and volume of TES, were sources of system flexibility. Whereas the remaining parameters provided opportunities for demand flexibility. The limits of variables were either assigned as percentage margins of the boundary conditions of BES in section 5.1 or with reference to the previous literature, as given in Table 5-20.

Table 5-20: Design variables for steady-state optimization

Variables	reference value	Lower bound	Upper bound	Remarks
Battery capacity (Wh)	5760	5184	6336	10% margin w.r.t., initial value
Volume of TES (m^3)	1.8	1.35	2.25	25% margin wrt initial value
Radius of borehole pipe (m)	0.0762	0.05715	0.09525	25% margin wrt initial value
Mass flow rate of brine in GHX (kg/h)	1136	681	1136	According to performance data of YAWS YORK HP [186]
Starting delay of HP (h)	0.25	0	0.5	[194]
Stopping delay of HP (h)	0.25	0	1	[194]
Cooling set point (°C)	25	24	28	[195]
Heating set point (°C)	20	18	23	[195]

Constraints: Two constraints were defined for the optimization problem, as given in Table 5-21. The first constraint of average PPD value maintained thermal comfort above a certain level by avoiding overheating/cooling or underheating/cooling. The average FSOC of the battery was given as the second constraint to extend the battery life to a minimum of 6.5 years.

FSOC depended on the BES's total electricity consumption and battery capacity. In comparison, PPD was mainly influenced by HP's temperature set points and starting/stopping delay.

Table 5-21: Constraints for steady-state optimization

Constraints	Criteria	Remarks
Average predicted percentage discomfort	= < 10	ASHRAE standard
Average fractional state of charge of battery	= > 0.45	for a minimum of 6.5 years of battery life

Objective functions: Two objective functions were set for SSO, the electricity consumption of BES ($\boldsymbol{P_{el,sys}}$) and $\boldsymbol{PER_{NRE}}$, while maintaining thermal comfort in the building. The goal was to minimize $P_{el,sys}$ and maximize the PER_{NRE}, i.e., meet the energy demand of the service system using a smaller share of primary energy from the grid network. The electricity consumption was the sum of the electricity consumption of the HP, electric heater in the storage tank, blower of water coils, pumps, controllers, and other auxiliary equipment. Eq. 3.12 was used to calculate the PER_{NRE} for BES. At each iteration, TRNSYS produced the values of these functions in a text file, forwarded to NSGA-III using Python to process the design variables for the next simulation. Since the household appliances' load profile was fixed, the variation in the design variables would influence the energy consumption of the HVAC system and DHW supply. For the designed optimization problem, all design variables had an impact on both objective functions except the battery capacity, which affected only the PER_{NRE}.

5.3.1.1 Optimization results

The optimization algorithm produced a PF between PER_{NRE} and $P_{el,sys}$. The solution with the maximum value of PER_{NRE} was also characterized by the lowest value of $P_{el,sys}$, as highlighted in Figure 5-10. The maximum PER_{NRE} of 1.03 was achieved for reduced $P_{el,sys}$ of 1707.77 kWh/year for the optimum solution. Moreover, both constraints had values of 6.52% and 0.46 for average PPD and average FSOC, respectively. The optimized values of design variables for the optimum solution on PF are listed in Table 5-22. Battery capacity was increased to 6000 Wh after optimization, which resulted in higher FSOC and, eventually, a larger share of PV supply to the building. The TES volume and borehole radius were reduced to 1.46 m^3 and 0.0602 m, respectively, in the optimum solution compared to the reference scenario. The mass flow rate of brine in GHX was also reduced from 1136 kg/h to 985 kg/h. After optimization, there was a minor change of 0.03 h and 0.01 h in starting and stopping delays of HP, respectively. The cooling set point was decreased to 24.63 °C, which resulted in lower energy

consumption during space cooling. On the other hand, the building was heated to a higher temperature of 21.18 °C during space heating in the optimal scenario.

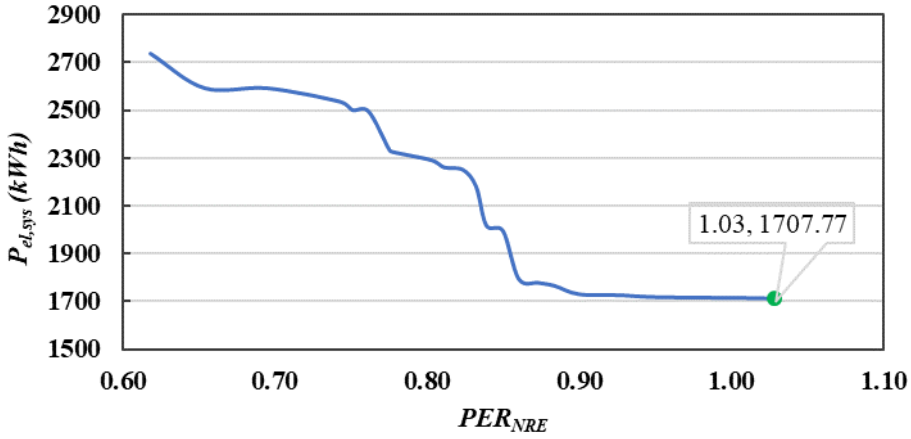

Figure 5-10: PF of steady-state optimization

Table 5-22: Optimized values of design variables

Variables	Optimal value
Battery capacity (Wh)	6000
Volume of TES (m^3)	1.46
Radius of borehole pipe (m)	0.0602
Mass flow rate of brine in GHX (kg/h)	985
Starting delay of HP (h)	0.28
Stopping delay of HP (h)	0.26
Cooling set point (°C)	24.63
Heating set point (°C)	21.18

5.3.1.2 Energy flexibility by steady-state optimization

Energy flexibility was evaluated by comparing reference and optimized energy consumption profiles of BES having brine-to-water heat pump with PV supply and emission heating. The DRE was assumed to be one year in SSO. Energy flexibility was achieved by system flexibility and demand flexibility in SSO. Thermal and electric storage capacities and borehole radius were responsible for system flexibility. On the other hand, the mass flow rate of brine, starting/stopping delays, and temperature set points provided demand flexibility through SSO. The EFIs for the SSO strategy are given below.

Storage capacity: The capacity of TES was reduced in the optimal SSO solution, which resulted in a down-flex storage capacity. The downward flexibility potential of the HP was evaluated for a simulation period of a whole year. Since the operation hours of the HP depended on the hot water's temperature and volume of TES, HP's power demand decreased for reduced TES volume. The annual power demand profiles of HP for reference and SSO scenarios are presented in Figure 5-11. Thermal storage capacity (C_{DF}) is also presented for each month on

the secondary vertical axis. The power demand in the SSO scenario kept lower than the reference scenario throughout the year. However, it was quite small in the summer because there was only DHW demand in those months. Similarly, in December, the CDF was high in winter, with a maximum value of 213.75 kWh. Overall, the energy flexibility was high in months having higher power demand of HP. In winter, the C_{DF} ranged between 42.35 kWh and 213.75 kWh. In comparison, it was only 4.50 kWh to 13.71 kWh in summer. Overall, the SSO strategy could incorporate 871.31 kWh storage capacity per year.

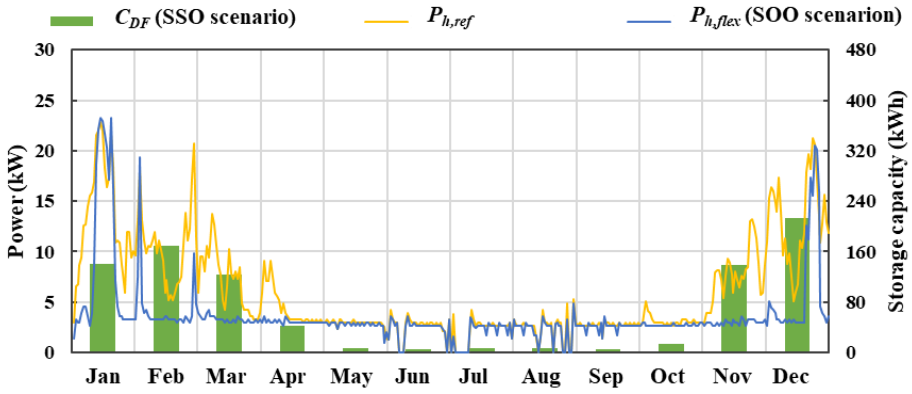

Figure 5-11: Storage capacity (down-flex) from SOO and power demand of HP in reference and SSO scenarios

Flexible energy: This EFI demonstrated how much energy consumption was saved after optimization. The main source of flexible energy was HP. Further, the flexible energy, like the storage capacity, was higher in the heating season. Figure 5-12 presents the flexible energy potential for each month. The maximum flexible energy was achieved in December (226.13 kWh), reaching 183.21 kWh, 153.36 kWh, and 147.71 kWh in February, November, and January, respectively. A total of 967.83 kWh of flexible energy was achieved by employing the SSO. The flexible energy potential varied between 5.73 kWh and 20.86 kWh from June to October.

Residual load: The residual load of the building evaluated the grid stress of the BES. The lower power demand of the HP and reduced energy consumption of BES substantially decreased the residual load after SSO. The annual profiles of residual loads for reference and SSO scenarios are presented in Figure 5-12. The electricity demand from the grid was also reduced in the heating season, as in the case of HP's power demand and energy consumption of BES. Nevertheless, the residual load in the SSO scenario was higher than the reference scenario from May to October. For example, the residual load reduced to 527.09 kWh from 7736.47 kWh in December. In contrast, it increased in May from 111.59 kWh to 124.47 kWh. Overall, the residual load in the SSO scenarios was 648.75 kWh less than in the reference scenario.

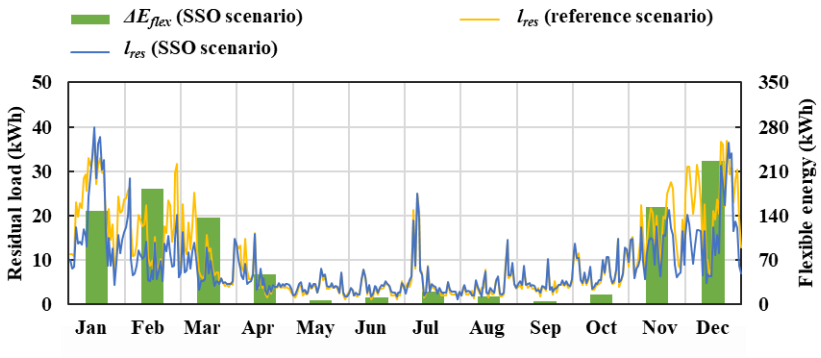

Figure 5-12: Flexible energy from SSO and residual loads in reference and SSO scenarios

Flexibility cost: Flexibility cost was computed by comparing the grid electricity cost during the operation of the BES in reference and SSO scenarios. Thus, the flexibility cost was directly related to the residual load of the building. The stacked column chart and scatter plot in Figure 5-13 show the grid electricity cost for both scenarios and the flexibility cost, respectively. The annual flexibility cost achieved by SSO was 196.81 €, with a grid electricity cost of 944.1 € in the SSO scenario. Since the residual load was increased after SSO from May to October, the flexibility cost was negative in those months, showing the increased grid electricity cost. The flexibility cost reached 63.53 € in December, 44.83 € in February, 40.53 € in January, and 35.13 € in November.

Flexibility emissions: This EFI provided information on the CO_2 emissions during the operation of BES. Flexibility emissions were also based on the residual load of the building. Thus, higher flexibility emissions were accomplished in winter months, 41.55 kgCo_2eq in January, 45.96 41.55 kgCo_2eq in February, 36.03 41.55 kgCo_2eq in November, and 65.12 41.55 kgCo_2eq in December. On the other hand, the SSO strategy increased the CO_2 emissions by minimal values from May to October, as shown in Figure 5-13. The net effect of SSO was reducing the CO_2 emissions from 1169.5 kgCo_2eq to 967.74 kgCo_2eq in a year.

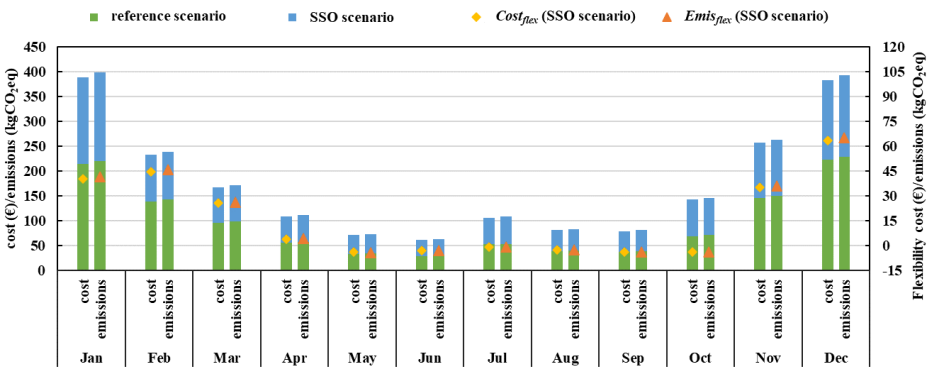

Figure 5-13: Total cost and emissions in reference and SSO scenarios with flexibility cost and emissions from SOO

5.3.2 MPC-based optimization

The functionality of the MPC optimization strategy was analyzed for three months, January, June, and October. Firstly, the performance of the MPC model was validated by comparing the predicted and simulated results for the thermal load of the reference building. Then the energy flexibility potential was computed for the dynamic control scheme. For MPC-based dynamic control, the boundary conditions and design parameters of BES were modified according to the findings of SSO. Finally, the energy consumption profile in investigated months was compared with the reference and SSO scenarios to better present dynamic control's energy flexibility potential.

5.3.2.1 Predictive model performance

The RandomForestRegressor predictive model was developed using the TRNSYS-generated training data for a residential building in Saarbrücken. The model was trained on the data set of 990 monthly TRNSY simulations with a 30-minute time step for each month. The correlation was initially computed between model outputs and possible inputs, including Tamb, RHamb, IT_H, internal gains, solar gains, SHD_w, Tset_H, Tset_C, Tzone, and relative humidity of zone RHzone. The variables with relatively higher correlations were selected as model inputs, as given in Table 5-23. Tamb was the most critical parameter for building thermal load, and Tzone highly influenced thermal comfort in the zone. Further, SHD_w was prominent in the summer but not considered in January and October due to low correlation scores. Then, the model was validated by comparing the energy demand of the building from the simulation and the predictive model for the reference building having similar boundary conditions.

Table 5-23: Correlation between inputs and outputs of predictive model

Features	January		June		October	
	Qth (kW)	***PPD (%)***	***Qth (kW)***	***PPD (%)***	***Qth (kW)***	***PPD (%)***
Tamb (°C)	-0.87	-0.13	0.24	-0.26	-0.49	-0.43
RHamb (%)	0.39	0.11	-0.18	0.27	0.25	0.19
IT_H (kWh/m2)	0.14	0.05	-0.14	0.17	0.10	0.10
SHD_w (fraction)	-	-	-0.28	-0.10	-	-
Tset_H (°C)	0.31	-0.89	-	-	0.38	-0.36
Tset_C (°C)	-	-	-0.21	0.03	-	-
Tzone (°C)	0.27	-0.91	0.15	0.51	-0.08	-0.71

Figure 5-14 to Figure 5-16 show the simulated and predicted thermal load (Q_{th}) plots during January, June, and October, respectively. Predicted results showed a good agreement with the simulated results. However, the accuracy of the predictive model was relatively lower in June. Moreover, the evaluation matrices of the predictive model were also calculated to measure the accuracy. Table 5-24 shows three evaluation matrices used in this study, i.e., mean absolute error (MAE), R2 (R squared) score, and root mean square error (RMSE). These matrices were within the acceptable range for all three months. Moreover, the evaluation scores were higher in January and October (heating-dominant months) than in June (a cooling-dominant month). Overall, higher R2 scores and lower values of MAE and RMSE in three months show that the predictive outcomes were near realistic.

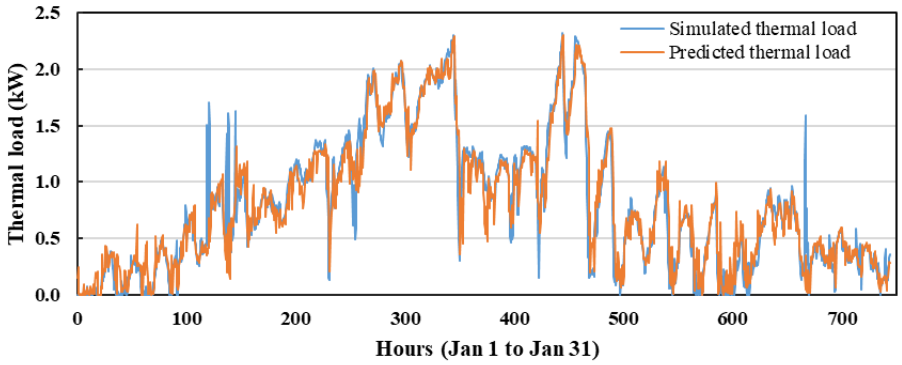

Figure 5-14: Comparison of simulated and predictive household's thermal load (January)

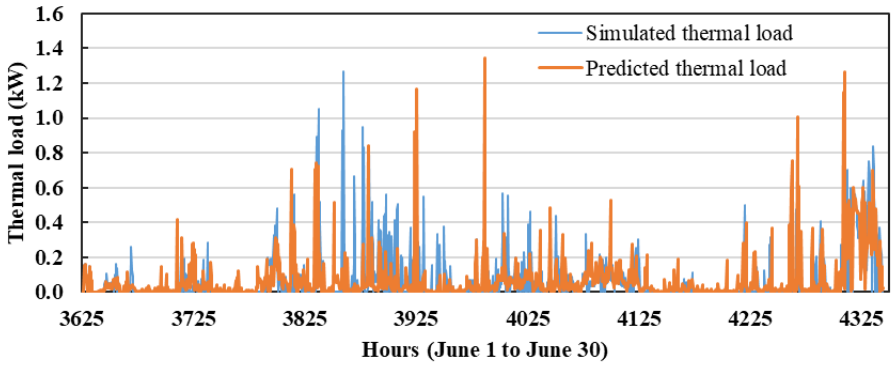

Figure 5-15: Comparison of simulated and predictive household's thermal load (June)

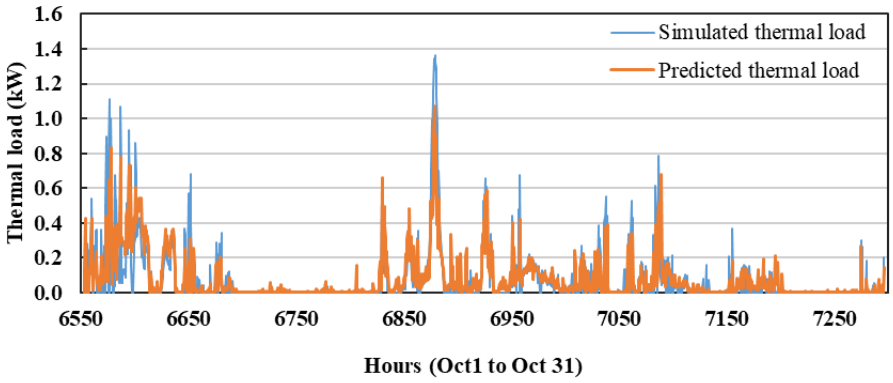

Figure 5-16: Comparison of simulated and predictive household's thermal load (October)

Table 5-24: Evaluation matrices of predictive model

Model evaluation matrices	January	June	October
MAE	0.0091	0.0652	0.0382
R2 score	0.998	0.967	0.991
RMSE	0.056	0.211	0.163

5.3.2.2 Energy flexibility by MPC

The employed optimization strategy was presumed to improve the energy flexibility of the building without compromising the thermal comfort in the zone. It should be noted here that the electricity consumption of household appliances was independent of the selected control variables and thus not considered in the formulation of the dynamic control. The MPC optimizer provided the reference set temperature to local PID controllers and shading fraction for the window blinds for each DRE of 30-minute. The PID controller generated a control signal by comparing the reference and zone temperature. That signal controlled the heating/cooling operational characteristics of the GHP, radiator, and cooling coils. Therefore, the goal was to achieve thermal comfort with the minimum possible electricity consumption of the HVAC system. The simulation results showed that the MPC-based optimization could further improve the energy flexibility of the building by delivering demand flexibility through optimal control of window shading and temperature set points. Moreover, the dynamic modulation of temperature set points reduced the energy consumption of BES while maintaining thermal comfort. As a result, the dynamic control provided better thermal comfort than the reference scenario, with an average PPD value of 11.18 % in January. However, it was slightly higher than the desired level and lower than the SSO scenario (7.261%) in January. MPC maintained thermal comfort at 7.49% and 6.95% PPD levels in June and October, respectively, which were almost the same in reference and SSO scenarios. The EFIs of the MPC-based optimization strategy are described below.

Storage capacity: The storage capacity (C_{DF}) and heating power demand resulting from MPC are presented in Figure 5-17. The stacked columns show the C_{DF} in MPC and SSO scenarios, whereas the scatter plots present the power demand of HP in all three scenarios. The simulation results showed that applying the MPC-based optimization after the SSO on BES could further induce energy flexibility. The C_{DF} was increased from 140.87 kWh (SSO scenario) to 289.81 kWh by the downward temperature modulation of the heating set point. It can be observed that the HP's power demand was much lower in the MPC scenario during high heating load hours, which was the source of energy flexibility in MPC-based optimization. A total of 21.34 kWh storage capacity was achieved in October, with a significant share of 7.63 kWh by the MPC strategy. The heating power demand in January and October decreased from 508.74 kW (reference scenario) to 354.16 kW (SSO scenario) and further decreased by 197.61 kW in the MPC scenario.

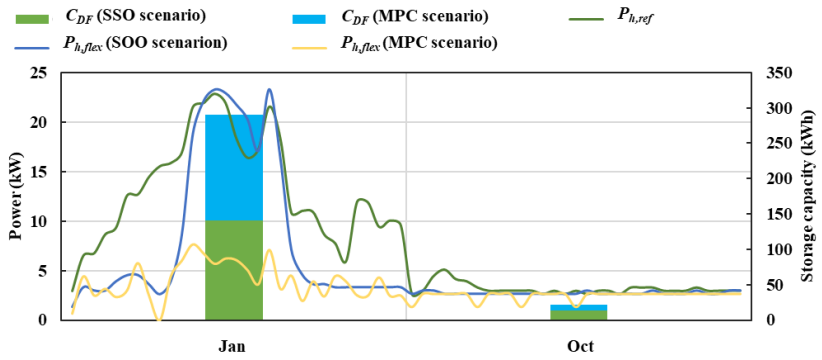

Figure 5-17: Storage capacities (down-flex) and HP's power demands in reference, SSO, and MPC scenarios

Flexible energy: The flexible energy from MPC-based optimization and its comparison with the SSO strategy is shown in Figure 5-18 on the secondary vertical axis. The flexible energy reached 97.26 kWh in January by employing dynamic control. The impact of MPC was increased energy consumption w.r.t. reference and SSO scenarios in June, resulting in -19.09 kWh flexible energy. In October, a month of low heating demand, the flexible energy kept to a low value of 4.25 kWh. Overall, the combined effect of SSO and MPC was an energy flexibility of 244.97 kWh in January and 19.53 kWh in October.

Residual load: The residual load was another indicator for assessing energy flexibility by activating the MPC of temperature set points and window shading. Figure 5-18 illustrates the variation in residual load profiles in simulated periods. Though SSO reduced the total annual residual load, the effect of SSO was increased residual load from May to October. In the case of MPC, the residual load was lower than the reference scenario in January and October and

higher in June with a minimal value of 1.45 kWh. The SSO and MPC strategies dropped the electricity requirement of the grid by a total of 233.72 kWh, including a 100.13 kWh reduction from MPC-based optimization.

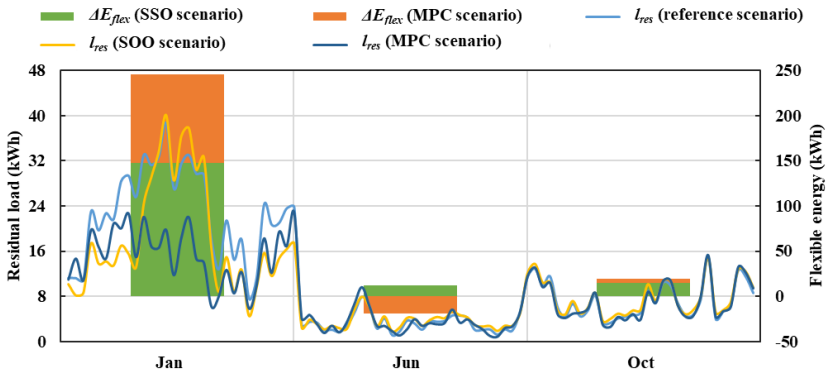

Figure 5-18: Flexible energies and residual loads in reference, SOO, and MPC scenarios

Flexibility cost: The electricity costs and flexibility costs in the investigated scenarios are presented in Figure 5-19. The flexibility cost depended on the grid electricity and showed a similar pattern as in residual load. The electricity cost was lower than the reference scenario in SSO and MPC scenarios during January. As a result, the flexibility costs were 40.53 € and 70.91 € in SSO and MPC scenarios, respectively, compared to the reference scenario. On the other hand, the electricity cost was higher than the reference scenario in June after applying the optimization strategies, as depicted by the negative flexibility costs. The SSO strategy's electricity cost in October was highest due to increased residual load. In comparison, the MPC strategy reduced the residual load in October by a nominal value and provided a flexibility cost of 1.34 €.

Flexibility emissions: The flexibility emissions were also a function of residual load and showed a pattern similar to the flexibility cost. MPC-based optimization was more effective than SSO for flexibility emissions. The dynamic temperature modulation in the heating season significantly reduced CO_2 emissions. Though SSO could achieve 41.55 $kgCO_2eq$ flexibility emissions in January, MPC further reduced the CO_2 emissions and provided flexibility emissions of 72.69 $kgCO_2eq$ regarding the reference scenario. The SSO could not achieve flexibility emissions in October, but the MPC strategy accomplished flexibility emissions of 1.38 $kgCO_2eq$ in October. Nevertheless, CO_2 emissions increased, as in the SSO scenario, by 0.45 $kgCO_2eq$ in June by activating MPC.

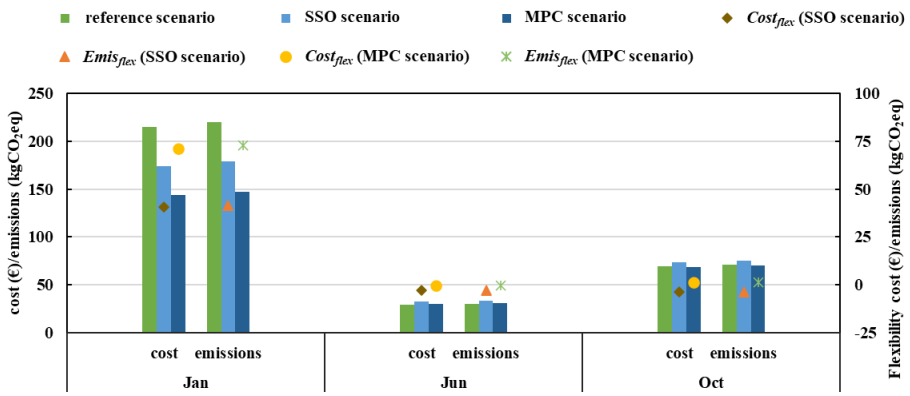

Figure 5-19: Total and flexibility cost and emissions in reference, SSO, and MPC scenarios

5.4 Discussion

The implantation of the proposed optimization framework can improve the energy flexibility of the building from the envelope design stage to the system selection and operation. A novel combination of EFIs was formulated to evaluate the energy flexibility potential for generation, system, and demand flexibilities. There were some limitations while conducting case studies, like constant grid tariff throughout the year, no feed-in tariff, and no national subsidies on renewable energy installations. Furthermore, annual simulations were carried out for generation and system flexibilities, and monthly simulations were conducted for demand flexibility through MPC. The EFIs were calculated for each flexibility category accordingly.

5.4.1 Flexible building envelope

The bi-objective optimization of the building envelope established two discussion areas about architectural design in different climate conditions: energy flexibility potential and optimal design parameters. The potential depended on the local building energy standards and heating/cooling demand for the flexible thermal load. For instance, the flexible thermal load was lower in Dfc (Oestersund) and Dfb (Stockholm) than in all other heating-dominant locations despite high heating demands due to good practices of the energy-efficient envelope. Contrary, other locations in the continental climate had significant potential for energy flexibility. Cfb (Saarbrücken), a temperate climate, showed low potential for flexible thermal load because of the highly insulated envelope. The locations in the Dry climate had higher cooling demand than other climates and showed the maximum potential of flexible cooling load. Similarly, the locations in tropical climates also achieved a significant flexible cooling load. Regarding the optimal envelope, the building design parameters depend on each other, and a complete set of optimal parameters should be adopted instead of individual parameters.

The locations with extreme weather conditions, either cold or hot, required very insulated envelopes to minimize transmission gains or losses. The insulation thickness of the external wall was higher in continental, dry-hot, and tropical climate zones. The insulation thickness of the roof was high in continental and temperate climate zones. The dry-cold climate was characterized by the lowest average insulation thickness for external walls and roofs.

Since the infiltration through the window aperture was active for passive cooling, the aperture angle was more effective in hot climates. Consequently, the aperture angle was higher in hot regions of temperate and dry climates. The dry-hot zone had a maximum mean aperture angle. Although the dominant thermal load was cooling in a tropical climate, it also had a higher humidity level throughout the year. As a result, the aperture angle was relatively lower than in dry climates, and it even reduced to 5 degrees in Jakarta, a tropical-monsoon region.

WWR was the most imperative element regarding solar gains in heating-dominant and cooling-dominant climates. As a matter of fact, the optimal solutions established that the heating-dominant regions require higher WWR to maximize the solar gains. Therefore, the continental-cold climate had the maximum WWR, continuously decreasing to the mean value of 0.27 in the temperate-hot summer climate. On the other hand, in the dry and tropical zone, the WWR remained equal to the lower bound in optimum solutions. The solar radiation value for activating the window shading was another factor in controlling the solar gains in the household. This parameter had relatively higher values in continental and temperate climates because the dominant thermal load is heating. In contrast, window shading was activated at low solar radiation, around 250W, in dry and tropical climates due to high cooling loads. The building orientation also strongly influenced the solar gains. The optimal orientation is an essential aspect of the building architecture since it can increase energy flexibility without additional investment costs. Optimization results showed that the South or North was the optimal orientation in the Northern hemisphere. In most of the locations, the front facade faced North. However, the locations in dry and temperate climate zones with minimal heating load had South-faced optimal building orientation.

5.4.2 Flexible energy system

Concerning the selection of flexible BES, the proposed framework devised a systematic methodology for a definite flexibility evaluation of BES based on performance indicators for system flexibility. It should be noted that the cost of energy system components in LCCA does not include value-added tax (VAT), cost of system accessories like piping, controllers, sensors,

and system installation costs, which is a limitation of this study. The methodology was applied to fourteen energy systems with various energy mixes and HVAC system configurations in four locations having different climates.

The alternatives with brine-to-water HP required less grid electricity in a heating-dominant climate. For a cooling-dominant climate, the alternatives having an absorption chiller consumed the minimum grid electricity. Further, QTA and JKT had larger *PER* and $f_{sav,NRE}$ due to higher solar radiation and ultimately higher electricity and heat supply from the PV system and FPCs. Similarly, the load cover factor prioritized the energy systems with brine-to-water HP in a heating-dominant climate and absorption chiller in a cooling-dominant climate. The GHG emissions were lowest for ground source brine-to-water HP energy systems during the operation in heating-dominant regions, but the emissions from the manufacturing process were the highest because of the BHX construction. The alternatives with air-to-water HPs were characterized by lower emissions during manufacturing. The low electricity rate and CO_2 emissions of grid utility make the alternative with A/WHP and PV system a suitable choice in STK. In contrast, the alternative with B/WHP and PV system became the appropriate energy system in SBK due to higher CO_2 emission and grid electricity tariffs. The energy systems with the absorption chiller had minimum environmental impacts in cooling-dominant climates, QTA and JKT.

Although the integration of PV, FPCs, and ground heat exchangers in the energy system reduced the cost of the utility grid, it also significantly increased the investment cost. The alternatives having GSHP required a significant investment, and consequently, the maintenance cost would also be high. The *LCCA* showed that air-to-air HP with no on-site generation was the best option in STK, QTA, and JKT. However, the energy system having air-to-water HP and the PV system was a good choice in SBK due to the high electricity rate and, therefore, the higher operating costs in the base case energy system. As far as the *LCCA* was concerned, the GSHPs were the least desired option in all climate zones. The $LCOE_{el}$ and $LCOE_{th}$ were computed using the five-year life cycle annualized cost. The $LCOE_{el}$ was strongly dependent on the grid utility rate. Thus, the optimal choice was the base case in locations with low utility rates like STK, QTA, and JKT. The high electricity rate in SBK made the alternative with A/WHP and PV an appropriate energy system. The alternatives with ASHPs and solar energy systems were associated with lower values of $LCOE_{th}$. As a result, the best energy system concerning $LCOE_{th}$ was A/WHP with PV generation and hot water coil in all investigated locations. GSHP was a favorable HVAC system regarding energy consumption and operating

GHG emissions in cold climates. On the other hand, the absorption chiller with FPCs was a suitable option for energy efficiency and LCEs in warm or hot climates.

Each EFI came up with a different alternative energy system w.r.t. other EFIs and locations. Selecting a BES configuration based on an individual EFI would result in subduing other EFIs. Therefore, choosing the BES based on the aggregated score of all EFIs was essential. The MCDM technique was applied using CRITIC and TOPSIS techniques to achieve this goal. The multi-criteria evaluation showed that the choice of suitable BES was quite different from the individual EFIs. It was also established that the selection of BES was strongly influenced by climate conditions, energy tariffs, and emissions during power production. According to the MCDM evaluation and sensitivity analysis, the energy systems with air-to-water HP + PV + radiator (STK), brine-to-water HP + PV + radiator (SBK), air-to-air HP + PV + FPC (QTA), and absorption chiller + PV + FPCs (JKT) were the most feasible BES in distinct locations.

5.4.3 Energy flexibility by BES optimization

The energy flexibility of the BES, identified by the MCDM process (reference scenario), was improved by a two-stage optimization approach. In the first stage (steady-state optimization), system and demand flexibilities were improved through MOO of BES design parameters, HP's starting/stopping delays, and temperature set points. In the second stage (MPC-based optimization), an MPC-based dynamic control was employed on the BES, optimized by SSO, to continuously modulate temperature set points of the zone and window shading fraction.

The optimization results showed a substantial flexibility potential in both SSO and MPC scenarios. EFIs of SSO were quite promising in heating mode, but the energy flexibility decreased in June. The BES was more flexible in the MPC scenario and performed better than the SSO scenario in the summer. However, the performance of BES in summer was optimum in the reference scenario. The critical aspect of the optimization framework was the design of an MPC-based dynamic control. The supervisory controller coupled the prediction model and optimization algorithm to determine the optimal control inputs. The predictive model was developed based on the dataset regarding the thermal load, boundary conditions, and control disturbances rather than the energy consumption profiles of a BES. The objective was to devise an MPC optimizer that could be employed on various energy systems for the reference building. The case study of MPC-based optimization illustrated the effectiveness of the proposed MPC model for improving demand flexibility. The heating power demand of the heat pump was 61.2% less than the reference scenario and 44.2% less than the SSO scenario for January and

October. The low heating power demand resulted in increased storage capacity (C_{DF}). Similarly, in these months, the residual load decreased by 25.4% and 14.3 % with reference and SSO scenarios. Moreover, the flexibility cost (72.25 €) and flexibility emissions (74.07 $kgCO_2eq$) during January and October indicated the significance of the MPC-optimizer for demand flexibility. The high energy flexibility achieved in the MPC scenario established that the MPC model based on heating/cooling demand and boundary conditions could be employed on a BES.

6 Conclusions

6.1 Summary of research

The high energy consumption and GHG emissions in the household sector, particularly in HVAC applications, have comprehended the importance of identifying a flexible BES at the design stage. Previous flexibility assessment studies are focused on energy flexibility of generation, system, and demand domains of a specific system, independently. The flexibility assessment indicators are also limited to demand response flexibility. Further, the indirect flexibility indicators for cost and emissions are evaluated during the operation of the energy system without considering the embodied emissions and life cycle costs of energy supply and BES. This work has proposed a systematic optimization framework to evaluate the energy flexibility of multiple building energy systems from an integrated perspective of the energy system and flexibility indicators. A novel set of EFIs is proposed so that an energy system's energy flexibility potential can be calculated for the complete life cycle. The EFIs are defined for the building architectural design to the energy system selection and operation, resulting in the evaluation of flexibility in all three domains of generation, system, and demand flexibilities.

Firstly, this study analyzed flexible thermal load against the optimized envelope design and its dependence on the climate. TRNSYS and Python-based NSGA-III were used for bi-objective optimization of a single-family household for twenty-four cities in twenty climate zones. The design variables of the optimization problem were insulation thickness of the envelope, window aperture angle, WWR, window shading fraction, radiation-based shading control, and orientation. The objective functions considered were the annual thermal load and the investment cost of insulation. An MCDM process was implemented through CRITIC and TOPSIS methods to find the best solution from the PFs. Even though the optimization reduced the thermal load in all investigated climates, it was more effective in the heating-dominant regions. Furthermore, it was observed that the weather conditions strongly influenced passive design parameters.

The passive design optimization results showed that thermal insulations of the envelope and WWR were the most perceptive design parameters as they determine the household's solar gains and transmission gains or losses. A highly insulated envelope was required in climates of high heating or cooling load. Therefore, the EPS thickness on external walls had higher ranges in continental-cold, continental-war summer, dry-hot, and tropical climate zones. The rockwool thickness on the roof was larger in heating-dominant locations of continental and temperate climate zones. The dry-cold climate zone was associated with mixed climate conditions and

required a lower level of insulation. The windows in the south direction, which were exposed to sunlight for an extended period, tended to increase the solar gains in continental and temperate climates. Similarly, the optimal orientation was North in those climates enabling the façade with maximum WWR to face South. On the contrary, dry-hot and tropical climate zones were characterized by cooling-dominant loads, minimum WWR, higher window shading, and the South (expect tropical-monsoon) as the optimal orientation.

In the second phase of the optimization framework, a set of fourteen energy system alternatives was defined as having different configurations of energy supply and HVAC systems. The energy systems were different combinations of the grid utility, PV with battery, FPCs, BHX, thermal energy storage, ASHPs, GSHPs, absorption chiller, radiator, and water coils. The EFIs of the alternatives were assessed by annual simulations of BESs and life-cycle analysis of costs and emissions. Although the EFIs provided an in-depth flexibility assessment of the energy system, the conflicting solutions from individual EFIs comprehended the MCDM approach for selecting the most suitable BES. Thus, the multi-criteria evaluation model used the flexibility assessment results to assign the weights of EFIs by the CRITIC weighting technique. Then, the TOPSIS method identified the most flexible energy system for a representative household building in four climates (severe cold, cold, mild, and hot). Finally, the stability of the MCDM results was assessed by creating five scenarios such that each scenario has different weights of EFIs. According to the MCDM results, the energy systems with air-to-water HP + PV + radiator (STK), brine-to-water HP + PV + radiator (SBK), air-to-air HP + PV + FPC (QTA), and absorption chiller + PV + FPCs (JKT) are the best options in the different locations.

Lastly, the energy flexibility potential of the BES was assessed by steady-state optimization of design parameters and temperature modulation by an MPC-based dynamic control. The SSO was based on annual simulations, whereas three representative months, January (cold), June (hot), and October (mild), were considered in the MPC scenario.

In SSO, the objectives were maximizing the primary energy ratio and minimizing the electricity demand of building service systems with constraints of thermal comfort level and fractional state of charge (FSOC) of battery storage. Thermal and electric storage capacities and borehole radius were the sources of system flexibility. Whereas mass flow rate of brine, starting/stopping delays, and temperature set points provided the demand flexibility. The annual assessments of EFIs indicated that the SSO strategy significantly improved the down-flex storage capacity and flexible energy throughout the year and, more prominently, during space heating. In contrast,

the residual load, operating cost, and operating emissions were higher than the reference scenario from May to October.

In MPC-based optimization, the building thermal load and boundary conditions dataset was used to develop a predictive model, communicating in a loop with a genetic algorithm to decide the control inputs. The supervisory controller modulated the reference temperatures of local PID controllers for space heating/cooling and windows' shading fraction to improve demand flexibility. The MPC optimizer significantly improved the demand flexibility in January, a month with high heating demand. On the other hand, the EFIs showed small flexibility potential in October, having low heating demand. In June, the residual load, operating cost, and operating emissions were higher than the reference scenario by a minimal value but lower than the SSO scenario.

6.2 Key findings

- The outcomes of this work provide comprehensive guidelines for the designers to make appropriate decisions about the household's passive design according to the climate. Previous building energy standards in the investigated locations provide only the limiting thermal transmittance values for the building envelope. These results set a benchmark for selecting energy-efficient envelope parameters and respective thermal transmittance ranges in the investigated climates, which can be applied worldwide, eliminating the traditional energy analysis process. It should be noted here that the optimal parameters strictly rely on one another and would not indicate remarkable improvement in energy demand if implemented individually.
- Selecting a flexible energy system in a location requires comprehensive flexibility indicators to understand the system performance and the interaction of its components rather than the individual performance criteria or operating characteristics. Since the choice of BES is strictly dependent on the local energy rates and associated GHG emissions, case-by-case evaluation should be conducted for energy system alternatives in each region. The outcome of this study could guide the energy system design for a household in different climates providing insight into energy flexibility.
- The MPC can improve the energy flexibility of the BES without compromising thermal comfort. This study elaborates on designing a thermal load-based prediction model and its coupling with the optimization algorithm to tackle the MPC problems in the context of different energy systems. The findings of this paper establish that the dataset of

building thermal load, boundary conditions, and control disturbances can be used to develop an MPC-based dynamic control. That controller could be employed on different building service systems to achieve energy flexibility.

6.3 Future work

Some ideas for future research have come up from this research work. Building envelope optimization considered limited locations in each climate zone and did not perform statistical analysis to validate the research findings. Therefore, further research should be conducted to statistically analyze these design parameters by considering more locations in each climate zone. It is also suggested to consider the variability in the price and GHG emissions of grid utility in different climate zones for employing the MCDM for selecting BES. The extended research would test the reliability of the MCDM approach for grid utility attributes in a climate. Since the MPC-optimizer did not improve energy flexibility in the summer in a cold climate, the MPC-based optimization strategy could be applied on various BESs in different climates to assess the certainty of the employed strategy.

References

[1] United Nations Environment Programme (2021), 2021 Global Status Report for Buildings and Construction: Towards a Zero-emission, Efficient and Resilient Buildings and Construction Sector, Nairobi, n.d. https://globalabc.org/resources/publications/2021-global-status-report-buildings-and-construction.

[2] Energy Information Administration (EIA), International Energy Outlook 2019, 2019.

[3] IEA (2017), Energy Technology Perspectives 2017, IEA, 2017. https://www.iea.org/reports/energy-technology-perspectives-2017.

[4] M. González-Torres, L. Pérez-Lombard, J.F. Coronel, I.R. Maestre, D. Yan, A review on buildings energy information: Trends, end-uses, fuels and drivers, Energy Reports. 8 (2022) 626–637. https://doi.org/10.1016/j.egyr.2021.11.280.

[5] D. Ürge-Vorsatz, L.F. Cabeza, S. Serrano, C. Barreneche, K. Petrichenko, Heating and cooling energy trends and drivers in buildings, Renewable and Sustainable Energy Reviews. 41 (2015) 85–98. https://doi.org/10.1016/j.rser.2014.08.039.

[6] European Commission, Energy performance of buildings directive, https://energy.ec.europa.eu/topics/energy-efficiency/energy-efficient-buildings/energy-performance-buildings-directive_en, 2018.

[7] European Commission, Energy efficiency directive, 2018. https://energy.ec.europa.eu/topics/energy-efficiency/energy-efficiency-targets-directive-and-rules/energy-efficiency-directive_en.

[8] W. Wu, H.M. Skye, P.A. Domanski, Selecting HVAC systems to achieve comfortable and cost-effective residential net-zero energy buildings, Appl Energy. 212 (2018) 577–591. https://doi.org/10.1016/j.apenergy.2017.12.046.

[9] U. Bac, K.A.M.S. Alaloosi, C. Turhan, A comprehensive evaluation of the most suitable HVAC system for an industrial building by using a hybrid building energy simulation and multi criteria decision making framework, Journal of Building Engineering. 37 (2021) 102153. https://doi.org/10.1016/j.jobe.2021.102153.

[10] M. Shahrestani, R. Yao, G.K. Cook, A fuzzy multiple attribute decision making tool for HVAC&R systems selection with considering the future probabilistic climate changes

and electricity decarbonisation plans in the UK, Energy Build. 159 (2018) 398–418. https://doi.org/10.1016/j.enbuild.2017.10.089.

[11] H. Yousefi, M.H. Ghodusinejad, Y. Noorollahi, GA/AHP-based optimal design of a hybrid CCHP system considering economy, energy and emission, Energy Build. 138 (2017) 309–317. https://doi.org/10.1016/j.enbuild.2016.12.048.

[12] S.Ø. Jensen, A. Marszal-Pomianowska, R. Lollini, W. Pasut, A. Knotzer, P. Engelmann, A. Stafford, G. Reynders, IEA EBC annex 67 energy flexible buildings, Energy Build. 155 (2017) 25–34.

[13] Z. Luo, J. Peng, J. Cao, R. Yin, B. Zou, Y. Tan, J. Yan, Demand Flexibility of Residential Buildings: Definitions, Flexible Loads, and Quantification Methods, Engineering. (2022). https://doi.org/10.1016/j.eng.2022.01.010.

[14] G. Reynders, R. Amaral Lopes, A. Marszal-Pomianowska, D. Aelenei, J. Martins, D. Saelens, Energy flexible buildings: An evaluation of definitions and quantification methodologies applied to thermal storage, Energy Build. 166 (2018) 372–390. https://doi.org/10.1016/j.enbuild.2018.02.040.

[15] Z. Liu, Y. Liu, B.-J. He, W. Xu, G. Jin, X. Zhang, Application and suitability analysis of the key technologies in nearly zero energy buildings in China, Renewable and Sustainable Energy Reviews. 101 (2019) 329–345. https://doi.org/10.1016/j.rser.2018.11.023.

[16] Z. Yu, Z. Gou, F. Qian, J. Fu, Y. Tao, Towards an optimized zero energy solar house: A critical analysis of passive and active design strategies used in Solar Decathlon Europe in Madrid, J Clean Prod. 236 (2019) 117646. https://doi.org/10.1016/j.jclepro.2019.117646.

[17] M. Usman, M. Ali, T. ur Rashid, H.M. Ali, G. Frey, Towards zero energy solar households – A model-based simulation and optimization analysis for a humid subtropical climate, Sustainable Energy Technologies and Assessments. 48 (2021) 101574. https://doi.org/10.1016/j.seta.2021.101574.

[18] Z. Zhou, L. Feng, S. Zhang, C. Wang, G. Chen, T. Du, Y. Li, J. Zuo, The operational performance of “net zero energy building”: A study in China, Appl Energy. 177 (2016) 716–728. https://doi.org/10.1016/j.apenergy.2016.05.093.

[19] D. Jonas, G. Frey, Model-based analysis of the performance and the environmental impact of solar thermal and heat pump systems, in: 2018 9th International Renewable Energy Congress (IREC), IEEE, 2018: pp. 1–6. https://doi.org/10.1109/IREC.2018.8362569.

[20] C. Far, H. Far, Improving energy efficiency of existing residential buildings using effective thermal retrofit of building envelope, Indoor and Built Environment. 28 (2019) 744–760. https://doi.org/10.1177/1420326X18794010.

[21] REN21, Renewables 2020 Global Status Report, REN21 Secretariat, Paris, 2020.

[22] R. Fardi Asrami, A. Sohani, E. Saedpanah, H. Sayyaadi, Towards achieving the best solution to utilize photovoltaic solar panels for residential buildings in urban areas, Sustain Cities Soc. 71 (2021) 102968. https://doi.org/10.1016/j.scs.2021.102968.

[23] A. Dashti, M. Gholami Korzani, Study of geothermal energy potential as a green source of energy with a look at energy consumption in Iran, Geothermal Energy. 9 (2021) 28. https://doi.org/10.1186/s40517-021-00210-2.

[24] R. Neves, H. Cho, J. Zhang, Pairing geothermal technology and solar photovoltaics for net-zero energy homes, Renewable and Sustainable Energy Reviews. 140 (2021) 110749. https://doi.org/10.1016/j.rser.2021.110749.

[25] R. Evins, Multi-level optimization of building design, energy system sizing and operation, Energy. 90 (2015) 1775–1789. https://doi.org/10.1016/j.energy.2015.07.007.

[26] W. Wu, H.M. Skye, Net-zero nation: HVAC and PV systems for residential net-zero energy buildings across the United States, Energy Convers Manag. 177 (2018) 605–628. https://doi.org/10.1016/j.enconman.2018.09.084.

[27] D. Jonas, G. Frey, D. Theis, Simulation and performance analysis of combined parallel solar thermal and ground or air source heat pump systems, Solar Energy. 150 (2017) 500–511. https://doi.org/10.1016/j.solener.2017.04.070.

[28] M. Mork, A. Xhonneux, D. Müller, Nonlinear Distributed Model Predictive Control for multi-zone building energy systems, Energy Build. 264 (2022) 112066. https://doi.org/10.1016/j.enbuild.2022.112066.

[29] Z. Wang, J. Calautit, S. Wei, P.W. Tien, L. Xia, Real-time building heat gains prediction and optimization of HVAC setpoint: An integrated framework, Journal of Building Engineering. (2022) 104103. https://doi.org/10.1016/j.jobe.2022.104103.

[30] Y. Guo, D. Bart, Optimization of design parameters for office buildings with climatic adaptability based on energy demand and thermal comfort, Sustainability (Switzerland). 12 (2020) 1–23. https://doi.org/10.3390/SU12093540.

[31] M. Balbis-Morejón, J.J. Cabello-Eras, J.M. Rey-Hernández, F.J. Rey-Martínez, Global Air Conditioning Performance Indicator (ACPI) for buildings, in tropical climate, Build Environ. 203 (2021) 108071. https://doi.org/10.1016/j.buildenv.2021.108071.

[32] T. Péan, R. Costa-Castelló, J. Salom, Price and carbon-based energy flexibility of residential heating and cooling loads using model predictive control, Sustain Cities Soc. 50 (2019) 101579. https://doi.org/10.1016/j.scs.2019.101579.

[33] J. Vivian, U. Chiodarelli, G. Emmi, A. Zarrella, A sensitivity analysis on the heating and cooling energy flexibility of residential buildings, Sustain Cities Soc. 52 (2020) 101815. https://doi.org/10.1016/j.scs.2019.101815.

[34] P. Munankarmi, J. Maguire, S.P. Balamurugan, M. Blonsky, D. Roberts, X. Jin, Community-scale interaction of energy efficiency and demand flexibility in residential buildings, Appl Energy. 298 (2021) 117149. https://doi.org/10.1016/j.apenergy.2021.117149.

[35] K. Foteinaki, R. Li, A. Heller, C. Rode, Heating system energy flexibility of low-energy residential buildings, Energy Build. 180 (2018) 95–108. https://doi.org/10.1016/j.enbuild.2018.09.030.

[36] TRANSSOLAR Energietechnik, Multizone Building modeling with Type56 and TRNBuild, in: Trnsys 18 Documantation, 2017. http://www.trnsys.com/.

[37] M. Usman, G. Frey, Multi-Objective Techno-Economic Optimization of Design Parameters for Residential Buildings in Different Climate Zones, Sustainability. 14 (2021) 65.

[38] M. Usman, D. Jonas, G. Frey, A methodology for multi-criteria assessment of renewable integrated energy supply options and alternative HVAC systems in a household, Energy Build. 273 (2022) 112397. https://doi.org/10.1016/j.enbuild.2022.112397.

[39] M. Usman, D.M. Minhas, G. Frey, Energy optimization of a residential building using model predictive control-A case study in temperate oceanic climate, in: 2022 International Conference on Electrical, Computer and Energy Technologies (ICECET), IEEE, 2022: pp. 1–6. https://doi.org/10.1109/ICECET55527.2022.9872555.

[40] H. Li, Z. Wang, T. Hong, M.A. Piette, Energy flexibility of residential buildings: A systematic review of characterization and quantification methods and applications, Advances in Applied Energy. 3 (2021) 100054. https://doi.org/10.1016/j.adapen.2021.100054.

[41] X. Ayón, J.K. Gruber, B.P. Hayes, J. Usaola, M. Prodanović, An optimal day-ahead load scheduling approach based on the flexibility of aggregate demands, Appl Energy. 198 (2017) 1–11. https://doi.org/10.1016/j.apenergy.2017.04.038.

[42] R. De Coninck, L. Helsen, Quantification of flexibility in buildings by cost curves – Methodology and application, Appl Energy. 162 (2016) 653–665. https://doi.org/10.1016/j.apenergy.2015.10.114.

[43] J. Ma, V. Silva, R. Belhomme, D.S. Kirschen, L.F. Ochoa, Evaluating and Planning Flexibility in Sustainable Power Systems, IEEE Trans Sustain Energy. 4 (2013) 200–209. https://doi.org/10.1109/TSTE.2012.2212471.

[44] K.O. Aduda, T. Labeodan, W. Zeiler, G. Boxem, Demand side flexibility coordination in office buildings: A framework and case study application, Sustain Cities Soc. 29 (2017) 139–158. https://doi.org/10.1016/j.scs.2016.12.008.

[45] H. Johra, P. Heiselberg, J. Le Dréau, Influence of envelope, structural thermal mass and indoor content on the building heating energy flexibility, Energy Build. 183 (2019) 325–339. https://doi.org/10.1016/j.enbuild.2018.11.012.

[46] H. Johra, A. Marszal-Pomianowska, J.R. Ellingsgaard, M. Liu, Building energy flexibility: A sensitivity analysis and key performance indicator comparison, in: J Phys Conf Ser, IOP Publishing, 2019: p. 12064.

[47] K. Foteinaki, R. Li, T. Péan, C. Rode, J. Salom, Evaluation of energy flexibility of low-energy residential buildings connected to district heating, Energy Build. 213 (2020) 109804. https://doi.org/10.1016/j.enbuild.2020.109804.

[48] T. Weiß, A.M. Fulterer, A. Knotzer, Energy flexibility of domestic thermal loads–a building typology approach of the residential building stock in Austria, Advances in

Building Energy Research. 13 (2019) 122–137. https://doi.org/10.1080/17512549.2017.1420606.

[49] K. Zhang, M. Kummert, Evaluating the impact of thermostat control strategies on the energy flexibility of residential buildings for space heating, in: Build Simul, Springer, 2021: pp. 1439–1452. https://doi.org/10.1007/s12273-020-0751-x.

[50] J. Le Dréau, P. Heiselberg, Energy flexibility of residential buildings using short term heat storage in the thermal mass, Energy. 111 (2016) 991–1002. https://doi.org/10.1016/j.energy.2016.05.076.

[51] Y. Zhou, S. Cao, Quantification of energy flexibility of residential net-zero-energy buildings involved with dynamic operations of hybrid energy storages and diversified energy conversion strategies, Sustainable Energy, Grids and Networks. 21 (2020) 100304. https://doi.org/10.1016/j.segan.2020.100304.

[52] J. Clauß, S. Stinner, I. Sartori, L. Georges, Predictive rule-based control to activate the energy flexibility of Norwegian residential buildings: Case of an air-source heat pump and direct electric heating, Appl Energy. 237 (2019) 500–518. https://doi.org/10.1016/j.apenergy.2018.12.074.

[53] F. Mancini, B. Nastasi, Energy retrofitting effects on the energy flexibility of dwellings, Energies (Basel). 12 (2019) 2788. https://doi.org/doi.org/10.3390/en12142788.

[54] A. Bampoulas, M. Saffari, F. Pallonetto, E. Mangina, D.P. Finn, A fundamental unified framework to quantify and characterise energy flexibility of residential buildings with multiple electrical and thermal energy systems, Appl Energy. 282 (2021) 116096. https://doi.org/10.1016/j.apenergy.2020.116096.

[55] G. Reynders, J. Diriken, D. Saelens, Generic characterization method for energy flexibility: Applied to structural thermal storage in residential buildings, Appl Energy. 198 (2017) 192–202. https://doi.org/10.1016/j.apenergy.2017.04.061.

[56] T. Méndez Echenagucia, A. Capozzoli, Y. Cascone, M. Sassone, The early design stage of a building envelope: Multi-objective search through heating, cooling and lighting energy performance analysis, Appl Energy. 154 (2015) 577–591. https://doi.org/10.1016/j.apenergy.2015.04.090.

[57] W. Yu, B. Li, H. Jia, M. Zhang, D. Wang, Application of multi-objective genetic algorithm to optimize energy efficiency and thermal comfort in building design, Energy Build. 88 (2015) 135–143. https://doi.org/10.1016/j.enbuild.2014.11.063.

[58] S.G. Yong, J.H. Kim, Y. Gim, J. Kim, J. Cho, H. Hong, Y.J. Baik, J. Koo, Impacts of building envelope design factors upon energy loads and their optimization in US standard climate zones using experimental design, Energy Build. 141 (2017) 1–15. https://doi.org/10.1016/j.enbuild.2017.02.032.

[59] J. Woolley, S. Schiavon, F. Bauman, P. Raftery, Side-by-side laboratory comparison of radiant and all-air cooling: How natural ventilation cooling and heat gain characteristics impact space heat extraction rates and daily thermal energy use, Energy Build. 200 (2019) 68–85. https://doi.org/10.1016/j.enbuild.2019.07.020.

[60] V. Lapinskienė, V. Motuzienė, R. Džiugaitė-Tumėnienė, R. Mikučionienė, Impact of internal heat gains on building's energy performance, 10th International Conference on Environmental Engineering, ICEE 2017. (2017). https://doi.org/10.3846/enviro.2017.265.

[61] U. Acar, O. Kaska, N. Tokgoz, Multi-objective optimization of building envelope components at the preliminary design stage for residential buildings in Turkey, Journal of Building Engineering. 42 (2021) 102499. https://doi.org/10.1016/j.jobe.2021.102499.

[62] Y. Dong, C. Sun, Y. Han, Q. Liu, Intelligent optimization: A novel framework to automatize multi-objective optimization of building daylighting and energy performances, Journal of Building Engineering. 43 (2021) 102804. https://doi.org/10.1016/j.jobe.2021.102804.

[63] P. Penna, A. Prada, F. Cappelletti, A. Gasparella, Multi-objectives optimization of Energy Efficiency Measures in existing buildings, Energy Build. 95 (2015) 57–69. https://doi.org/10.1016/j.enbuild.2014.11.003.

[64] M. Rabani, H. Bayera Madessa, N. Nord, Achieving zero-energy building performance with thermal and visual comfort enhancement through optimization of fenestration, envelope, shading device, and energy supply system, Sustainable Energy Technologies and Assessments. 44 (2021) 101020. https://doi.org/10.1016/j.seta.2021.101020.

[65] F. Ascione, R.F. De Masi, F. de Rossi, S. Ruggiero, G.P. Vanoli, Optimization of building envelope design for nZEBs in Mediterranean climate: Performance analysis of

residential case study, Appl Energy. 183 (2016) 938–957. https://doi.org/10.1016/j.apenergy.2016.09.027.

[66] M. Ferrara, J.C. Vallée, L. Shtrepi, A. Astolfi, E. Fabrizio, A thermal and acoustic co-simulation method for the multi-domain optimization of nearly zero energy buildings, Journal of Building Engineering. 40 (2021) 102699. https://doi.org/10.1016/j.jobe.2021.102699.

[67] S. Chang, D. Castro-Lacouture, Y. Yamagata, Decision support for retrofitting building envelopes using multi-objective optimization under uncertainties, Journal of Building Engineering. 32 (2020) 101413. https://doi.org/10.1016/j.jobe.2020.101413.

[68] J. Zhao, Y. Du, Multi-objective optimization design for windows and shading configuration considering energy consumption and thermal comfort: A case study for office building in different climatic regions of China, Solar Energy. 206 (2020) 997–1017. https://doi.org/10.1016/j.solener.2020.05.090.

[69] F. Harkouss, F. Fardoun, P.H. Biwole, Passive design optimization of low energy buildings in different climates, Energy. 165 (2018) 591–613. https://doi.org/10.1016/j.energy.2018.09.019.

[70] S. Naji, L. Aye, M. Noguchi, Multi-objective optimisations of envelope components for a prefabricated house in six climate zones, Appl Energy. 282 (2021) 116012. https://doi.org/10.1016/j.apenergy.2020.116012.

[71] F. Harkouss, F. Fardoun, P.H. Biwole, Multi-objective optimization methodology for net zero energy buildings, Journal of Building Engineering. 16 (2018) 57–71. https://doi.org/10.1016/j.jobe.2017.12.003.

[72] N. Delgarm, B. Sajadi, S. Delgarm, F. Kowsary, A novel approach for the simulation-based optimization of the buildings energy consumption using NSGA-II: Case study in Iran, Energy Build. 127 (2016) 552–560. https://doi.org/10.1016/j.enbuild.2016.05.052.

[73] O. Ayadi, S. Al-Dahidi, Comparison of solar thermal and solar electric space heating and cooling systems for buildings in different climatic regions, Solar Energy. 188 (2019) 545–560. https://doi.org/10.1016/j.solener.2019.06.033.

[74] I. Siksnelyte-Butkiene, E.K. Zavadskas, D. Streimikiene, Multi-Criteria Decision-Making (MCDM) for the Assessment of Renewable Energy Technologies in a Household: A Review, Energies . 13 (2020). https://doi.org/10.3390/en13051164.

[75] J. Wang, Y. Liu, F. Ren, S. Lu, Multi-objective optimization and selection of hybrid combined cooling, heating and power systems considering operational flexibility, Energy. 197 (2020) 117313. https://doi.org/10.1016/j.energy.2020.117313.

[76] M. Shahrestani, R. Yao, G.K. Cook, Characterising the energy performance of centralised HVAC&R systems in the UK, Energy Build. 62 (2013) 239–247. https://doi.org/10.1016/j.enbuild.2013.03.016.

[77] A. Avgelis, A.M. Papadopoulos, Application of multicriteria analysis in designing HVAC systems, Energy Build. 41 (2009) 774–780. https://doi.org/10.1016/j.enbuild.2009.02.011.

[78] H. Wang, R. Lahdelma, MCDM for sustainability ranking of district heating systems considering uncertainties, in: Life Cycle Sustainability Assessment for Decision-Making, Elsevier, 2020: pp. 139–153. https://doi.org/10.1016/B978-0-12-818355-7.00007-5.

[79] K. Alanne, A. Salo, A. Saari, S.-I. Gustafsson, Multi-criteria evaluation of residential energy supply systems, Energy Build. 39 (2007) 1218–1226. https://doi.org/10.1016/j.enbuild.2007.01.009.

[80] H. Ren, W. Gao, W. Zhou, K. Nakagami, Multi-criteria evaluation for the optimal adoption of distributed residential energy systems in Japan, Energy Policy. 37 (2009) 5484–5493. https://doi.org/10.1016/j.enpol.2009.08.014.

[81] K. Kontu, S. Rinne, V. Olkkonen, R. Lahdelma, P. Salminen, Multicriteria evaluation of heating choices for a new sustainable residential area, Energy Build. 93 (2015) 169–179. https://doi.org/10.1016/j.enbuild.2015.02.003.

[82] R. Džiugaitė-Tumėnienė, V. Motuzienė, G. Šiupšinskas, K. Čiuprinskas, A. Rogoža, Integrated assessment of energy supply system of an energy-efficient house, Energy Build. 138 (2017) 443–454. https://doi.org/10.1016/j.enbuild.2016.12.058.

[83] Y. Yang, J. Ren, H.S. Solgaard, D. Xu, T.T. Nguyen, Using multi-criteria analysis to prioritize renewable energy home heating technologies, Sustainable Energy Technologies and Assessments. 29 (2018) 36–43. https://doi.org/10.1016/j.seta.2018.06.005.

[84] F. Harkouss, F. Fardoun, P.H. Biwole, Optimal design of renewable energy solution sets for net zero energy buildings, Energy. 179 (2019) 1155–1175. https://doi.org/10.1016/j.energy.2019.05.013.

[85] M. Babatunde, D. Ighravwe, A CRITIC-TOPSIS framework for hybrid renewable energy systems evaluation under techno-economic requirements, Journal of Project Management. 4 (2019) 109–126. https://doi.org/10.5267/j.jpm.2018.12.001.

[86] T. Salameh, E.T. Sayed, M.A. Abdelkareem, A.G. Olabi, H. Rezk, Optimal selection and management of hybrid renewable energy System: Neom city as a case study, Energy Convers Manag. 244 (2021) 114434. https://doi.org/10.1016/j.enconman.2021.114434.

[87] T.Q. Péan, J. Salom, R. Costa-Castelló, Review of control strategies for improving the energy flexibility provided by heat pump systems in buildings, J Process Control. 74 (2019) 35–49. https://doi.org/10.1016/j.jprocont.2018.03.006.

[88] J.C. Beagon, C. Finck, P. Vogler-Finck, Paul, Control strategies for building energy systems to unlock demand side flexibility – A review, (n.d.). https://doi.org/10.26868/25222708.2017.462.

[89] D. Mariano-Hernández, L. Hernández-Callejo, A. Zorita-Lamadrid, O. Duque-Pérez, F. Santos García, A review of strategies for building energy management system: Model predictive control, demand side management, optimization, and fault detect & diagnosis, Journal of Building Engineering. 33 (2021) 101692. https://doi.org/10.1016/j.jobe.2020.101692.

[90] M. Killian, M. Kozek, Ten questions concerning model predictive control for energy efficient buildings, Build Environ. 105 (2016) 403–412. https://doi.org/10.1016/j.buildenv.2016.05.034.

[91] M. Ławryńczuk, P. Ocłoń, Model Predictive Control and energy optimisation in residential building with electric underfloor heating system, Energy. 182 (2019) 1028–1044. https://doi.org/10.1016/j.energy.2019.06.062.

[92] A. Marszal-Pomianowska, H. Johra, T. Weis, A. Knotzer, S.Ø. Jensen, H. Kazmi, I. Vigna, R. Pernet, J. Le Dréau, K. Zhang, International Energy Agency-Characterization of Energy Flexibility in Buildings: Energy in Buildings and Communities Programme Annex 67 Energy Flexible Buildings, Danish Technological Institute, 2019.

[93] J. Salpakari, P. Lund, Optimal and rule-based control strategies for energy flexibility in buildings with PV, Appl Energy. 161 (2016) 425–436. https://doi.org/10.1016/j.apenergy.2015.10.036.

[94] F. Mancini, S. Romano, G. Lo Basso, J. Cimaglia, L. de Santoli, How the italian residential sector could contribute to load flexibility in demand response activities: A methodology for residential clustering and developing a flexibility strategy, Energies (Basel). 13 (2020) 3359. https://doi.org/10.3390/en13133359.

[95] R. Dott, J. Ruschenburg, F. Ochs, J. Bony, M. Haller, The Reference Framework for System Simulation of the IEA SHC Task 44 / HPP Annex 38 - Part B: Buildings and Space Heat Load, 2013. https://doi.org/10.13140/2.1.2221.4727.

[96] R. Mikulits, T. Wolfgang, OIB-Directives 6: Energy saving and thermal protection, (2015).

[97] Pacific Northwest National Laboratory, Country Report on Building Energy Codes in China, (2009).

[98] H. Ramin, H. Karimi, Optimum envelope design toward zero energy buildings in Iran, in: E3S Web of Conferences, EDP Sciences, Tallinn, Estonia, 2020: p. 16004. https://doi.org/10.1051/e3sconf/202017216004.

[99] A. Council, Energy efficiency building standards in Japan, Acesso Em Março. (2007) 1–9.

[100] C.F. Hansen, M.L. Hansen, Executive Order on the Publication of the Danish Building Regulations 2015 (BR15), The Danish Transport and Construction Agency, 2015.

[101] F.U. Vogdt, M. Walsdorf-Maul, K. Schwabe, F. Schaudienst, A. Baumbach, Comparison between calculating methods of energy saving regulations and their economic efficiency, Czasopismo Techniczne. Budownictwo. 109 (2012) 423–430.

[102] G. Britain, The Building Regulations 2010: Conservation of Fuel and Power: Approved Document L1A, NBS, 2014.

[103] R. Bordier, N. Rezaï, Implementing the Energy Performance of Buildings Directive-EPBD implementation in France, 2018.

[104] R.V. Bruke, M.S. Gil, D.J. Gonzalez, J.S. Rodriguez, Guía de aplicación del DB-HE 2019 - CTE, 2020.

[105] S.S. Longo, M. Cellura, M.A. Cusenza, F. Guarino, Marotta, Selecting insulating materials for building envelope: A life cycle approach., A Life Cycle Approach. TECNICA ITALIANA-Italian Journal of Engineering Science. 65 (2021) 312–316. https://doi.org/10.18280/ti-ijes.652-426.

[106] D. Bienvenido-Huertas, M. Oliveira, C. Rubio-Bellido, D. Marín, A comparative analysis of the international regulation of thermal properties in building envelope, Sustainability. 11 (2019) 5574. https://doi.org/10.3390/su11205574.

[107] M. Mahboob, T. ur Rashid, M. Amjad, Assessment of Energy Saving Potential in Residential Sector of Pakistan through Implementation of NEECA and PEC Building Standards, in: 2019 15th International Conference on Emerging Technologies (ICET), IEEE, 2019: pp. 1–6. https://doi.org/10.1109/ICET48972.2019.8994750.

[108] Government of Dubai, A PRACTICE GUIDE FOR BUILDING A SUSTAINABLE DUBAI, Dubai Green Building System, 2020.

[109] Building, C. Authority, Code for environmental sustainability of buildings, (2012).

[110] Bureau of Energy Efficiency, Energy Conservation Building Code, (2017).

[111] ASHRAE, Standard 90.2-2018, Energy Efficient Design of Low-Rise Residential Buildings, The American Society of Heating, Refrigerating and Air-Conditioning Engineers, 2018.

[112] Boverket, The National Board of Housing, Building and Planning's building regulations, BBR 18, BFS 2011:26, (2011).

[113] J. Widén, M. Lundh, I. Vassileva, E. Dahlquist, K. Ellegård, E. Wäckelgård, Constructing load profiles for household electricity and hot water from time-use data-Modelling approach and validation, Energy Build. 41 (2009) 753–768. https://doi.org/10.1016/j.enbuild.2009.02.013.

[114] Verein Deutscher Ingenieure, VDI 4655 – Reference Load Profiles of Single-family and Multi-family Houses for the Use of CHP Systems, 2008.

[115] H. Wang, H. Fang, X. Yu, S. Liang, How real time pricing modifies Chinese households' electricity consumption, J Clean Prod. 178 (2018) 776–790. https://doi.org/10.1016/j.jclepro.2017.12.251.

[116] S.M. Hakimi, Multivariate stochastic modeling of washing machine loads profile in Iran, Sustain Cities Soc. 26 (2016) 170–185. https://doi.org/10.1016/j.scs.2016.06.004.

[117] H. Shiraki, S. Nakamura, S. Ashina, K. Honjo, Estimating the hourly electricity profile of Japanese households – Coupling of engineering and statistical methods, Energy. 114 (2016) 478–491. https://doi.org/10.1016/j.energy.2016.08.019.

[118] G. Trotta, An empirical analysis of domestic electricity load profiles: Who consumes how much and when?, Appl Energy. 275 (2020) 115399. https://doi.org/10.1016/j.apenergy.2020.115399.

[119] J.-P. Zimmermann, M. Evans, T. Lineham, J. Griggs, G. Surveys, L. Harding, N. King, P. Roberts, Household Electricity Survey: A study of domestic electrical product usage, 2012. https://www.gov.uk/government/uploads/system/uploads/attachment_data/file/208097/10043_R66141HouseholdElectricitySurveyFinalReportissue4.pdf.

[120] T. Csoknyai, J. Legardeur, A.A. Akle, M. Horváth, Analysis of energy consumption profiles in residential buildings and impact assessment of a serious game on occupants' behavior, Energy Build. 196 (2019) 1–20. https://doi.org/10.1016/j.enbuild.2019.05.009.

[121] A. Alberini, G. Prettico, C. Shen, J. Torriti, Hot weather and residential hourly electricity demand in Italy, Energy. 177 (2019) 44–56. https://doi.org/10.1016/j.energy.2019.04.051.

[122] S.E. Policy, D. Francisco, M. Freire, C. Ferreira, Residential Sector Energy Consumption at the Spotlight : From Data to Knowledge, 2017.

[123] The Energy Informatics Group, PRECON Pakistan Residential Electricity Consumption Dataset, (2019). https://opendata.com.pk/dataset/precon-pakistan-residential-electricity-consumption-dataset.

[124] I. Almohanna, Solar Dcathlon Middle East, TEAM KSU :PROJECT MANUAL, 2019.

[125] P. Gupta, T.T.T. Zan, J. Dauwels, A. Ukil, Flow-Based Estimation and Comparative Study of Gas Demand Profile for Residential Units in Singapore, IEEE Trans Sustain Energy. 10 (2019) 1120–1128. https://doi.org/10.1109/TSTE.2018.2861821.

[126] A. Garg, P.R. Shukla, J. Maheshwari, J. Upadhyay, An assessment of household electricity load curves and corresponding CO2 marginal abatement cost curves for

Gujarat state, India, Energy Policy. 66 (2014) 568–584. https://doi.org/10.1016/j.enpol.2013.10.068.

[127] T. Kubota, U. Surahman, O. Higashi, A comparative analysis of household energy consumption in Jakarta and Bandung, 30th International PLEA Conference: Sustainable Habitat for Developing Societies: Choosing the Way Forward - Proceedings. 2 (2014) 260–267.

[128] P. Kuusela, I. Norros, R. Weiss, T. Sorasalmi, Practical lognormal framework for household energy consumption modeling, Energy Build. 108 (2015) 223–235. https://doi.org/10.1016/j.enbuild.2015.09.008.

[129] M.Y. Haller, R. Dott, J. Ruschenburg, F. Ochs, J. Bony, The Reference Framework for System Simulations of the IEA SHC Task 44/HPP Annex 38 Part A: General Simulation Boundary Conditions, International Energy Agency, A Technical Report of Subtask CReport C1 Part A. (2013).

[130] ASHRAE Project Committee 90.1, Schedules and internal loads for Appendix C, n.d. https://web.ashrae.org/90_1files/.

[131] R. Parsons, ed., ASHRAE Handbook - Fundamental, American Society of Heating Refrigerating and Air-Conditioning Engineers, 2001.

[132] D. Jonas, D. Theis, G. Frey, Implementation and Experimental Validation of a Photovoltaic-Thermal (PVT) Collector Model in TRNSYS, in: Proceedings of the 12th International Conference on Solar Energy for Buildings and Industry (EuroSun2018), Rapperswil, Switzerland, 2018. https://doi.org/10.18086/eurosun2018.02.16.

[133] D. Jonas, M. Lämmle, D. Theis, S. Schneider, G. Frey, Performance modeling of PVT collectors: Implementation, validation and parameter identification approach using TRNSYS, Solar Energy. 193 (2019) 51–64. https://doi.org/10.1016/j.solener.2019.09.047.

[134] R. Heimrath, M. Haller, The reference heating system, the template solar system of task 32, A Report of IEA Solar Heating and Cooling Programme–Task. 32 (2007).

[135] ASHRAE, 2019 ASHRAE Handbook - HVAC Applications, Chapter 35, 2019. https://www.ashrae.org/technical-resources/ashrae-handbook.

[136] R. Dott, M.Y. Haller, J. Ruschenburg, F. Ochs, J. Bony, The reference framework for system simulations of the IEA SHC Task 44/HPP Annex 38 Part B: buildings and space heat load, International Energy Agency. (2013).

[137] J. Salom, A.J. Marszal, Analysis of load match and grid interaction indicators in NZEB with high-resolution data, (2014).

[138] Greenhouse gas emission intensity of electricity generation in Europe, (n.d.). https://www.eea.europa.eu/data-and-maps/indicators/overview-of-the-electricity-production-3/assessment-1.

[139] I. Yousuf, A.R. Ghumman, H.N. Hashmi, M.A. Kamal, Carbon emissions from power sector in Pakistan and opportunities to mitigate those, Renewable and Sustainable Energy Reviews. 34 (2014) 71–77. https://doi.org/10.1016/j.rser.2014.03.003.

[140] THE G20 TRANSITION TOWARDS A NET-ZERO EMISSIONS ECONOMY, (2019). https://www.climate-transparency.org/wp-content/uploads/2019/11/Brown-to-Green-Report-2019.pdf.

[141] A.K. Hunter, Comparative Life Cycle Assessment: ground source heat pump system versus gas furnace and air conditioner system, (2017). https://doi.org/10.32920/ryerson.14665932.v1.

[142] I. Gounaris, Environmental Performance Assessment of Heat Pumps, (2015). https://repository.ihu.edu.gr//xmlui/handle/11544/136 (accessed March 19, 2022).

[143] M. Beccali, M. Cellura, F. Ardente, S. Longo, B. Nocke, P. Finocchiaro, A. Kleijer, C. Hildbrand, J. Bony, S. Citherlet, Task 38 Solar Air-Conditioning and Refrigeration "Life Cycle Assessment of Solar Cooling Systems" A technical report of subtask D Subtask Activity D3, (2010).

[144] L.C. Stages, Life cycle greenhouse gas emissions from solar photovoltaics, J. Ind. Ecol. (2012). https://www.nrel.gov/docs/fy13osti/56487.pdf (accessed April 20, 2022).

[145] Q. Dai, J.C. Kelly, L. Gaines, M. Wang, Life cycle analysis of lithium-ion batteries for automotive applications, Batteries. 5 (2019) 48.

[146] M. Zheng, R. Fang, Z. Yu, Life cycle assessment of residential heating systems: a comparison of distributed and centralized systems, Energy Procedia. 104 (2016) 287–292.

[147] M. Nyman, C.J. Simonson, Life cycle assessment of residential ventilation units in a cold climate, Build Environ. 40 (2005) 15–27. https://doi.org/10.1016/j.buildenv.2004.04.011.

[148] Life cycle assessment of SWEP 25 heat exchanger through SSP G8 tool, (n.d.). https://www.swep.net/support/ssp-calculation-software/ssp-g8/.

[149] STROM-REPORT-STROMPREISE VERGLEICHEN, (n.d.). https://strom-report.de/strompreise/ (accessed March 23, 2022).

[150] National Electric Power Regulatory Authority Pakistan, Consumer-End Applicable Tariff, (2022). https://nepra.org.pk/consumer.

[151] State Electricity Company (PLN) Indonesia, ELECTRICITY TARIFF, (n.d.). https://web.pln.co.id/pelanggan/tarif-tenaga-listrik.

[152] International Energy Agency, Technology Roadmap Energy-efficient Buildings: Heating and Cooling Equipment, (2011). https://sustainable.stanford.edu/sites/default/files/IEA_buildings_roadmap.pdf.

[153] F. Asdrubali, G. Baldinelli, A. Presciutti, Solar coolng with small size chiller: State of the art, 14th European Conference - Renewable Energy in Heating and Cooling. (2011).

[154] Heat exchanger SWEP 25TH, (n.d.). https://www.heat-exchangers.uk/shop/exchanger.php?vymenik=B25TH&desek=40.

[155] Reflex Storatherm Heat, (n.d.). https://www.reflex-winkelmann.com/int/products/reflex_products/Heat/.

[156] The Unico System, Modular Water Coils, (n.d.). https://www.unicosystem.com/Shop/indoor-units/modular-coils/.

[157] J.N. Mayer, Current and Future Cost of Photovoltaics:Long-term Scenarios for Market Development, System Prices and LCOE of Utility-Scale PV Systems, (2015). https://www.agora-energiewende.de/en/publications/current-and-future-cost-of-photovoltaics/ (accessed March 20, 2022).

[158] B. Carlsson, H. Persson, M. Meir, J. Rekstad, A total cost perspective on use of polymeric materials in solar collectors – Importance of environmental performance on suitability, Appl Energy. 125 (2014) 10–20. https://doi.org/10.1016/j.apenergy.2014.03.027.

[159] Hoppecke 2 OPzV bloc solar.power, (n.d.). https://www.europe-solarstore.com/hoppecke-2-opzv-bloc-solar-power-120-12v.html.

[160] J. Morrissey, R.E. Horne, Life cycle cost implications of energy efficiency measures in new residential buildings, Energy Build. 43 (2011) 915–924. https://doi.org/10.1016/j.enbuild.2010.12.013.

[161] B.H. Goh, Y. Sun, The development of life-cycle costing for buildings, Building Research & Information. 44 (2016) 319–333. https://doi.org/10.1080/09613218.2014.993566.

[162] E. and I.S. Department of Business, Whole Life Cost of Energy (WLCOE) Calculator – User Guide, n.d. https://assets.publishing.service.gov.uk/government/uploads/system/uploads/attachment_data/file/860772/whole-life-cost-of-energy-calculator-user-guide.pdf (accessed May 6, 2021).

[163] A.R. Starke, J.M. Cardemil, R. Escobar, S. Colle, Multi-objective optimization of hybrid CSP+PV system using genetic algorithm, Energy. 147 (2018) 490–503. https://doi.org/10.1016/j.energy.2017.12.116.

[164] Z. Jalali, E. Noorzai, S. Heidari, Design and optimization of form and facade of an office building using the genetic algorithm, Sci Technol Built Environ. 26 (2020) 128–140. https://doi.org/10.1080/23744731.2019.1624095.

[165] A. Zhang, R. Bokel, A. van den Dobbelsteen, Y. Sun, Q. Huang, Q. Zhang, Optimization of thermal and daylight performance of school buildings based on a multi-objective genetic algorithm in the cold climate of China, Energy Build. 139 (2017) 371–384. https://doi.org/0.1016/j.enbuild.2017.01.048.

[166] Nasruddin, Sholahudin, P. Satrio, T.M.I. Mahlia, N. Giannetti, K. Saito, Optimization of HVAC system energy consumption in a building using artificial neural network and multi-objective genetic algorithm, Sustainable Energy Technologies and Assessments. 35 (2019) 48–57. https://doi.org/10.1016/j.seta.2019.06.002.

[167] M.-D. Yang, M.-D. Lin, Y.-H. Lin, K.-T. Tsai, Multiobjective optimization design of green building envelope material using a non-dominated sorting genetic algorithm, Appl Therm Eng. 111 (2017) 1255–1264. https://doi.org/10.1016/j.applthermaleng.2016.01.015.

[168] K. Li, L. Pan, W. Xue, H. Jiang, H. Mao, Multi-Objective Optimization for Energy Performance Improvement of Residential Buildings: A Comparative Study, Energies (Basel). 10 (2017). https://doi.org/10.3390/en10020245.

[169] J. Ferdyn-Grygierek, K. Grygierek, Multi-Variable Optimization of Building Thermal Design Using Genetic Algorithms, Energies (Basel). 10 (2017). https://doi.org/10.3390/en10101570.

[170] M.J. Mayer, A. Szilágyi, G. Gróf, Environmental and economic multi-objective optimization of a household level hybrid renewable energy system by genetic algorithm, Appl Energy. 269 (2020) 115058. https://doi.org/10.1016/j.apenergy.2020.115058.

[171] M. Ghaderian, F. Veysi, Multi-objective optimization of energy efficiency and thermal comfort in an existing office building using NSGA-II with fitness approximation: A case study, Journal of Building Engineering. 41 (2021) 102440. https://doi.org/10.1016/j.jobe.2021.102440.

[172] A. Benítez-Hidalgo, A.J. Nebro, J. García-Nieto, I. Oregi, J. Del Ser, jMetalPy: A Python framework for multi-objective optimization with metaheuristics, Swarm Evol Comput. 51 (2019) 100598. https://doi.org/10.1016/j.swevo.2019.100598.

[173] H. Li, K. Deb, Q. Zhang, P.N. Suganthan, L. Chen, Comparison between MOEA/D and NSGA-III on a set of many and multi-objective benchmark problems with challenging difficulties, Swarm Evol Comput. 46 (2019) 104–117. https://doi.org/10.1016/j.swevo.2019.02.003.

[174] J. Iwaro, A. Mwasha, R.G. Williams, R. Zico, An Integrated Criteria Weighting Framework for the sustainable performance assessment and design of building envelope, Renewable and Sustainable Energy Reviews. 29 (2014) 417–434. https://doi.org/10.1016/j.rser.2013.08.096.

[175] F. Pedregosa, G. Varoquaux, A. Gramfort, V. Michel, B. Thirion, O. Grisel, M. Blondel, P. Prettenhofer, R. Weiss, V. Dubourg, Scikit-learn: Machine learning in Python, The Journal of Machine Learning Research. 12 (2011) 2825–2830.

[176] A. Bampoulas, F. Pallonetto, E. Mangina, D.P. Finn, An ensemble learning-based framework for assessing the energy flexibility of residential buildings with multicomponent energy systems, Appl Energy. 315 (2022) 118947. https://doi.org/10.1016/j.apenergy.2022.118947.

[177] C. Fan, F. Xiao, S. Wang, Development of prediction models for next-day building energy consumption and peak power demand using data mining techniques, Appl Energy. 127 (2014) 1–10. https://doi.org/10.1016/j.apenergy.2014.04.016.

[178] H. Deng, D. Fannon, M.J. Eckelman, Predictive modeling for US commercial building energy use: A comparison of existing statistical and machine learning algorithms using CBECS microdata, Energy Build. 163 (2018) 34–43. https://doi.org/10.1016/j.enbuild.2017.12.031.

[179] J.T. Wen, S. Mishra, Intelligent building control systems: A survey of modern building control and sensing strategies (advances in industrial control) 2018 edition, ISBN-13. (2018) 978–3319684611.

[180] R. Parsons, ed., ASHRAE Handbook - Fundamentals, American Society of Heating Refrigerating and Air-Conditioning Engineers, 1997.

[181] J. Xiong, A. Tzempelikos, Model-based shading and lighting controls considering visual comfort and energy use, Solar Energy. 134 (2016) 416–428. https://doi.org/10.1016/j.solener.2016.04.026.

[182] F. Bre, A.S. Silva, E. Ghisi, V.D. Fachinotti, Residential building design optimisation using sensitivity analysis and genetic algorithm, Energy Build. 133 (2016) 853–866. https://doi.org/10.1016/j.enbuild.2016.10.025.

[183] ASHRAE, Standard 90.1-2019, Energy Standard for Buildings Except Low-Rise Residential Buildings, 2019.

[184] D. Jonas, TRNSYS Type 835: PV model for the coupling with solar thermal absorber and collector models as PVT model, (2019). https://doi.org/10.5281/zenodo.1446414.

[185] M. Usman, Energy Flexibility, Germany, n.d. https://github.com/UdSAES/Energy-flexibility.

[186] YORK®, Residential Geothermal Heat Pumps, (2021). https://www.yorkgeothermal.com/residential/products/geothermal-heat-pumps/yaws/ (accessed November 14, 2021).

[187] BOSCH, Bosch IDS 2.0 Split System Heat Pump, (2021). https://www.bosch-thermotechnology.us/us/en/ocs/residential/inverter-ducted-split-family-ids–18527266-p/.

[188] DAIKIN, Daikin Altherma low temperature air-to-water Heat Pumps, (2021). https://www.daikin.eu/en_us/product-group/air-to-water-heat-pump-low-temperature.html.

[189] MAYA-YAZAKI, YAZAKI Water Fired Chiller, (2021). https://maya-airconditioning.com/eng/assorbitori-ad-acqua.html.

[190] ASHRAE, Standard 55, Thermal environmental conditions for human occupancy, 2020.

[191] M. Kottek, J. Grieser, C. Beck, B. Rudolf, F. Rubel, World Map of the Köppen-Geiger climate classification updated, Meteorologische Zeitschrift. 15 (2006) 259–263. https://doi.org/10.1127/0941-2948/2006/0130.

[192] Insulation materials, (n.d.). https://www.obi.de/baustoffhalle/daemmstoffe/c/233#/.

[193] M.Z. Jacobson, V. Jadhav, World estimates of PV optimal tilt angles and ratios of sunlight incident upon tilted and tracked PV panels relative to horizontal panels, Solar Energy. 169 (2018) 55–66. https://doi.org/10.1016/j.solener.2018.04.030.

[194] P. Satrio, T.M.I. Mahlia, N. Giannetti, K. Saito, Optimization of HVAC system energy consumption in a building using artificial neural network and multi-objective genetic algorithm, Sustainable Energy Technologies and Assessments. 35 (2019) 48–57. https://doi.org/10.1016/j.seta.2019.06.002.

[195] Z. Yong, Y. Li-Juan, Z. Qian, S. Xiao-Yan, Multi-objective optimization of building energy performance using a particle swarm optimizer with less control parameters, Journal of Building Engineering. 32 (2020) 101505. https://doi.org/10.1016/j.jobe.2020.101505.

Appendix A

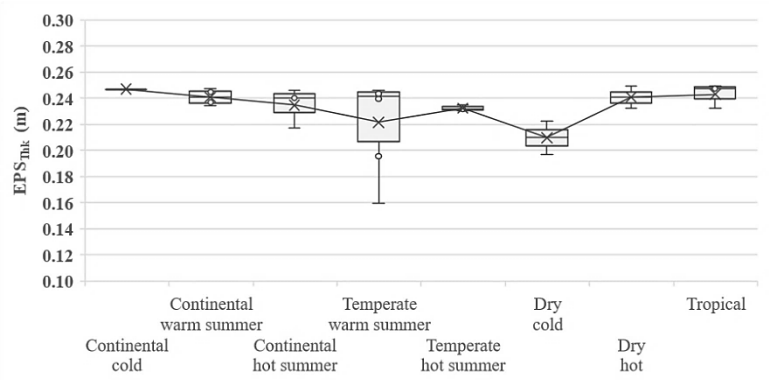

Fig A1: Variability in thickness of EPS insulation in different climate zones

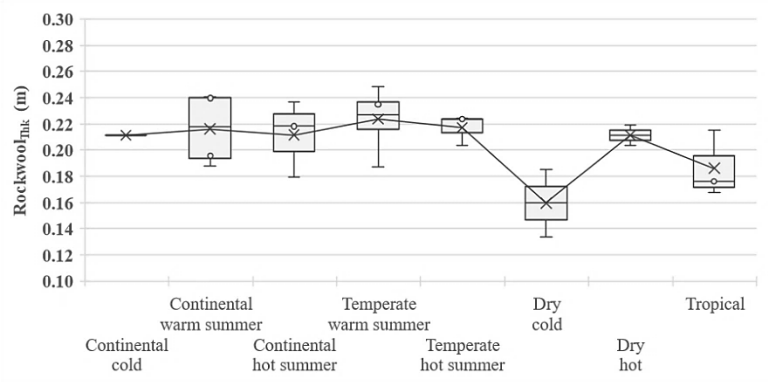

Fig A2: Variability in thickness of rockwool insulation in different climate zones

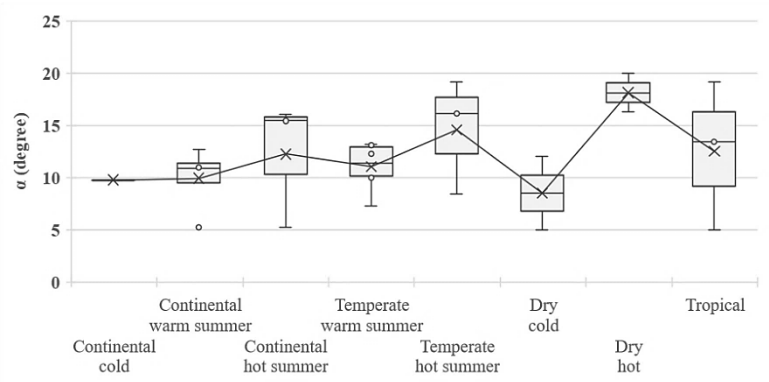

Fig. A3: Variability in window aperture angel in different climate zones

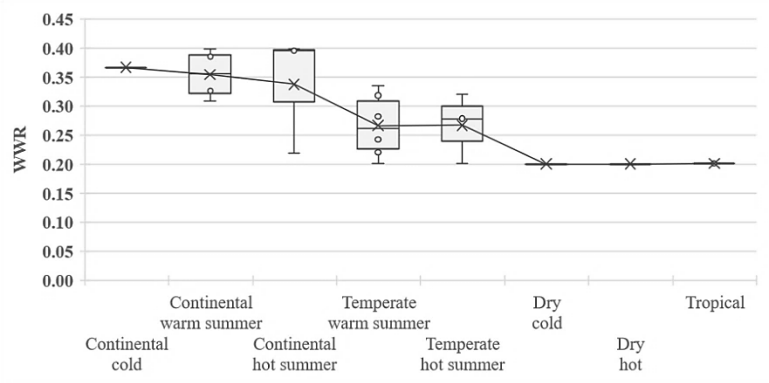

Fig. A4: Variability in WWR in different climate zones

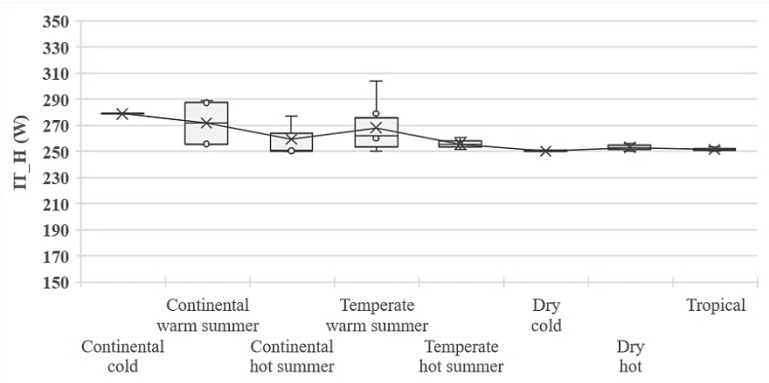

Fig. A5: Variability in solar radiation for shading control in different climate zones

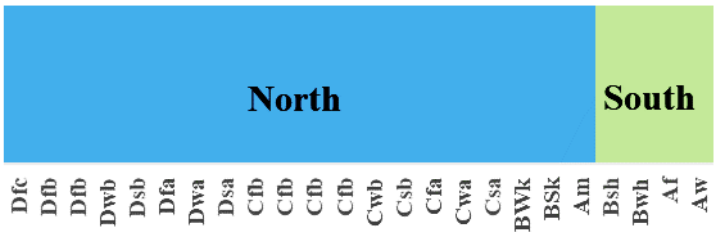

Fig. A6: Optimal household orientation in different climate zones